Development and Evaluation of Glucose-Responsive Biomaterials as Self-Regulated Insulin Delivery Systems

by

Lisa Rae Volpatti

B.S. Chemical Engineering
University of Pittsburgh, 2013

M.Phil. Chemistry
University of Cambridge, 2014

M.S. Chemical Engineering Practice
Massachusetts Institute of Technology, 2016

Submitted to the Department of Chemical Engineering in Partial Fulfillment of the Requirements for the Degree of

DOCTOR OF PHILOSOPHY

at the

MASSACHUSETTS INSTITUTE OF TECHNOLOGY

February 2020

Signature of Author: Signature redacted .....
Lisa R. Volpatti
Department of Chemical Engineering
January 10, 2020

Certified by: Signature redacted .....
Daniel G. Anderson
Samuel A. Goldblith Professor of Applied Biology,
Chemical Engineering and Health Sciences & Technology
Thesis Supervisor

Accepted by: Signature redacted .....
Patrick S. Doyle
Robert T. Haslam Professor of Chemical Engineering
Chairman, Committee for Graduate Students

Development and Evaluation of Glucose-Responsive Biomaterials as Self-Regulated Insulin Delivery Systems

by

Lisa Rae Volpatti

Submitted to the Department of Chemical Engineering on January 10, 2020 in Partial Fulfillment of the Requirements for the Degree of Doctor of Philosophy

Abstract

Motivation: Diabetes mellitus is a disease characterized by poor glycemic control which often leads to severe complications including cardiovascular disease and kidney failure Many diabetic patients must continually monitor their blood sugar and self-administer multiple daily doses of exogenous insulin to combat hyperglycemia To reduce this patient burden, limit the occurrence of hypoglycemic events, and better mimic native insulin activity, therapies which can self-regulate insulin delivery are an attractive option This work begins to address current limitations of such glucose-responsive insulin delivery systems by developing novel biomaterial-based formulations

Results This Thesis presents 3 types of glucose-responsive insulin delivery systems developed during my PhD Each system employs the enzyme glucose oxidase as a glucose sensor, which converts glucose to gluconic acid and reduces the pH of the microenvironment when glucose levels are high. This change in pH acts as a trigger to release insulin on demand The first system uses the pH-responsive polymer acetalated-dextran to formulate nanoparticles that physically encapsulate both insulin and glucose oxidase The particles rapidly degrade in the presence of acid, making this system a fast acting therapeutic that reduces blood sugar within an hour of administration in diabetic mice The second system is comprised of alginate microgels that encapsulate nanoparticles to create a depot of insulin for sustained glucose-responsive release *in vivo* for over 3 weeks with just 2 doses. The third system is based on the electrostatic complexation of insulin to positively charged polymers, such as polyethyleneimine When the pH is reduced below the isoelectric point of insulin, the complex dissociates and releases insulin only in response to elevated levels of glucose. These complexes are afforded a prolonged functional lifetime by decreasing the rate of insulin release under normal glucose concentrations The synthesis, formulation, *in vitro* characterization, and *in vivo* results in diabetic mouse models for each of these systems are discussed

Conclusion: The development and characterization of the glucose-responsive insulin delivery systems described here marks an important step in the advancement of self-regulated insulin delivery. Furthermore, these formulations may provide generalized strategies for the development of future stimuli-responsive drug delivery systems

Thesis Supervisor Daniel G Anderson
Title Samuel A Goldblith Associate Professor

Acknowledgements

First and foremost, I would like to thank my advisor, Prof. Dan Anderson for his support and mentorship throughout my Ph.D. Thank you for giving me the flexibility and independence to develop my own ideas and work on what truly interests me. Next, I would like to thank Prof. Robert Langer for being an outstanding mentor and role model. The Langer Lab is a diverse community full of brilliant people and amazing opportunities, and I'm very thankful to be a part of it. Thank you Bob for your unparalleled leadership, expertise, and support. I would also like to thank Prof. Sangeeta Bhatia for serving as a member of my Thesis Committee, providing valuable scientific and professional advice, and being a source of inspiration as an extremely successful female professor.

Thank you to the administrative staff who work endlessly behind the scenes to keep the Anderson and Langer Labs running efficiently. Specifically, I would like to thank Tara Fawaz for her outstanding organizational skills in managing the Anderson Lab, always going above and beyond expectations, and being a good friend. Thank you to the many members of the Langer Lab Administrative Office who have been instrumental to the success of the lab, specifically Connie Beal who also goes above and beyond expectations to efficiently manage the Langer Lab. Thank you also to the members of the Department of Chemical Engineering Student Office, past and present, including Suzanne Maguire, Joel Dashnaw, Eileen Demarkles, and Sharece Corner.

I am very appreciative for all of the members of the Anderson and Langer Labs for helpful scientific discussions, collaborations, and mentorship. In particular, I would like to thank Dr. Arijit Basu, Dr. Crystal Chu, Dr. Abel Cortinas, Dr. Kevin Daniel, Dr. Asha Patel, Dr. Arnab Rudra, and Dr. Matthew Webber. I would also like to thank my officemates for providing helpful discussions and general banter: Dr. Chandra Bhattacharya, Dr. Matt Bochenek, Dr. Suman Bose, Dr. Derfogail Delcassian, Amanda Facklam, Corina MacIsaac, and Luke Rhym. Special thanks to Suman and Amanda for their friendship.

I would like to the board of Graduate Women in Chemical Engineering, especially Kara Rodby for co-founding the group with me. It has been such a pleasure working with them over the past year in an effort to enhance diversity, equity, and inclusion. Thank you also to Prof. Paula Hammond, Department Head, for supporting our group, mandating inclusivity trainings, and being a mentor and role model.

Thank you to my best ChemE friends Nick Schickel, Mike Orella, and Connor Coley for their unwavering support from the first semester onwards. Thanks to the rest of our friend group – Laura, Caroline, Kassi, Justin, Catie, Craig, Ryan, and Meg. I really could not ask for better or more supportive friends. Thanks to my Practice School friends for making our time in Washington D.C. and Australia such great experiences.

Finally, I would like to thank my family for their love and support every step of the way. Thank you to my mom and dad for helping me move to Cambridge, flying to Boston to visit, and providing a welcoming home every time I visit. Thank you Kim for always being my best friend and amigo #1. Thanks to you and Angelina for your daily FaceTime calls and of course to the puppers, Gigi and Leroy, for their cuddles and love. Thank you Grandma Mem, Grandma Caroline, and the late Grandpap Joe and Grandpa Earl. I'm very thankful to have had the support of friends and family throughout this Ph.D.

Table of Contents

List of Figures

List of Tables

Chapter 1: Background and Significance

1.1 Motivation

Diabetes mellitus is a class of diseases characterized by lack of sufficient control of blood glucose levels attributed to deficient insulin production or signaling In 2017, diabetes was estimated to affect 451 million people (aged 18-99) worldwide and was responsible for approximately 5 million deaths (aged 20-99) [1] Additionally, care for diagnosed diabetics (including institutional care, outpatient care, and outpatient medications and supplies) accounted for 1 in 4 health care dollars in the U S in 2017 [2]

Insulin, a 51 amino acid residue protein first discovered by Banting and Best,[3] is a natural hormone responsible for the uptake, metabolism, and storage of glucose in the body [4-5] In healthy individuals, a rise in blood glucose levels causes β-cells of islets of Langerhans in the pancreas to secrete insulin into the blood Insulin then binds to extracellular receptors in liver, muscle, and adipose tissues, signaling these cells to uptake, metabolize, and store excess glucose as glycogen When glucose levels return to normal, the insulin levels in the blood correspondingly recede. In diabetic patients, however, this fine control of insulin and blood glucose levels is disrupted

Type 1 diabetes is an autoimmune disorder that develops when the body's immune system attacks the insulin-producing β-cells in the pancreas [6] Therefore, Type 1 diabetics are no longer able to produce and secrete insulin independently and require exogenous insulin dosing to maintain glucose levels. Type 2 diabetes, on the other hand, typically begins when the body develops a resistance to insulin, that is, the cells within the muscles, liver, and fat tissue do not take up and use insulin as efficiently.[7] This resistance often leads to the β-cells in the pancreas slowly losing the ability to produce sufficient quantities of insulin Therefore, Type 2 diabetes is characterized by both insulin

resistance and β-cell dysfunction. The risk for developing Type 2 diabetes is positively correlated with age, genetic predisposition, physical inactivity, and obesity.[8]

Chronic hyperglycemia may lead to severe complications including cardiovascular disease, kidney failure, and cancer.[9-10] These complications may be limited in both Type 1 and Type 2 diabetic patients with intensive insulin therapy, which involves consistent self-monitoring of blood glucose levels from finger pricks in conjunction with multiple daily subcutaneous injections of insulin in attempt to achieve normoglycemia.[11-12] However, self-administered intensive insulin therapy fails to tightly regulate blood glucose levels, results in decreased patient compliance,[13-14] and increases the risk of hypoglycemia.[15] Acute episodes of hypoglycemia can cause brain damage, seizures, loss of consciousness, or even death.[16-17]

A variety of insulin analogs have been developed since its discovery in 1921 in attempt to offer better control over diabetes. These may be classified as rapid-acting (e.g. Insulin Lispro), short-acting (e.g. regular insulin), intermediate-acting (e.g. neutral protamine Hagedorn insulin; NPH), or long-acting (e.g. Insulin Detemir; Figure 1.1a).[18-20]

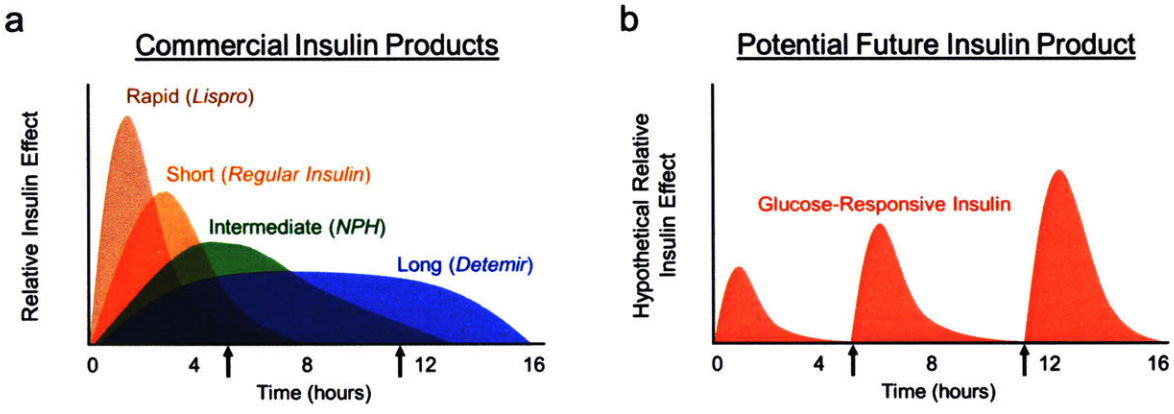

Figure 1.1. Comparison of relative insulin effects over time. (a) Relative insulin effect for existing commercial rapid-, short-, intermediate-, and long-acting insulin analogs. (b) Hypothetical relative insulin effect of a potential future glucose-responsive insulin formulation. Arrows represent meals that result in an increase in systemic blood sugar.

However, no commercially available formulations dynamically regulate insulin activity in response to glucose levels according to individual patient needs A self-regulated delivery system that mimics the native insulin secretion of a healthy pancreas would result in fewer hypoglycemic events and better long-term glycemic control Such a system would respond to increases in blood glucose levels resulting from meals by releasing insulin into the blood (Figure 1 1b).

One realization of such a delivery system comes in the form of an insulin pump that combines continuous glucose sensing with insulin infusions [21-22] While insulin pumps have had recent commercial success, there are still many challenges associated with current devices Most continuous glucose monitors require recalibration with blood glucose levels from a finger prick and have a limited lifetime [23-25] Insulin pump technology also requires patients to be educated on its use for proper insertion, removal, decision making, and response to alarms.[26] Therefore, although these systems may be considered closed-loop, they still place a burden of responsibility on the patient.

Since patient compliance and adherence to medication regimens is a major challenge in combating diabetes,[14, 27-28] reducing dosing frequency through extended release formulations could enhance compliance and therapeutic outcomes [13, 29] For many therapeutics, sustained release drug delivery systems are designed to exhibit zero-order release kinetics through Fickian diffusion to keep the concentration of drug in the blood in a constant range over a long period of time However, in the case insulin delivery, the concentration of insulin in the blood and subsequently the rate of insulin release should be proportional to blood glucose levels, thus posing an additional difficulty in developing an environmentally-responsive drug delivery system To this end, chemically glucose-

responsive biomaterial formulations have been developed that respond to local changes in glucose with an associated change in insulin release rate [30] These systems can be broadly classified as nanoparticles, microparticles, hydrogels, or membranes that encapsulate insulin and may shrink, swell, or degrade in response to glucose to release the therapeutic protein on demand [30-31] The most commonly employed glucose sensors in such systems fall into three primary categories. glucose-binding proteins, phenylboronic acid (PBA)-functionalized polymers, and glucose oxidase

1.2 Glucose-Binding Proteins

Carbohydrate-binding proteins, such as lectins and membrane receptors, have been used in drug delivery systems as glucose-recognition molecules for their ability to reversibly bind to monosaccharides including glucose and mannose Early work primarily focused on delivering exogenous glucose-binding proteins, while more recent advances in this area have exploited the natural ability of endogenous membrane proteins to recognize glucose.

1 2 1 Exogenous lectins

The most well-studied lectin for applications in glucose-responsive insulin delivery is concanavalin A (Con A), which reversibly binds to α-D-glucosyl and α-D-mannosyl groups with relatively high affinity as indicated by dissociation constants in the low mM range [32-33] The potential of Con A to provide glucose-responsive insulin delivery was demonstrated with the synthesis of a glycosylated insulin derivative complementary to the binding site of Con A [34] While the unmodified insulin did not bind, the maltose-modified insulin derivative was able to bind to Con A and could be displaced from the binding sites in response to excess free glucose [34]

The feasibility of using a Con A-based glucose-responsive insulin delivery system in vivo was later determined with an implantable insulin delivery reservoir device in streptozotocin (STZ)-induced type 1 diabetic rats [35] The insulin reservoir is separated from the intraperitoneal space by a glucose-sensitive hydrogel comprised of Con A bound to dextran derivatives.[35] Since Con A is a tetrameric protein with 4 binding sites, the same lectin molecule may bind to several glycosylated proteins, polymers, or polysaccharides, creating a crosslinked hydrogel network (Figure 1 2) When the ambient glucose

concentrations are high, the free glucose will preferentially bind to Con A through the process of competitive displacement. The crosslinks of the hydrogel will thus be disrupted, resulting in an increase in the gel's porosity and permeability (Figure 1.2). In the case of the implantable device, an increase in glucose causes a disruption in the equilibrium binding between Con A and dextran which decreases the viscosity of the gel and increases insulin permeability.[35] The device was thus reported to control daily blood glucose measurements of the diabetic rats until the insulin was exhausted.[35] Several other Con A-based hydrogel delivery platforms rely on this same principle with many encapsulating insulin inside the gel itself (Table 1).

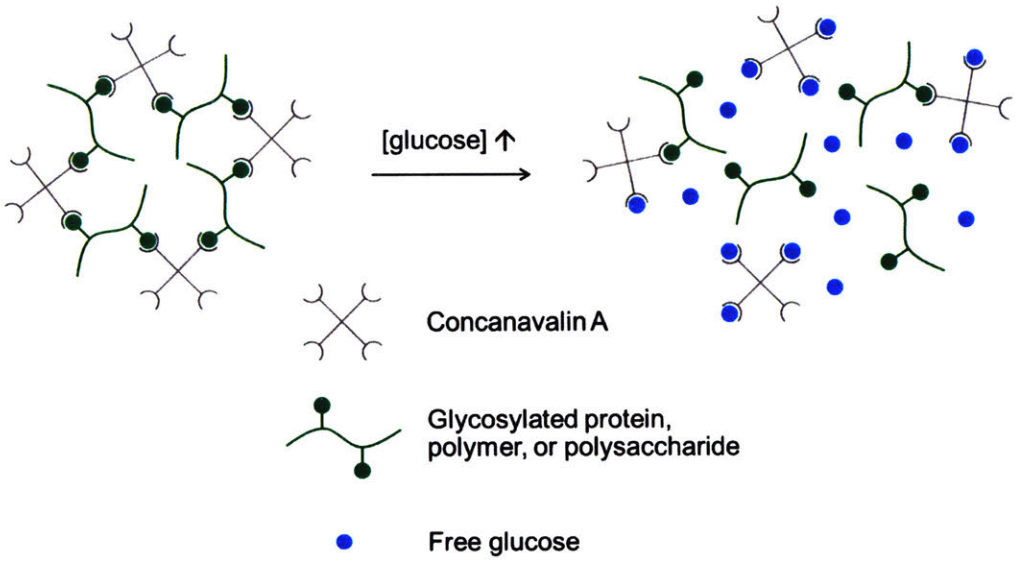

Figure 1.2. Schematic of glucose-responsive hydrogels based on concanavalin A.

Another strategy for glucose-responsive insulin delivery using Con A is based on the gating of mesoporous silica nanoparticles (MSNs). The pores of the MSNs serve as the insulin reservoir. The surface of the MSNs may be functionalized, for example with mannose ligands, and bound with Con A to provide a gated delivery vehicle.[36] When glucose levels are

elevated, the mannose-Con A interactions are disrupted through competitive binding of glucose, and insulin is released [36]

1.2.2 Endogenous glucose-binding proteins

In addition to exogeneous lectins, such as Con A, endogenous carbohydrate-binding membrane proteins have been employed in the development of glucose-responsive insulin delivery systems. One formulation developed by Merck, MK-2640, consists of a mannosylated insulin derivative [37-38] MK-2640 has affinity for the mannose receptor C-type 1 which functions in the clearance of glycoproteins by endosomal degradation. The ability of MK-2640 to bind to either the mannose receptor or the insulin receptor is the basis for its glucose-responsiveness When blood sugar levels are elevated, glucose will competitively bind to the mannose receptor As a result, a larger fraction of MK-2640 should be available to bind to the insulin receptor and subsequently reduce blood glucose levels Conversely, when glucose levels are low, more MK-2640 is expected to be degraded upon binding to the mannose receptor Thus, the fraction of MK-2640 cleared by either pathway should in principle be mediated by the amount of glucose present Despite success in glucose-mediated insulin clearance in preclinical studies in large animal models,[37] there was no significant glucose-dependent change in MK-2640 clearance in a clinical trial of 16 subjects with type 1 diabetes [39] Nevertheless, these results may provide valuable information that aids in the design of the next-generation of glucose-responsive insulins

In another approach, researchers have taken advantage of glucose transporters on cell membranes to mediate insulin availability in the blood [40] Insulin conjugated with glucosamine (Glc-Insulin) was reported to reversibly bind to the membrane of red blood

cells (RBCs).[40] An elevation of surrounding glucose levels in vitro resulted in the release of bound Glc-Insulin. Mouse RBCs were then incubated with Glc-Insulin and injected intravenously into diabetic mice. While the Glc-Insulin-conjugated RBCs provided enhanced glycemic control, free Glc-Insulin responded similarly to unmodified insulin,[40] suggesting that pre-incubation of Glc-Insulin with the delivery vehicle is required for glucose-responsiveness. To create an insulin analog that can bind to glucose transporters in situ, the same group conjugated insulin with a glucose transporter inhibitor, Glut-i2.[41] Upon subcutaneous injection, this analog was reported to enhance the duration of action of insulin and mitigate its hypoglycemic effect in mice.[41]

Table 1.1. Recent Glucose-Responsive Insulin Formulations Based on Glucose-Binding Proteins

Glucose-binding protein	**Formulation type**	**Primary biomaterial component(s)**
Exogeneous concanavalin A	Hydrogels	Dextran,[35] dextran/PEG,[42] dextran/PEG/chitosan,[43] pullulan[44]
	Microgels	Chitosan,[45] dextran,[46-47] poly(DMAEMA)[48]
	Microparticles	Chitosan/dextran[49]
	Nanogels	PNIPAM[50]
	Nanoparticles	MSNs[36]
Endogenous glucose transporter	Insulin conjugates	Glucosamine-modified insulin,[40] Glut-i2-modified insulin[41]
Endogenous mannose receptor C-type 1	Insulin conjugates	Insulin-carbohydrate conjugate[37, 39]

MSNs: mesoporous silica nanoparticles
PNIPAM: poly(N-isopropylacrylamide)
poly(DMAEMA): poly(dimethylamino ethyl methacrylamide) or poly(dimethylamino ethyl methacrylate)

1.3 Phenylboronic Acid-Functionalized Polymers

Phenylboronic acids (PBAs) reversibly bind to 1,2-cis-diols to form boronic esters and can as such be used as carbohydrate sensors (Figure 1.3) Like lectins, they may be used crosslink hydrogels by binding to glycosylated proteins, polymers, or polysaccharides. These reversible covalent bonds can be disrupted through the competitive binding of glucose, resulting in a glucose-responsive delivery system Moreover, PBAs exist in equilibrium between the neutral boronic acid species and the boronate anion in solution Since esters formed from the charged species are more stable, binding to diols may shift the equilibrium to the boronate form, leading to a macroscopic change in the material and subsequent insulin release

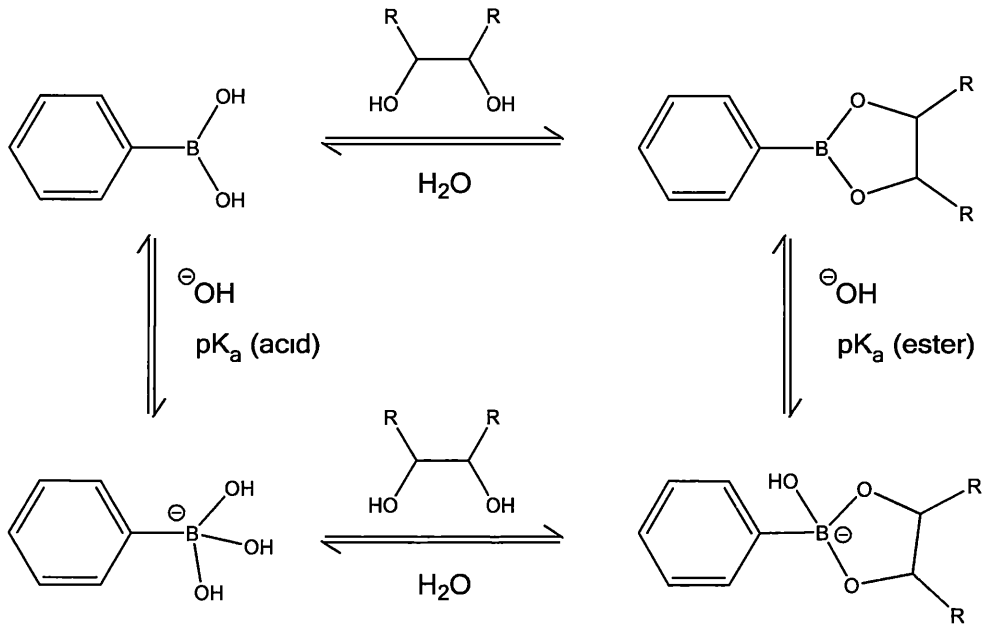

Figure 1.3 Schematic of phenylboronic acid binding of 1,2- or 1,3-cis-diols The equilibrium between the boronate and the boronic acid can be shifted by adjusting the solution pH

Boronate ester formation is generally favored near or above the pK_a of the boronic acid, and the pK_a of PBA is 8 8.[51] Therefore, early efforts in this field focused on reducing the apparent pK_a of PBA to achieve glucose-responsiveness under physiological pH

Methods of facilitating ester formation include adding electron withdrawing groups as substituents on the aromatic ring (Figure 1 4a),[51] forming benzoboroxoles as cyclic analogs of PBAs (Figure 1 4b),[52] and generating a nitrogen center adjacent to the boron in a Wulff-type PBA (Figure 1 4c) [53] Amino groups can also be incorporated into the polymer backbone to improve solubility and enhance diol binding under physiological conditions.[54] However, the optimal pH for binding is not always higher than the pK_a and many other factors must be taken into account in determining binding affinities and designing glucose-responsive insulin delivery systems [51]

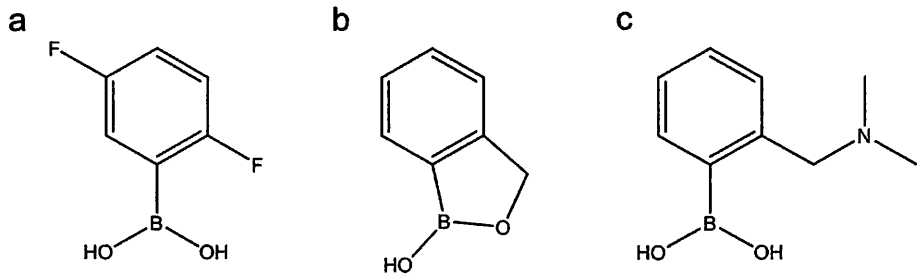

Figure 1.4 Examples of phenylboronic acid analogs with reduced pK_a values a) 2,5-difluorophenylboronic acid, pK_a = 7 0,[51] b) benzoxaborole, pK_a = 7 3,[55] c) 2-(N,N-dimethylaminomethyl)phenylboronic acid, pK_a = 6 7 [51]

1 3 1 Competitive displacement

In a manner similar to hydrogels fabricated from Con A, hydrogels synthesized from PBA-modified macromolecules can be dynamically crosslinked through reversible sugar binding When external sugar concentrations are high, the glucose will out-compete the diols in the delivery matrix, crosslinks will be displaced, and the gel will swell These dynamic covalent bonds impart with the hydrogels with self-healing and shear-thinning behavior For example, an injectable, self-healing hydrogel was synthesized from 4-arm PEG macromers [56] The arms of the PEG were modified with either PBA derivatives or

glucose-like diols Upon mixing, the crosslinked polymers formed a self-healing hydrogel network that exhibited glucose-mediated release of immunoglobulins.[56] In order to simplify the complexity of the system, single component glucose-responsive polymeric materials have been synthesized from monomers containing PBA pendant groups or glucose modifications (Table 1.2) In one such study, polymers containing between 10-60% PBA monomers were able to form shear-thinning, self-healing hydrogels that exhibit glucose-responsive behavior.[57] In addition to shear-thinning hydrogels, injectable hydrogels can be comprised of temperature-responsive materials that undergo a sol-gel transition at physiological temperature. For example, hydrogels that respond to temperature in addition to glucose and pH can formed by incorporating N-isopropylacrylamide monomers into the polymer backbone [58]

Several types of nanomaterials, including micelles, nanoparticles, vesicles, and nanogels, have also been reported as glucose-responsive delivery vehicles based on the competitive displacement of PBA-diol interactions (Table 1 2) For example, the self-assembly of two polymers generated glucose-responsive complex micelles with PEG comprising the micelle shell and PBAs complexed with glycosyl groups forming the micelle core [59] In another approach, MSNs have been gated by exploiting reversible PBA-diol binding in a similar manner to Con A-gated MSNs [60-61] The surface of the MSNs can be grafted with PBA-containing molecules, and polysaccharides[60] or sugar-modified β-cyclodextrins[61] can sterically block the nanopores through the formation of boronate esters These pores are then opened by the competitive binding of glucose, providing glucose-mediated cargo release To eliminate the need of a delivery vehicle, insulin directly conjugated with PBA derivatives has been reported to show glucose-

responsiveness in diabetic mice, possibly due to the glucose-dependent binding of the insulin analog to endogenous immobilized diols [62]

1 3.2 Ionization equilibrium shift

In addition to disrupting covalent PBA-diol interactions, the binding of sugars to free PBA may shift the ionization equilibrium from the neutral state toward the charged state This shift often results in an increased osmotic pressure which causes hydrogels to swell By changing the configuration of the PBA, hydrogels can also be designed to shrink in response to glucose[63-64] Additionally, the equilibrium shift to the charged boronate form may result in a change in hydrophobicity that leads to the disruption of micellar structures or electrostatic complexes.

PBAs coupled to hydrogel backbones can act as glucose sensors by shifting the ionization equilibrium toward the charged species upon binding to 1,2- or 1,3-cis-diols The resulting osmotic pressure gradient causes a change in hydration of the hydrogel, ultimately resulting in a volume change of the bulk gel. Swelling of the hydrogel enhances its permeability and permits encapsulated insulin release in response to elevated glucose concentrations. An abrupt change in hydration under optimized conditions may also result in localized dehydration of the hydrogel surface that impedes insulin release in normoglycemic conditions Poly(acrylamide)-based hydrogels form this so-called "skin layer" that reversibly rehydrates when equilibrated in hyperglycemic concentrations [65] A catheter-combined device has been developed from these materials that was reported to control glucose metabolism in both insulin-deficient (Type 1) and insulin-resistant (Type 2) diabetic mouse models [66] Similar "skin layer"-forming poly(N-isopropylacrylamide)

(PNIPAM)-based hydrogels have also been formulated with silk fibroin in microneedle-array patches [67-68]

In addition to bulk hydrogels, PBA-based nanostructures that exploit the shift in ionization equilibrium can be designed for glucose-responsive insulin delivery For example, micelles can be self-assembled from amphiphilic polymers with a hydrophilic block such as PEG and a hydrophobic block containing PBA The hydrophilic block comprises the outer shell phase of the micelle, while the hydrophobic PBA-containing block represents the inner core. Upon binding to glucose, the PBA will exist primarily in the charged, hydrophilic form This switch from amphiphilic to double hydrophilic disrupts the micellar structure, resulting in the release of encapsulated cargo [69-74] By tuning the degree of polymerization of the boroxole block in co-polymers containing a hydrophilic PEG block, Kim et al were able to form several nanostructures including spherical micelles, cylindrical micelles, and larger polymersomes, as confirmed by transmission electron microscopy (TEM) [71] Moreover, the shift in PBA ionization equilibrium can alter the net charge of a polycation and disrupt electrostatic interactions with insulin, resulting in particle disassembly and protein release [75]

Table 1.2 Recent Glucose-Responsive Insulin Formulations Based on Phenylboronic Acid

Main mechanism of release	Formulation type	Primary biomaterial component(s)
Displacement of PBA-diol interactions	Films	Polystyrene/alginate[76]
	Hydrogels	Multi-arm PEG,[56, 77-78] poly(APBA-b-LAMA),[79] PEO-b-PVA,[80] PNIPAM,[58] poly(BG)[57]
	Insulin complexes	β-cyclodextrin[81]
	Insulin conjugates	PBA-modified insulin[62]
	Micelles	PEG/poly(aspartic acid),[59, 82] PEG/poly(aspartic acid)/PNIPAM,[83] PNAM[84]
	Microparticle-hydrogel hybrids	PLGA/hyaluronic acid
	Nanogels	PEG/poly(glutamic acid)[85-86]
	Nanoparticles	MSNs,[60-61] poly(APBA-b/r-GAMA),[87-90] PEO-b-PHOS,[91] PMAPBA/chitosan,[92] poly(acrylic acid),[93] poly(glutamic acid)/chitosan,[94]
	Vesicles	α-cyclodextrin/PEG/poly(aspartic acid)[95]
Shifting of the ionization equilibrium leading to changes in solubility, swelling, or contracting	Dendrimers	poly(amidoamine)/poly(aspartic acid)/PEG[96]
	Hydrogels	poly(acrylamide),[65-66, 97] PNIPAM[98]
	Membranes	poly(ε-caprolactone)[99]
	Micelles	PEG-b-PBDEMA,[70, 72] PEG/poly(2-nitrobenzyl acrylate),[73] PEG/poly(glutamic acid),[69] PNIPAM/PEG/poly(aspartic acid),[100] starch[74, 101]
	Microgels	PNIPAM[63-64, 102]
	Microneedles hydrogels	silk fibroin/PNIPAM[67-68]
	Microparticles	Alginate/polyvinylpyrolidone,[103] PLGA[104], poly(N-(2-aminoethyl)acrylamide)[75]
	Nanogels	Chitosan/alginate[105] PNIPAM/dextran[106]
	Polymersomes	Polystyrene/PEG[71, 107]

PBDEMA poly[(2-phenylboronic esters-1,3-dioxane-5-ethyl) methylacrylate]
PEO-b-PVA poly(ethylene oxide)-*block*-poly(vinyl alcohol)
PEO-b-PHOS poly(ethylene oxide)-*block*-poly(4-hydroxystyrene)
PLGA poly(lactic-*co*-glycolic acid)
PMAPBA poly(3-methacrylamido phenylboronic acid)
PNAM poly(N-acryloylmorpholine)
poly(APBA-r-GAMA) poly(3-acrylamidophenyl boronic acid-*random*-D-gluCon Amidoethyl methacrylate)
poly(APBA-b-LAMA) poly(3-acrylamidophenyl boronic acid-*block*-2-lactobionamidoethyl methacrylate)
poly(BG) poly(3- propionamidophenyl)boronic acid (N-(3-((2,3,4,5,6-pentahydroxyhexyl)amino)propyl)propionamide)

1.4 Glucose Oxidase

Glucose oxidase (GOx) is an enzyme found in certain species of insects and fungi. It converts glucose into gluconolactone, which is rapidly hydrolyzed into gluconic acid (Figure 1.5). This reaction consumes oxygen and produces hydrogen peroxide as a byproduct. A second enzyme, catalase, is often coupled to this reaction for applications in glucose-responsive insulin delivery to disproportionate the reactive oxidative species and reproduce oxygen to enhance the kinetics of conversion. Many commercial glucometers employ glucose oxidase as a sensor due to its stability, specificity for glucose, and rapid turnover rate.[108-109] Several glucose-responsive insulin delivery systems therefore also employ this enzyme as a sensor coupled with pH-, peroxide-, or hypoxia-sensitive biomaterials.

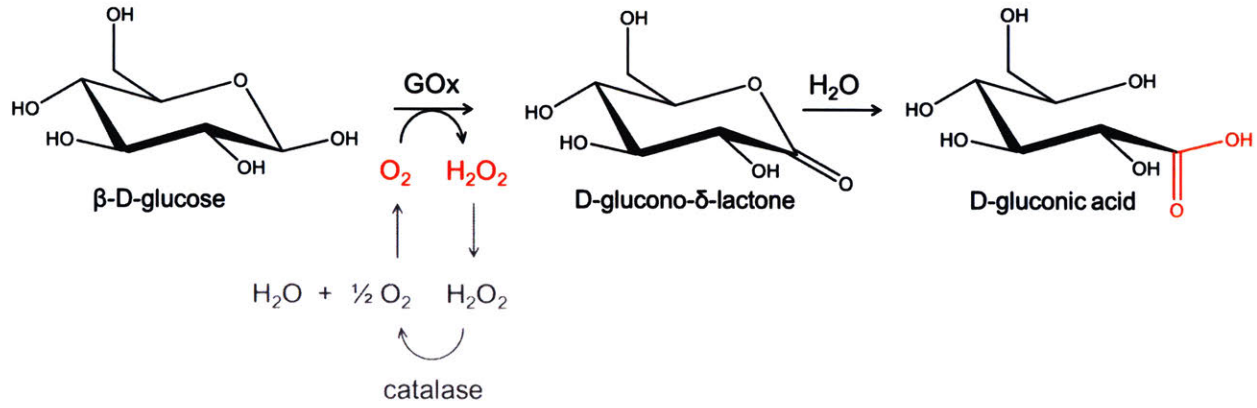

Figure 1.5. Enzymatic action of glucose oxidase (GOx). GOx converts glucose to gluconolactone which is then hydrolyzed into gluconic acid. Catalase can be added to disproportionate the hydrogen peroxide and regenerate the oxygen required for the enzymatic conversion of glucose.

1.4.1 Decreased pH

The majority of glucose-responsive delivery systems that employ GOx are based on pH-sensitive biomaterials. Early studies using GOx for glucose-responsive insulin release involved the immobilization of the enzyme onto a charged polymeric membrane.

Insulin permeation through the membrane can be increased due to the swelling of polycationic polymers[110-111] or the shrinking of polyanionic polymers[112] causing the opening of pores in response to protonation at lowered pH values. Implantable polymeric matrices[113] and hydrogels[114-116] were then developed to release insulin with potential in vivo applications.

Over the past decade, materials have been reported that degrade, disassemble, solubilize, or swell under acidic conditions and have been formulated into films, hydrogels, membranes, microparticles, and nanostructures (Table 1.3). One example using membrane technology in an implantable device consists of an insulin reservoir made from PEGylated silicone with a glucose-responsive plug.[117] The polymeric membrane plug contains hydrogel nanoparticles that shrink in acidic conditions, resulting in the formation of a porous network that enables the release of insulin. These devices were reported to achieve normoglycemia for several days when implanted in STZ-induced diabetic rats.[117] An injectable network comprised of surface-coated modified-dextran nanoparticles was also reported to reduce blood sugar levels of STZ-induced diabetic mice for several days.[118] In this system, the acetal groups of the modified dextran are cleaved in response to acid, producing the soluble polysaccharide which results in the release of encapsulated insulin.[118] In another report, chitosan microgels containing GOx and catalase nanoparticles were shown to swell in response to glucose and sustain normoglycemia in diabetic mice for up to 10 hours.[119]

More recently, biomimetic materials have been used in conjunction with GOx and evaluated in vivo for glucose-mediated insulin delivery. For example, a pH-sensitive peptide with β-sheet-rich structure was developed that reversibly self-assembles into a

hydrogel under physiological conditions [120] In response to reduced pH, the hydrogel disassembles due to electrostatic repulsions between ornithine residues. This self-assembling system shows reversibility in response to changing high and low glucose concentrations in vitro and provides up to 8 days of glycemic control when subcutaneously administered to diabetic rats [120] Another report of biomimicry involves the coating of GOx, catalase, and insulin-encapsulated modified-dextran nanoparticles with RBC-derived lipid bilayers.[121] The RBC-derived membranes contain glucose transporters to facilitate the internalization of glucose and are shown to enhance the circulation time and efficacy of the nanoparticles upon intravenous administration in diabetic mice [121] Thus, a diverse array of delivery routes in addition to materials and formulations have been reported for glucose-responsive release of insulin triggered by the enzymatic conversion of glucose to gluconic acid.

1 4.2 Generation of hydrogen peroxide

The generation of H_2O_2 may provide a fast-acting stimulus for glucose-responsive insulin delivery Several formulations—including gated MSNs,[122] polymeric vesicles,[123] core-shell hydrogels,[124] and even red blood cells[125]—have shown glucose-mediated insulin release from H_2O_2-sensitive materials (Table 1 3) In addition to their ability to bind diols, phenylboronic acids are readily oxidized in the presence of H_2O_2 to form free boronic acid This property has been exploited to create H_2O_2-sensitive MSNs through surface modification with pendant PBAs.[122] The PBA modifications enable host-guest interactions with α-cyclodextrin that sterically shield the pores When the PBA is cleaved through H_2O_2-mediated hydrolysis, the host-guest interactions are disrupted, and the pores are openedd to release the preloaded insulin [122] In another report, amphiphilic block copolymers were synthesized from PEG and PBA-modified poly(serine) [123] Similar to the

hydrophobicity switch of PBA-based micelles, the H_2O_2-mediated degradation of the PBA moieties causes the polymers to become water soluble and the vesicles to dissociate [123]

These glucose-responsive MSNs and vesicles have been integrated into microneedle patches for transdermal insulin delivery in diabetic mice.[122-123] To scavenge excess H_2O_2 that does not react with the delivery materials, core-shell microneedles have also been developed with a H_2O_2-sensitive hydrogel core and a catalase-containing shell.[124] The catalase shell was reported to limit inflammation compared to a similar gel without the scavenging enzyme [124]

In a different approach, RBCs were used as a H_2O_2-responsive drug delivery vehicle [125] RBCs were isolated from rats and loaded with insulin using a hypotonic dialysis method prior to membrane conjugation with biotinylated GOx. The glucose-dependence of this system stems from the enzymatic generation of H_2O_2 near the surface of the RBCs in response to elevated glucose concentrations As a result, the RBC membranes are reported to rupture, forming pores in the lipid bilayers through which insulin can escape. In vitro release occurred within minutes upon exposure to elevated glucose levels, and the modified RBCs were able to maintain normoglycemia in diabetic rats for up to 9 days.[125]

1 4.3 Hypoxic conditions

The consumption of oxygen by the enzymatic conversion of glucose has also been used as a trigger for glucose-responsive delivery by encapsulating GOx and insulin in hypoxia-sensitive biomaterials For example, hyaluronic acid has been conjugated with reduction-sensitive 2-nitroimidazole [126] Vesicles were then be self-assembled from the modified hyaluronic acid with a hydrophobic core and hydrophilic shell Under hypoxic conditions, hydrophobic 2-nitroimidazole is converted to hydrophilic 2-aminoimazole [126]

The conversion from amphiphilic to hydrophilic results in the dissociation of the vesicles and release of insulin To eliminate the H_2O_2 byproduct, dual-responsive vesicles have been developed employing a H_2O_2-sensitive thioether linkage to attach the 2-nitroimidazole to a PEG-poly(serine) backbone [127] These vesicles can further be formulated in microneedle array patches to facilitate their delivery [126-127]

Table 1.3. Recent Glucose-Responsive Insulin Formulations Based on Glucose Oxidase

Trigger(s)	Formulation type	Primary biomaterial component(s)
Acid	Coacervates	Peptides[128]
	Films	Star poly(DMAEMA)[129-130]
	Hydrogels	Chitosan/PEG/poly(acrylamide),[131] β-cyclodextrin/PEI,[132] peptides[120, 133]
	Membranes	Bovine serum albumin/MnO_2 nanoparticles/PNIPAM-MAA,[117, 134-135] PVDF/poly(acrylic acid)[136]
	Metal-organic frameworks	Zeolitic imidazolate framework-8[137-138]
	Micelles	PEG-b-PDPA[139]
	Microgels	poly(AM-*co*-APMA),[140] PNIPAM[141]
	Microgels and nanoparticles	Chitosan,[119, 142] hyaluronic acid/dextran[143]
	Microparticles	Mesoporous silica microparticles[144]
	Nanonetwork	Dextran/alginate/chitosan[118]
	Nanoparticles	β-cyclodextrin/MSNs[145-146], dextran,[147] dextran/erythrocyte vesicles,[121] oleic acid- β-cyclodextrin,[148] silica vesicles/PEI[149]
	Polymersomes	PEG/polyserine[150]
Hydrogen peroxide	Films	poly(amidoamine)[151]
	Hydrogels	Multi-arm PEG,[152] poly(MPC)[153]
	Micelles	PEG/poly(DMAEMA)[154]
	Microgels	Alginate/MSNs[155]
	Microneedles: hydrogels	PVA[124]
	Microneedles: nanoparticles	α-cyclodextrin/MSNs[122]
	Microneedles: vesicles	PEG,[156] PEG/polyserine[123]
	Microparticles	poly(allylamine)[157]
	Nanogels	PEG[158]
	Red blood cells	GOx-modified erythrocytes[125]
	Vesicles	Pillar[5]arene[159]
Hypoxia	Microneedles: vesicles	Hyaluronic acid,[126] PEG/polyserine[127]

PEG-b-PDPA: poly(ethylene glycol)-*block*-poly(2-diisopropylaminoethyl methacrylate)
PEI: polyethyleneimine
PNIPAM-MAA: poly(N-isopropyl acrylamide-*co*-methacrylic acid)
poly(AM-co-APMA): poly(acrylamide-*co*-*N*-(3-aminopropyl)methacrylamide)
poly(MPC): poly(2-methacryloyloxyethyl phosphorylcholine)
PVDF: poly(vinylidene fluoride)

1.5 Summary and Perspective

The most common sensors used in glucose-responsive insulin delivery include glucose-binding proteins, phenylboronic acid-functionalized polymers, and glucose oxidase (Table 1.4). While delivering exogenous lectins may present immunogenicity, the targeting of endogenous glucose-binding proteins reduces potential toxicity associated with the delivery vehicle However, this approach may suffer in terms of specificity and sensitivity PBA-functionalized polymers are perhaps the most stable delivery vehicle but the least specific to glucose and are often not sensitive to small changes in blood glucose concentration. GOx is the most specific sensor and can be sensitive to physiologically relevant changes in blood glucose levels However, its potential immunogenicity and toxicity present barriers for its translation into the clinic Further engineering of this enzyme may potentially reduce these challenges in the future Moreover, novel glucose sensors may be developed to surmount the issues associated with each of these sensors

Here, we focus on delivery systems involving GOx due to its high specificity and sensitivity to glucose We use the chemical engineering concepts of kinetics, transport, and thermodynamics to overcome some of the challenges associated with glucose-responsive insulin delivery and provide a basis for future work in the field.

Table 1.4 Comparison of Glucose Sensing Molecules for Glucose-Responsive Insulin Delivery

	Glucose-binding proteins	**Phenylboronic acid-functionalized polymers**	**Glucose oxidase**
Specificity	Typically glucose and mannose	1,2-cis-diols	Glucose
Sensitivity	Medium	Low	High
Immunogenicity	Potentially immunogenic if delivered exogenously	Dependent on polymer backbone	Potentially immunogenic
Toxicity	Typically low	Dependent on polymer backbone	Potential toxicity from H_2O_2 byproduct
Stability	Medium	High	Medium

1.6 Thesis Overview

This Thesis is divided into 4 additional chapters In Chapter 2, we describe a nanoparticle-based glucose-responsive insulin delivery system comprised of modified dextran, glucose oxidase, and catalase In Chapter 3, we discuss the potential of this nanoparticle system to be encapsulated in porous microgels to allow for extended glucose-responsive insulin delivery. In Chapter 4, we describe an alternative method to achieve glucose-responsive insulin release based on the electrostatic complexation of insulin to a polycation. Finally, in Chapter 5, we conclude the Thesis and offer perspectives on future directions

Chapter 2: Glucose-Responsive Nanoparticles for Rapid and Extended Self-Regulated Insulin Delivery

The work presented in this chapter is published in

L R Volpatti, M A Matranga, A B Cortinas, D Delcassian, K B Daniel, R Langer, D G Anderson, Glucose-Responsive Nanoparticles for Rapid and Extended Self-Regulated Insulin Delivery *ACS Nano* 2019, https //doi org/10 1021/acsnano 9b06395

2.1 Introduction

The kinetics of insulin release remains a major hurdle in glucose-responsive insulin delivery. To develop a system that responds on a therapeutically relevant timescale and can afford sustained glucose-responsive insulin delivery in vivo, we co-formulate rapid-release and prolonged-release acetalated dextran nanoparticles (Ac-dex NPs) encapsulating GOx, catalase, and insulin. When the surrounding glucose concentration is high, glucose diffuses into the NPs and is converted to gluconolactone by encapsulated GOx. Gluconolactone is then rapidly hydrolyzed to gluconic acid which reduces the pH of the microenvironment of the NPs. The acetal groups of the modified dextran are subsequently cleaved, solubilizing the NPs and releasing the encapsulated insulin on-demand (Figure 2.1). Thus, locally regulating the pH near the NPs allows for the controlled release of insulin.

We found that a combination of two types of materials is required to achieve the desired kinetics of both rapid-onset and extended release of insulin. Analyses in both healthy and diabetic mouse models show direct evidence of glucose-responsiveness in vivo, rapid glycemic control, and prolonged normoglycemia for 16 hours with a single subcutaneous injection in a diabetic mouse model.

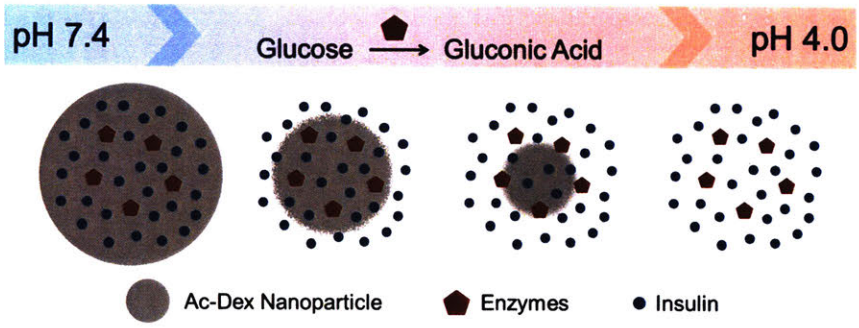

Figure 2.1. Schematic of glucose-responsive insulin release from acid-degradable nanoparticles.

2.2 Preparation and Characterization of Ac-dex Nanoparticles

Ac-dex is a pH-responsive polymer synthesized by reacting dextran with methoxypropene (Figure 2.2).[160-161] Acyclic acetal modifications are formed first which then react with neighboring hydroxyl groups to form the more stable cyclic modifications. The acetal groups are cleaved in the presence of acid to reform the native, soluble polysaccharide.

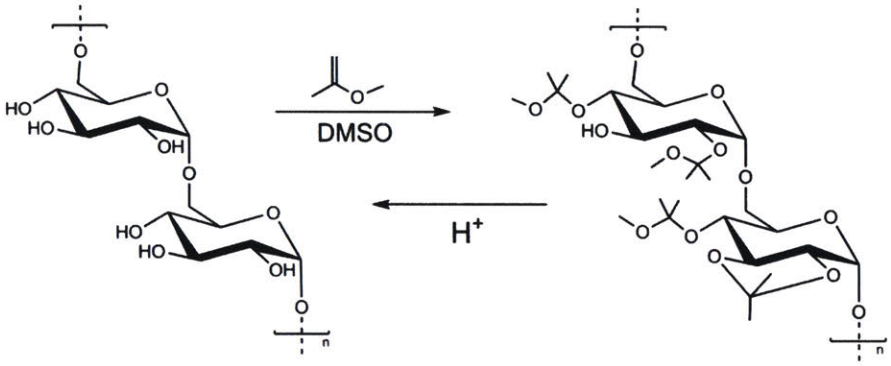

Figure 2.2. Acetalated-dextran (Ac-dex) synthesis.

Following acetal cleavage, the resultant degradation products are analyzed by ^{1}H NMR to determine the amount of each type of modification (Figure A.2-1). Polymers with high acyclic acetal content degrade quickly while those with high cyclic acetal content have longer half-lives. A combination of nanoparticles made from these polymers can therefore provide both rapid and prolonged release kinetics (Figure 2.3).

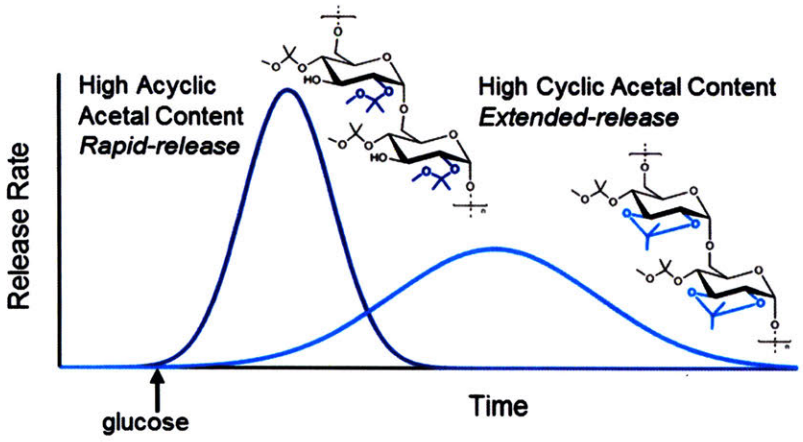

Figure 2.3. Schematic of release kinetics from rapid-release (high acyclic acetal content) and extended-release (high cyclic acetal content) Ac-dex nanoparticles.

In order to develop a system with desired release kinetics, we synthesized several derivatized dextran polymers with varying degrees of modification. For reaction times between 10 and 60 min, the fraction of acyclic modifications decreases as more cyclic modifications are formed. The percentage of residues containing a single cyclic modification increases from 55% (C55) after 10 min of reaction to 83% (C83) after 60 min while the percentage of acyclic modifications decreases from 94% to 83% (Figure 2.4a).

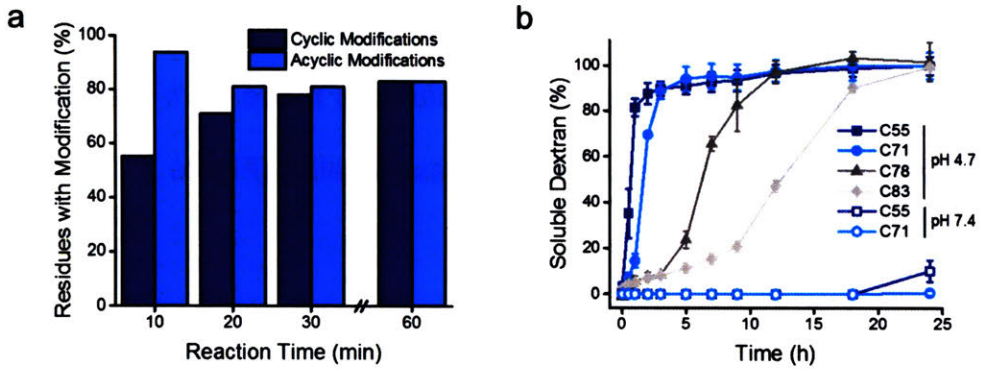

Figure 2.4. Degradation rate can by tuned according to percentage of polymer modifications. a) Percentage of total residues of the dextran polymer containing a cyclic or acyclic modification for various reaction times determined by 1H NMR of the degradation products. b) Rate of degradation of Ac-dex nanoparticles by percent cyclic modification as determined by concentration of soluble dextran in the supernatant. Nanoparticles were incubated in either acetate buffer (pH 4.7) or PBS (pH 7.4) at 37 °C with agitation.

To probe the kinetics of acetal cleavage, nanoparticles (NPs) were synthesized from a range of polymers using a sonication, solvent evaporation method. The NPs were then incubated in either acetate buffer (pH 4.7) or phosphate buffered saline (PBS, pH 7.4) at 37 °C with agitation, and the amount of soluble dextran in the supernatant was measured over time to represent polymer degradation. NPs synthesized from the least modified polymer (C55NPs) were > 80% degraded within the first hour, while those from polymers with increasing percentage of modifications were more stable in acidic solution (Figure 2.4b). Notably, NPs from the two least modified polymers showed minimal degradation upon incubation at pH 7.4 for 24 hours (Figure 2.4b).

To better understand the process of degradation, C55NPs were exposed to acidic solution, and their size was monitored by dynamic light scattering (DLS) over time (Figure 2.5a). The NPs reduced in size over the first hour reaching 67% of their original diameter before becoming undetectable by DLS (Figure 2.5b), suggesting that they degrade at least partially by surface erosion.

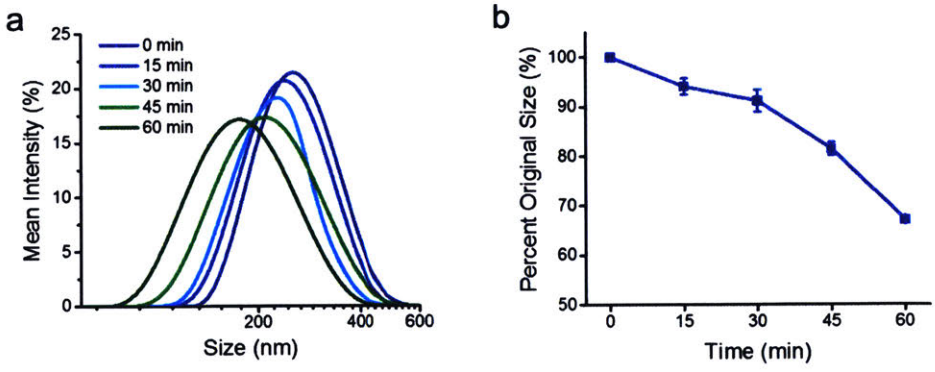

Figure 2.5. The diameter of nanoparticles decreases as they degrade in acidic conditions. a) Dynamic light scattering for C55NPs over time upon incubation in acetate buffer (pH 4.7) at 37 °C. b) Average relative diameter of NPs showing reduction in size over time.

The size of the NPs was further characterized by DLS and cryo-transmission electron microscopy (TEM). The average mean diameter of Ac-dex NPs was 252 ± 25 nm, and their sizes were consistent across varying polymer modifications (Figure 2.6a). NPs encapsulating insulin, GOx, and catalase were then synthesized using a double emulsion, solvent evaporation method. DLS measurements of protein-encapsulated NPs similarly show a consistent diameter across polymer modification with a slightly larger average of 274 ± 22 nm (Figure 2.6b). Cryo-TEM micrographs show spherical NPs with diameters that corroborate DLS measurements (Figure 2.6c,d). In both DLS and cryo-TEM measurements, the C71NPs are slightly smaller than the C55NPs. Nonetheless, the diameters remain fairly consistent across different formulations, allowing us to isolate the variable of polymer modification and determine its effect on degradation and release.

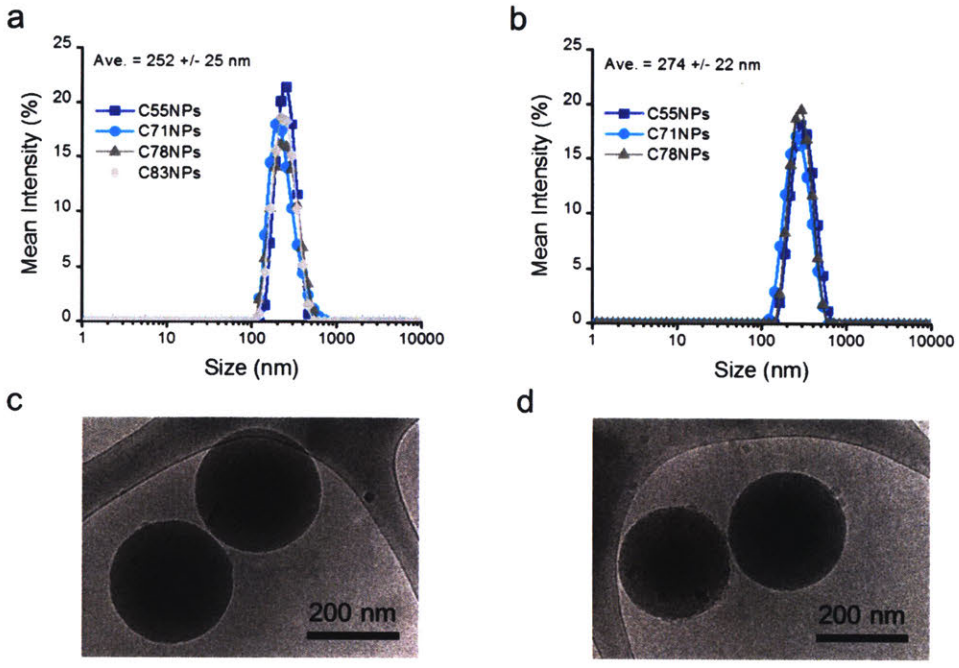

Figure 2.6. Nanoparticle size is consistent across formulations. a) Dynamic light scattering of Ac-dex NPs made from polymers with various degrees of modification. b) Dynamic light scattering of protein-encapsulated NPs made from polymers with various degrees of modification. c) Cryo-transmission electron micrograph of protein-encapsulated C55NPs. d) Cryo-transmission electron micrograph of protein-encapsulated C71NPs.

The insulin loading of C55NPs is 8.3% by mass, nearly double the amount in C71NPs and over 6 times that in C78NPs, which suggests that the insulin loading capacity decreases exponentially with acetalation reaction time (Figure 2.7a). The C55NPs contain ~ 1 U GOx / mg NP, and the loading of GOx similarly decreases with percent modification (Figure 2.7b). The increased hydrophobicity of highly modified dextran may limit the amount of total protein loading. Thus, by varying the percent modification of the dextran, we can systematically alter the material properties to tune both the release profile and the protein loading efficiency.

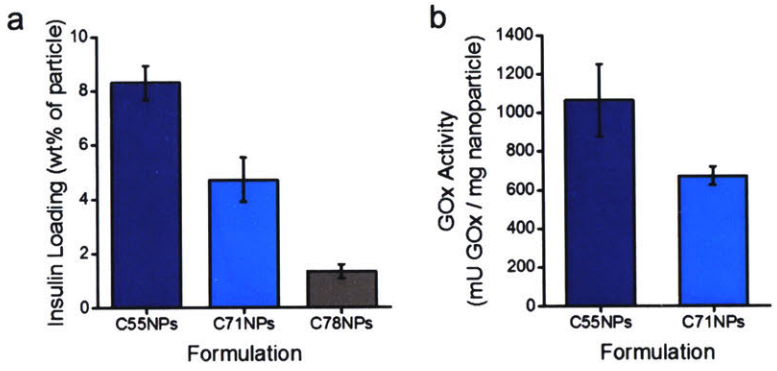

Figure 2.7. Protein loading decreases with increasing polymer modifications. Loading efficiency of (a) insulin and (b) glucose oxidase in nanoparticles synthesized from Ac-dex with varying extent of modification.

2.3 Insulin Release Kinetics from NPs

To determine the kinetics of insulin release, protein-encapsulated NPs were incubated in either acetate buffer or PBS (20 mg/mL). The resultant release profiles closely follow the degradation profiles for both the C55NPs and C71NPs (Figure 2.8a).

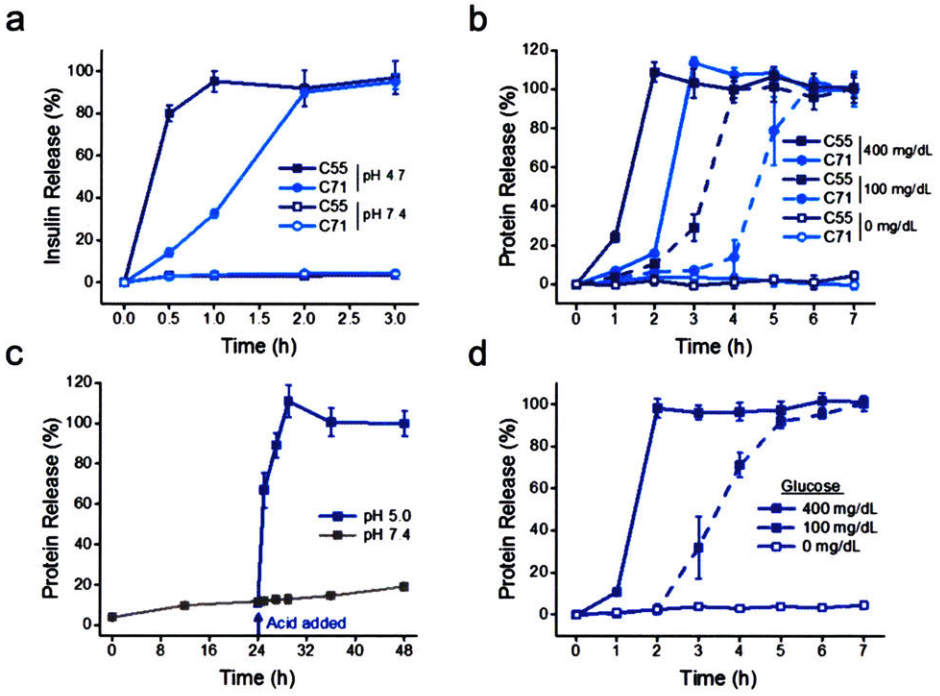

Figure 2.8. A co-formulation of 55% and 71% (% cyclic acetalation) Ac-dex NPs have fast-acting and long-acting insulin release characteristics. a) Insulin release from C55NPs or C71NPs incubated in either acetate buffer (pH 4.7) or phosphate buffered saline (PBS, pH 7.4) at 37 °C with agitation. b) Glucose-mediated protein release from C55NPs or C71NPs (20 mg/mL) upon incubation in PBS, PBS + 100 mg/dL glucose, or PBS + 400 mg/dL glucose at 37 °C with agitation. c) Two regimes of protein release resulting from the addition of acid (HCl) to a mixture of C55NPs and C71NPs after 24 hours of incubation. d) Glucose-mediated protein release from a mixture of C55NPs and C71NPs (20 mg/mL).

The release kinetics were then studied in response to elevated (400 mg/dL) or physiological (100 mg/dL) glucose concentrations. The C55NPs show a rapid response to elevated glucose levels with virtually all insulin released after 2 hours; however, they are completely degraded under physiological glucose concentrations after 4 hours of incubation (Figure 2.8b). The C71NPs, on the other hand, have a delayed onset of release (after 2 hours) with a prolonged release of insulin under lower glucose conditions (up to

6 hours, Figure 2.8b). Based on these results, we hypothesized that a mixture of NPs could provide fast- and long-acting delivery options.

A co-formulation containing equal parts by mass of C55NPs (rapid-release) and C71NPs (extended-release) shows two regimes of release in response to an acidic environment (Figure 2.8c). The same formulation affords a rapid onset of release in elevated glucose conditions with more prolonged release under physiological concentrations of glucose (Figure 2.8d). The pH profiles are similar for the C55NPs alone, the C71NPs alone, or a mixture of the two (Figure 2.9). In high glucose conditions, a period of ~ 2 h is required to overcome the buffering effects of the solution and decrease the pH below 5 accounting for the delayed onset of insulin release. In low glucose conditions, the pH reaches 5 after ~ 4 h. Therefore, the differences in release kinetics may be attributed to the prolonged degradation of the more highly modified polymeric nanoparticles.

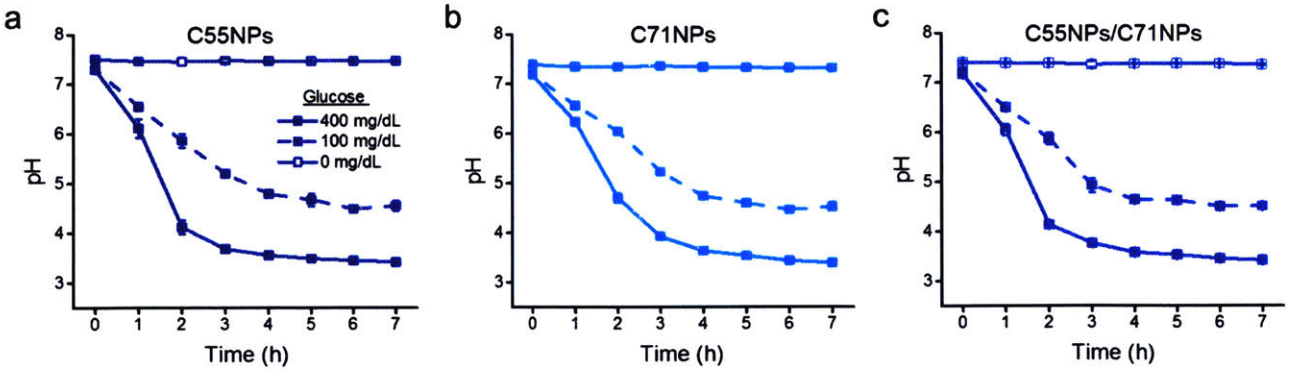

Figure 2.9. pH curves are similar for different formulations. Effect of glucose concentration on pH over time for (a) C55NPs, (b) C71NPs, or (c) a mixture of C55NPs and C71NPs incubated in phosphate buffered saline (pH 7.4) at 37 °C with agitation.

At a lower concentration of NPs (10 mg/mL), there is a greater distinction in the onset of insulin release across a range of glucose concentrations (Figure 2.10a).

Furthermore, insulin is released in < 1 h when NPs are first preincubated in physiological glucose conditions before being exposed to elevated glucose (Figure 2.10b).

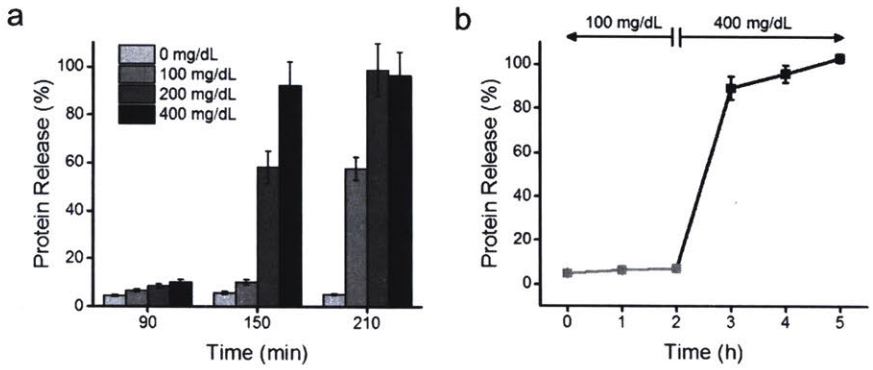

Figure 2.10. Protein release kinetics are altered by lowering concentration of NPs. Total protein release (a) for a range of glucose concentrations and (b) upon increasing the concentration of glucose after a 2 hour incubation (b) for a mixture of C55NPs and C71NPs at a concentration of 10 mg NP/mL.

2.4 Activity and Biocompatibility

After analyzing the release kinetics in response to varying glucose concentrations, we then confirmed that the released insulin retains its structure and function. Insulin-encapsulated C55NPs were incubated at 37 °C with agitation in buffer containing trypsin (0.025%) for 24 h. Circular dichroism (CD) spectra of the released insulin shows excellent agreement with that of fresh insulin (Figure 2.11a), confirming its protection from proteolytic degradation and retention of its characteristic alpha helix structure. To show that insulin remains bioactive after formulation and release, a cell-based assay was performed to quantify the amount of AKT phosphorylation caused by the activation of the insulin receptor (see methods). The resultant dose-response curves (Figure A.2-2) were used to calculate the EC_{50} of the sample. No significant differences in activity are observed between fresh insulin and insulin that has been incubated in NPs up to 24 h (Figure 2.11b). These results suggest that insulin is unaltered during NP processing, incubation, and release. Furthermore, NP components show minimal toxicity to these cells at the concentrations tested.

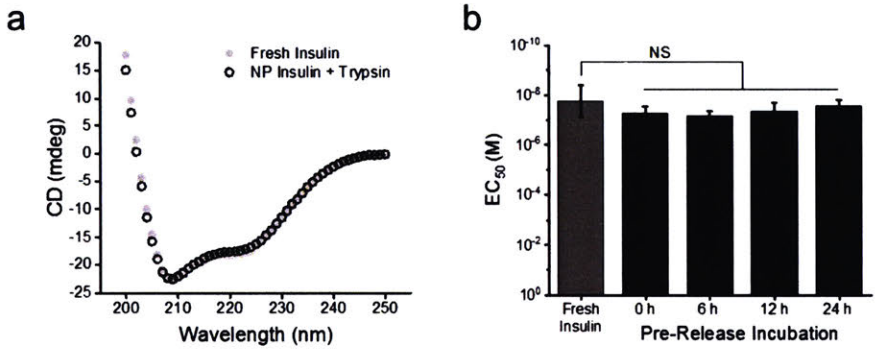

Figure 2.11. Insulin structure and function are retained after formulation and release. a) Circular dichroism of released insulin after incubating NPs with 0.025% trypsin-EDTA for 24 hours compared to unprocessed fresh insulin confirming retention of secondary structure. b) EC_{50} determined by AKT phosphorylation of C2C12 cells exposed to fresh insulin or insulin released from nanoparticles after various incubation times. Statistical significance is indicated by NS: $p > 0.05$.

To further probe cytotoxicity of intact NPs, we performed a hemolysis assay for blood compatibility (Figure 2.12). Hemolysis of erythrocytes is < 1% for relevant doses of NPs when compared to PBS (negative control) and 1% Triton X-100 (positive control), providing further evidence of their biocompatibility.

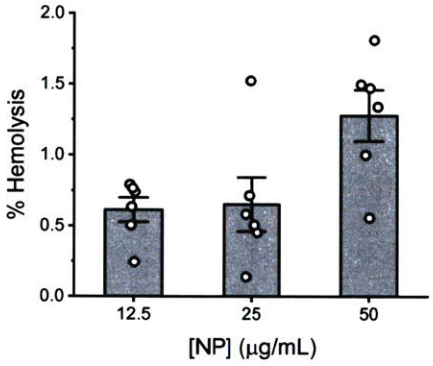

Figure 2.12. Hemolysis of erythrocytes is < 1.5% for NP concentrations up to 50 μg/mL. Blood compatibility of nanoparticles determined by the percent hemolysis upon incubation with nanoparticles at 37 °C for 1 h. Data represent mean ± standard error of the mean (N = 6).

Before determining the efficacy of the NPs in vivo, we tested whether they remain at the site of injection after subcutaneous (s.c.) administration in a mouse model. To study particle migration, we formulated Ac-dex NPs without proteins encapsulating a fluorescently labeled dextran (AF680). We then s.c. injected these NPs into immunocompetent, hairless, albino SKH1E mice and quantified their fluorescence over time using an in vivo imaging system (IVIS; Figure 2.13a). Since these NPs do not contain the glucose-sensing enzyme, they are not expected to rapidly degrade and release their cargo, and the decrease in fluorescence can largely be attributed to particle migration. On Day 3, the total fluorescence is on average 76.5% that of Day 1, suggesting limited particle migration away from the site of injection during the time of therapeutic effect (Figure 2.13b).

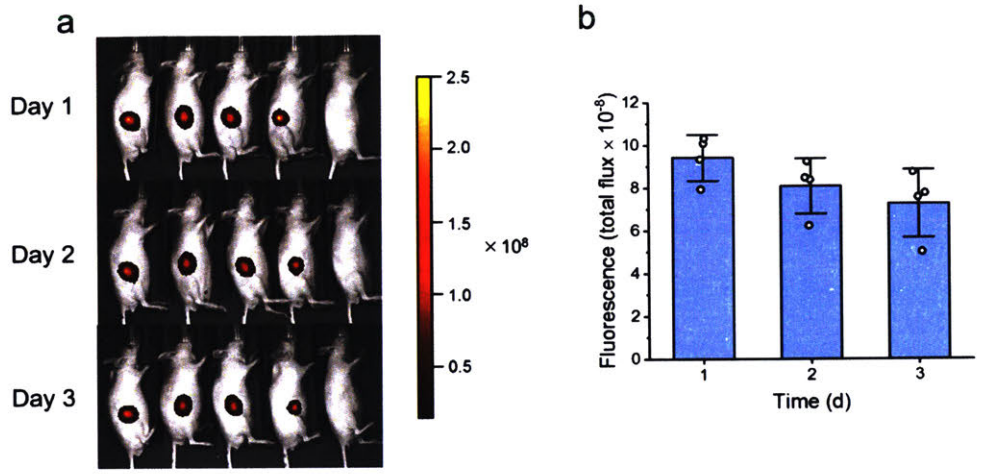

Figure 2.13. NPs experience limited migration away from the injection site over therapeutically relevant timescales. a) In vivo fluorescent images of Ac-dex NPs (– Enzymes, – Insulin) containing AF680-dextran (10 kDa) subcutaneously injected in mice at a total nanoparticle dose of 8 mg/kg. b) Quantification of total flux of fluorescence in (a). Data is normalized to background fluorescence of control mouse and represents mean ± standard deviation; N = 4.

To determine if the persistence of NPs causes an inflammatory response with long-term effects, 5 mm sections of mouse skin were biopsied 1, 7, and 28 days following injection of empty NPs or a saline control and processed for histological analysis (Figure 2.14). The presence of neutrophils in the resulting H&E stained histological images indicated that 4/5 mice exhibited an inflammatory response 1 day after NP injection. After 1 week 2/5 mice had few macrophages present, and after 1 month there were no signs of inflammation in any of the 5 mice. These results are consistent with previous reports of in vivo biocompatibility of Ac-dex[162] and suggest that Ac-dex NPs do not cause a severe or prolonged inflammatory response when s.c. injected in mice.

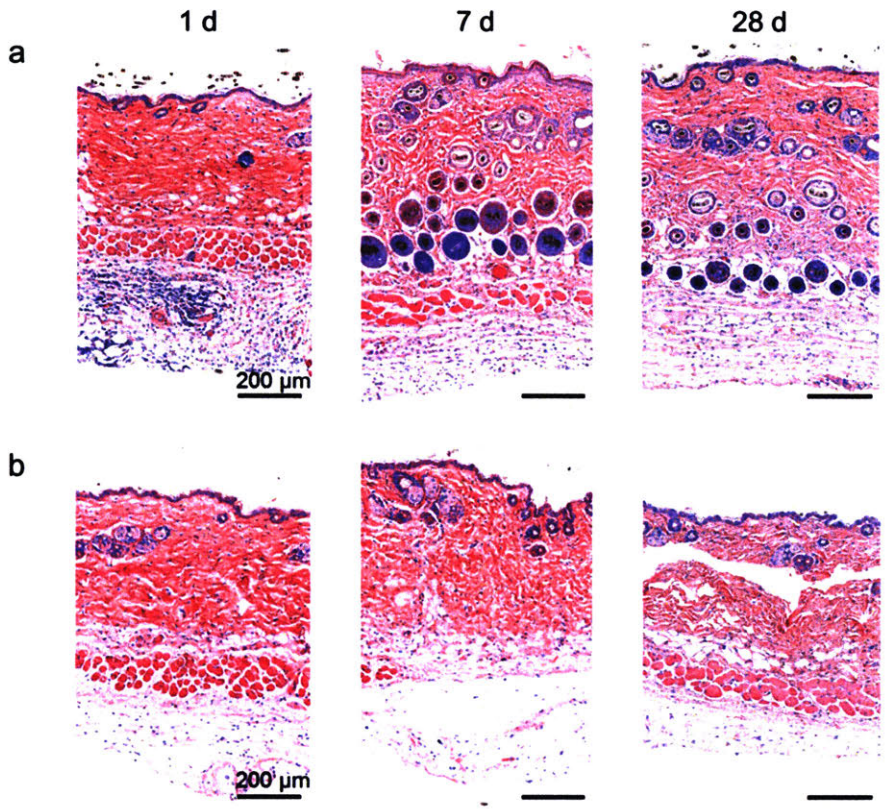

Figure 2.14. Skin biopsies show no signs of inflammation 4 weeks after injection of Ac-dex nanoparticles. Histological images (H&E staining) of mouse skin surrounding the injection of a) Ac-dex NPs (– Enzymes, – Insulin) or b) PBS. Representative images of 5 biological replicates.

2.5 In Vivo Glycemic Control

To evaluate the ability of the nanoparticles to provide glucose-responsive glycemic control in vivo, we employed both streptozotocin (STZ)-induced type 1 diabetic mouse and healthy mouse models. Fasted diabetic mice were subcutaneously injected with a dose of 3 IU/kg naked insulin, a co-formulation of C55NPs and C71NPs at an insulin dose of 14.4 IU/kg (0.5 mg/kg), or a co-formulation of empty NPs, and their blood glucose (BG) levels were monitored over time (Figure 2.15a).

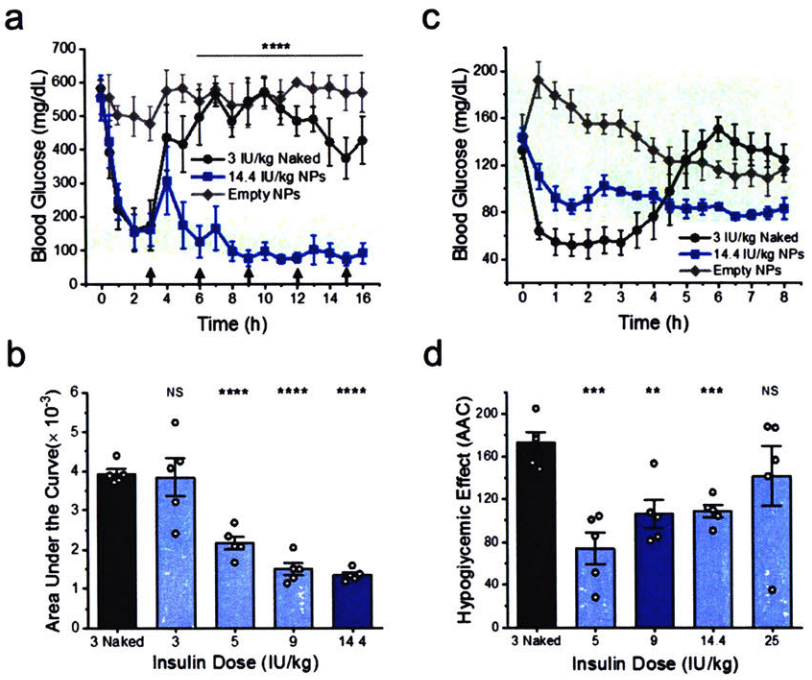

Figure 2.15. Doses between 5 and 14 IU/kg insulin in co-formulated Ac-dex NPs achieve effective glycemic control in diabetic mice with limited risk of hypoglycemia in healthy mice. a) Blood glucose levels of streptozotocin-induced type 1 diabetic mice following administration of empty NPs, 3 IU/kg naked insulin, or 14.4 IU/kg insulin in Ac-dex NPs. Arrows represent intraperitoneal glucose tolerance tests (GTTs, 1.5 g/kg) every 3 h. b) Area under the curve for the first 9 hours of (a) in addition to doses of 3, 5, and 9 IU/kg NPs. c) Blood glucose levels of healthy mice following administration of empty NPs, 3 IU/kg naked insulin, or 14.4 IU/kg insulin in Ac-dex NPs. d) The hypoglycemic effect calculated as the area above the curve of (c) for the first 2.5 h in addition to doses of 5, 9, and 25 IU/kg NPs. Data represent mean ± standard deviation (a,c) or standard error of the mean (b,d). Statistical significance is indicated by $^{**}p < 0.01$, $^{***}p < 0.001$, $^{****}p < 0.0001$.

The BGs of the 14.4 IU/kg NPs group were reduced at virtually the same rate as those in the naked insulin group, indicating a rapid onset of insulin release in elevated glucose conditions in vivo. To test if this initial reduction in BG levels was due to nonspecific burst release, NPs were incubated for an hour in vitro and transferred to fresh buffer prior to injection (Figure A.2-3a). The resultant BG profile and area under the curve (AUC) of the pre-incubated NPs was similar to that of directly injected NPs (Figure A.2-3b), suggesting that this initial rapid release is specific to the in vivo environment.

Diabetic mice were administered an intraperitoneal glucose tolerance test (GTT, 1.5 g/kg) after 3 h to test the efficacy of the NPs in responding to a glucose challenge (Figure 2.15a). The mice receiving 3 IU/kg naked insulin returned to their initial hyperglycemic state directly following the GTT. In contrast, the NP group successfully regained glycemic control after an initial spike in BG levels and maintained BGs in the normoglycemic range (70 – 200 mg/dL) following 4 additional GTTs, thus providing 16 h of glycemic control with a single dose. The mice returned hyperglycemic 2 d post-injection, indicating the potential of NPs as a once-daily treatment (Figure A.2-4). The AUCs following 9 h and 2 GTTs show that NP doses of 5, 9, or 14.4 IU/kg insulin provide significantly enhanced glycemic control compared to 3 IU/kg naked insulin (Figure 2.15b, A.2-5).

NPs were next s.c. administered to healthy mice to determine their in vivo response to normoglycemic conditions (Figure 2.15c). While mice receiving 3 IU/kg naked insulin experienced hypoglycemia, defined as having an average blood sugar concentration less than 70 mg/dL, the NP group, receiving almost 5 times the dose of insulin, remained in the normoglycemic range. The area above the curve (AAC) and

below the initial BG value for the first 2.5 h is used to quantify the hypoglycemic effect. With this metric, NP doses of 5, 9, or 14.4 IU/kg insulin provide significantly reduced risk of a hypoglycemic event compared to 3 IU/kg naked insulin (Figure 2.15d, A.2-6). Thus, doses between 5 and 14.4 IU/kg NPs enhance glycemic control in diabetic mice and reduce the hypoglycemic effect in healthy mice compared to a single dose of 3 IU/kg naked insulin.

Since healthy mice have lower fasting BG levels than diabetic mice, they may initially experience hypoglycemia more rapidly. However, they may also respond to the insulin more rapidly by secreting counterregulatory hormones such as glucagon. Therefore, we also examined the potential for hypoglycemia in a diabetic mouse model. Mice receiving 9 IU/kg NPs were divided into 3 groups and administered i) a 1.5 g/kg GTT at 3 h and a 2 g/kg GTT at 6 h, ii) a 2 g/kg GTT at 6 h alone, or iii) no GTTs over the 8 h study (Figure 2.16a). Different GTT doses were given to represent variability in glucose intake throughout the day. AUCs for groups (ii) and (iii) were not significantly different than that of group (i) (Figure 2.16b), and the average BGs of each group remained above 70 mg/dL for the duration of the study. These results indicate that a dose of 9 IU/kg NPs is able to attain tight glycemic control despite small differences in glucose intake and poses limited risk of hypoglycemia under these conditions in diabetic mice.

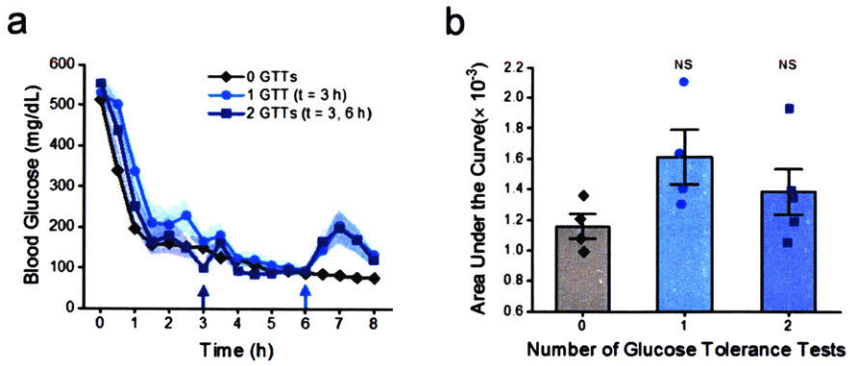

Figure 2.16. NPs provide similar blood glucose profiles with 0, 1, or 2 glucose tolerance tests. a) Blood glucose levels of diabetic mice following administration of 9 IU/kg NPs with 0, 1 (1.5 g/kg at 3 h), or 2 GTTs (1.5 g/kg at 3 h, 2 g/kg at 6 h). b) Area under the curve for (a). Shaded regions and error bars represent standard error of the mean. Statistical significance is indicated by NS: $p > 0.05$ in comparison to 0 GTT.

To distinguish between glucose-responsive and non-responsive insulin release, fasted diabetic mice were administered nanoparticles containing enzymes and insulin (NPs), nanoparticles without enzymes (NPs (– Enzymes)), or nanoparticles without insulin (NPs (– Insulin)). While the in vitro data suggest NPs will be glucose-responsive in vivo, NPs(– Enzymes) are expected to slowly release insulin over time, representing basal insulin delivery. Following a 3 g/kg GTT 2 h post-injection, the average BG of all groups rises above 400 mg/dL within 30 min. After 30 min at this elevated BG level, the NP group reduces the BGs over the next 2 h and is the only group with an average BG in the normoglycemic range at the end of the 5 h study (Figure 2.17a).

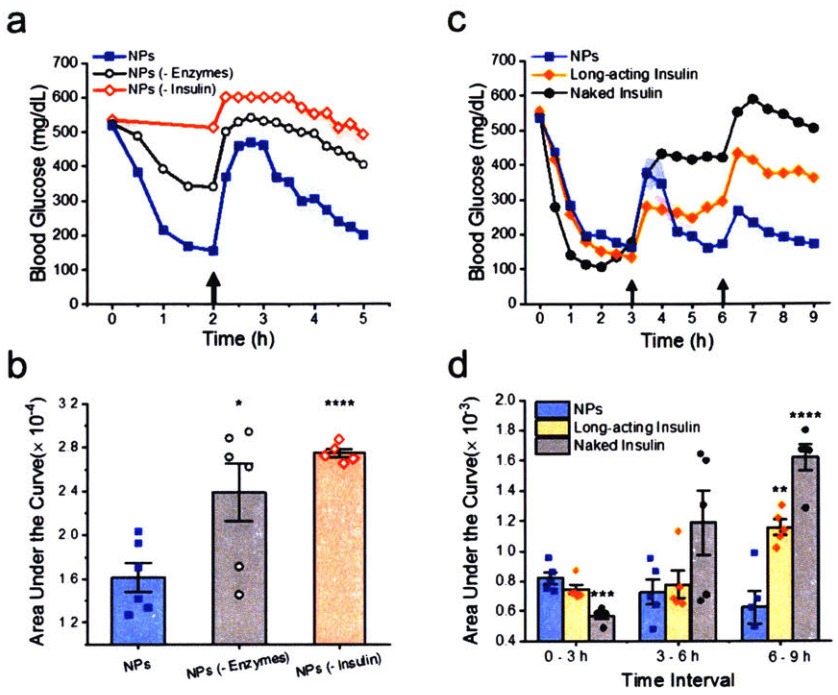

Figure 2.17. Glucose-responsive NPs enhance glycemic control relative to constituent components and free long-acting or native insulin. a) Response of diabetic mice to a GTT (3 g/kg) following injection of 9 IU/kg NPs, 9 IU/kg NPs(– Enzymes), or an equivalent dose of NPs(– Insulin). b) Area under the curve for (a). c) Blood glucose levels of diabetic mice following administration of 5 IU/kg NPs, long-acting insulin, or naked insulin with GTTs at 3 h and 6 h (1.5 g/kg). d) Area under the curve for (c) by 3 h time interval. Shaded regions and error bars represent standard error of the mean. Statistical significance is indicated by *$p < 0.05$, **$p < 0.01$, ***$p < 0.001$, ****$p \leq 0.0001$ in comparison to NPs (blue bar).

These kinetics are slightly delayed compared to the rapid initial BG reduction which may have resulted from a larger release of insulin upon initial exposure to high glucose concentrations. Nevertheless, the NPs begin to reduce the BG levels 1 h after bolus glucose administration and are ultimately able to regain glycemic control. These results suggest that all components of the nanoparticle are necessary to produce consistent glycemic control with significantly reduced AUCs (Figure 2.17b).

To further probe the difference between basal and glucose-responsive insulin, we next evaluated the BG levels of diabetic mice in response to equivalent doses (5 IU/kg) of NPs, a long-acting acylated analog of insulin (commercially known as insulin

detemir),[163-164] and naked insulin (Figure 2.17c). Compared to NPs, naked insulin initially reduces BGs more rapidly at this dose, as shown by a significantly decreased AUC for the first 3 h following administration (Figure 2.17d). However, the NP group is the only group with average BGs < 200 mg/dL following either of the 1.5 g/kg GTTs at 3 h and 6 h (Figure 2.17c). Moreover, for the time interval between 6 – 9 h, the long-acting insulin and naked insulin groups both have significantly higher AUCs than the NP group (Figure 2.17d). Therefore, for the same dose of insulin (5 IU/kg), glucose-responsive NPs provide better extended glycemic control compared to long-acting basal or naked insulin treatments.

2.6 Glucose-Responsive Insulin Release in Vivo

To provide direct evidence of the translation of glucose-responsive delivery in vivo, we conducted time course measurements of serum human insulin concentrations in healthy and diabetic mice. Healthy mice receiving NPs (– Enzymes) or NPs experienced similar low levels of serum insulin (< 20 μIU/mL) after 1 h (Figure 2.18a). This result corroborates our findings that the NPs do not experience a large glucose-independent burst release of insulin.

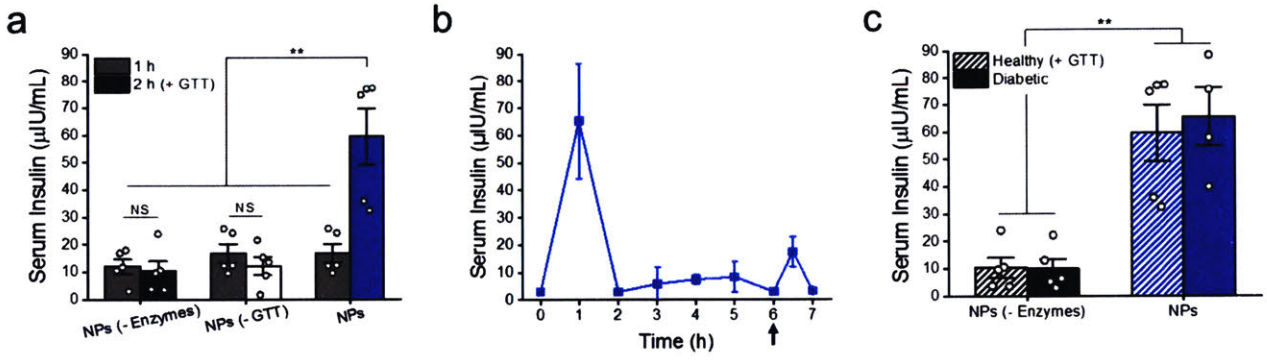

Figure 2.18. Co-formulated Ac-dex NPs show glucose-responsive insulin release in vivo. a) Human serum insulin levels of healthy mice 1 h after administration or 2 h after administration with a GTT after 1 h (3 g/kg). b) Human serum insulin of diabetic mice following injection of NPs with a GTT at 6 hours (2 g/kg). c) Human serum insulin of healthy mice (1 h post-GTT) or diabetic mice (1 h post-administration) receiving NPs(– Enzymes) or NPs. Data represent mean ± standard error of the mean (a,c) or standard deviation (b). Statistical significance is indicated by $^{**}p < 0.01$.

At the 1 h time point, the mice were administered a GTT (3 g/kg), and the serum insulin concentration was measured after an additional hour (2 h total). Mice injected with NPs (– Enzymes) and mice that did not receive a GTT (NPs (– GTT)) had similar serum insulin levels at the 1 and 2 h time points. Conversely, there was > 3-fold increase in the amount of serum insulin in the NPs group after the GTT. These results indicate that there is limited basal insulin release with a spike in release in response to glucose and both enzymes and elevated glucose concentrations are required for enhanced insulin release in vivo. Serum insulin of mice injected with NPs (– Insulin) were mostly below the range of

detection both before and after the GTT, confirming that mouse insulin shows minimal cross reactivity with the human insulin ELISA (ALPCO) used for analysis (Figure A.2-7).

Human insulin in diabetic mouse serum was monitored over time to quantify glucose-responsive insulin release in a diseased state. Serum insulin levels reach a maximum 1 h after injection, followed by low levels of basal serum insulin until the concentrations modestly increase immediately after a GTT at 6 h (Figure 2.18b). The relative heights of these peaks suggest that insulin release is greatest upon first exposure of the NPs to glucose, consistent with the BG reduction rates from Figure 4. Mice receiving NPs (– Enzymes) had low serum insulin concentrations for the duration of the study with no significant increase after the GTT (Figure A.2-8a). Serum insulin concentrations are comparable in diabetic mice and healthy mice following the initial exposure of the NPs to elevated glucose levels, whether after administration or a glucose injection (Figure 2.18c). In both cases, serum insulin concentrations are significantly higher in the NPs group compared to the NPs (– Enzymes) group (Figure 2.18c, A.2-8b). These results support the conclusion that both enzymes and hyperglycemia are required for enhanced insulin release in vivo.

2.7 Discussion and Conclusions

Insulin adherence of Type 2 diabetic patients is low,[165-166] with at least 35% of patients reporting dosing omission or irregularities.[167-168] Inflexibility of scheduled insulin doses as well as interference with daily activities are commonly cited as contributing factors of non-adherence to prescribed insulin regimens.[168-170] A once-daily insulin injection with some flexibility of timing and dose is expected to increase patient adherence and improve quality of life of diabetic patients [14] Furthermore, glucose-responsive insulin may have the additional therapeutic benefits of improved glycemic control by smoothing out the peaks and valleys associated with multiple self-administered doses of insulin and reduced risk of hypoglycemia corresponding to fewer visits to the emergency department [171]

In order for a glucose-responsive delivery system to be effective, the kinetics must be rapid to quickly counteract a spike in blood sugar Here, we report an example of fine tuning insulin release kinetics from polymeric NPs in response to glucose by controlling the extent of polymer modification We expect this approach to aid in the development of future glucose-responsive insulin delivery systems based on GOx Most commercial implantable continuous glucose monitoring systems employ GOx as a sensor [172-173] A limitation of using GOx and catalase in an injectable delivery system, however, is their potential toxicity and immune response from repeated administrations Therefore, to make steps toward the translation of GOx-based glucose-responsive insulin delivery, methods of physically isolating the enzymes or chemically shielding them from the immune system should be further investigated

In summary, we have developed a co-formulation of rapid-release (55% cyclic modifications) and prolonged-release (71% cyclic modifications) acetalated-dextran nanoparticles encapsulating insulin and enzymes that enhances glucose-responsive delivery Glucose-responsiveness is directly evidenced in vivo with an increase in serum insulin following a glucose challenge in both healthy and diabetic mice (Figure 2 18) A main advantage of these co-formulated NPs is their ability to reduce elevated blood glucose levels in a diabetic mouse model on a timescale comparable to that of naked insulin and provide sustained delivery to afford 16 h of glycemic control after 5 simulated meals In addition to providing enhanced glycemic control relative to free insulin when comparing the same dose of 5 IU/kg, co-formulated NPs also reduce the risk of hypoglycemia Thus, the development and characterization of these co-formulated, glucose-responsive nanoparticles marks an important step in the advancement of self-regulated insulin delivery

2.8 Materials and Methods

Materials/reagents. All chemicals were obtained from Sigma-Aldrich (St Louis, MO) and cell culture reagents from Life Technologies (Carlsbad, CA) unless otherwise noted. Recombinant human insulin (Gibco™) was purchased from ThermoFisher Scientific (Waltham, MA) AlphaLISA SureFire ULTRA kits were purchased from Perkin-Elmer (Waltham, MA) to quantify AKT phosphorylation, and an insulin ELISA kit was purchased from ALPCO (Salem, NH) to measure serum insulin

Synthesis of acetalated dextran Dextran (1 g, MW = 9 – 11 kDa) and pyridinium p-toluenesulfonate (0.0617 mmol) were added to a round-bottom flask and purged with nitrogen Anhydrous DMSO (10 mL) was subsequently added under nitrogen After complete dissolution of the dextran, 2- methoxypropene (37 mmol) was added to start the reaction The reaction was quenched with Et_3N after various predetermined reaction times (10, 20, 30, 60 min) The product was precipitated and washed with pH 8 water three times and collected by centrifugation (10 min, 8000 rcf, Avanti JXN-26, Beckman Coulter) The product (Ac-dex) then was lyophilized for two days to yield a white powder

NMR functionalization analysis. Ac-dex (5 mg/mL) was hydrolyzed in D_2O containing DCl (10 mM) for 2 h The samples were analyzed with a 500 MHz 1H NMR (Varian). Cyclic and acyclic acetal content was measured by quantifying the amount of acetone and methanol produced by the hydrolysis of Ac-dex and normalizing by the protons on the anameric carbon of the glucose ring

Nanoparticle synthesis Empty Ac-dex nanoparticles were prepared with a single-emulsion, solvent evaporation technique. Briefly, Ac-dex was dissolved in dichloromethane (DCM, 40 mg/mL) and added to a 3% poly(vinyl alcohol) (PVA) in PBS

solution This two-phase mixture was sonicated for 90 s (Q-500, QSonica, 65% amplitude) with 1 s pulse and immediately poured into a 0 3% PVA solution. After stirring for 2 h, the mixture was centrifuged (15 min, 8000 rcf, Avanti JXN-26, Beckman Coulter) and washed twice with basic water (pH 8) before lyophilization. To form protein encapsulated nanoparticles, insulin was dissolved in carbonate buffer (pH 9.5, 100 mg/mL) with or without GOx (168.1 units/mg, 15 mg/mL) and catalase (≥20,000 units/mg, 2 mg/mL) and added to DCM containing Ac-dex (40 mg/mL). The mixture was sonicated, added to a 3% PVA solution, and sonicated a second time to form a double emulsion, which was processed in the same manner as the single-emulsion nanoparticles

Acetalated-dextran degradation analysis Empty Ac-dex nanoparticles were suspended in triplicate in acetate buffer (pH 4 7) or in PBS (pH 7.4) at 5 mg/mL and incubated at 37 °C on a shaker plate. At indicated time points, aliquots were withdrawn and centrifuged The supernatants were removed and analyzed with a microplate bicinchoninic acid assay (BCA, Pierce) according to the manufacturer's protocol using a dextran standard The absorbance was measured at 562 nm with a plate reader (Infinite M200, Tecan)

Nanoparticle characterization. Nanoparticles were characterized by dynamic light scattering (DLS, Zetasizer Nano ZS, Malvern Instruments) and cryo-transmission electron microscopy (TEM, JEOL 2100F) Lyophilized nanoparticles were suspended in ultrapure water and filtered through 0 8 μm membrane filters before analysis by DLS or cryo-TEM To determine degradation kinetics, nanoparticles were suspended in acetate buffer, incubated in a 37 °C shaker, and analyzed at various time points (0, 15, 30, 45, 60 min).

Loading capacity. The loading capacities of protein were determined by degrading a known mass of nanoparticles in a solution of PBS + acetic acid (pH 2) and measuring protein content Insulin was quantified by high performance liquid chromatography (HPLC, Agilent 1100 Series) with an Atlantis® T3 column (5 µm, Waters) The activity of GOx was measured using an Amplex® Red Glucose/Glucose Oxidase Assay Kit (Life Technologies)

In vitro insulin release Nanoparticles containing insulin (5 mg/mL) or insulin and enzymes (10 mg/mL or 20 mg/mL) were suspended in triplicate in PBS alone or with the addition of 100 mg/dL or 400 mg/dL glucose and incubated at 37 °C with agitation At indicated time points, aliquots were withdrawn and centrifuged. The supernatants were removed and protein content was analyzed with a Coomassie Plus protein assay (Pierce) according to the manufacturer's protocol

Insulin structure. Secondary structural motifs were elucidated using high-performance circular dichroism (CD) Nanoparticles containing insulin (2 5 mg/mL) were incubated in a 1.10 solution of 0 25% Trypsin-EDTA·PBS at 37 °C with agitation After 24 h, the nanoparticles were washed thrice to remove the trypsin and degraded with HCl (pH 2) NaOH was used to return the pH to 7.4. This sample and fresh recombinant human insulin (200 µg/mL) were analyzed with a high-performance CD spectrometer (J-1500, JASCO Inc) using a 0.1 cm pathlength cell.

In vitro activity. The in vitro activity of released insulin was determined with a cellular AKT assay To prepare for the AKT assay, C2C12 cells (American Type Culture Collection) were cultured in Dulbecco's modified Eagle medium (DMEM) containing L-

glutamine, 4.5 g/L D-glucose, and 110 mg/L sodium pyruvate supplemented with 10% fetal bovine serum and 1% penicillin–streptomycin Cells were seeded and incubated in 96-well plates at a density of 5,000 cells per well After 24 h, the cells were washed twice with serum-free DMEM and incubated for 4 h. The media was then removed, and the cells were stimulated with insulin samples or controls for 30 min. The cells were then washed twice with cold Tris-buffered saline and lysed with cold Lysis Buffer (Perkin-Elmer) for 10 min Concentrations of pAKT 1/2/3 (Ser473) and total AKT 1 in the cell lysates were determined with AlphaLISA SureFire ULTRA kits (Perkin-Elmer) according to the manufacturer's instructions Data were analyzed using GraphPad Prism 6.0 and fit to four parameter dose-response curves to determine the EC_{50} of each insulin sample

Blood compatibility. All animal protocols were approved by the MIT Committee on Animal Care, and animals were cared for under supervision of MIT's Division of Comparative Medicine Blood was collected from healthy 8-week-old male C57BL/6 mice (Jackson Labs) in EDTA-coated centrifugation tubes. The serum fraction was separated and removed upon centrifugation (5 min, 500 rcf) and replaced with an equal volume of PBS This step was repeated twice, and the final suspension was diluted 1 50 in PBS 10 µL of sample and 190 µL diluted red blood cells were added to a 96-well plate using PBS as a negative control and 20%Triton X-100 as a positive control The plate was incubated for 1 h at 37 C and then centrifuged for 5 min at 500 rcf The absorbance of the supernatant was measured at 540 nm, and the % hemolysis was calculated by normalizing the PBS samples to 0% and the Triton X-100 samples to 100% hemolysis

In vivo imaging studies. For in vivo imaging, 8-week-old male SKH1E mice were fed an alfalfa-free diet (AIN-76A, Bio-Serv) for 1 week leading up to the study to limit

background fluorescence Mice were anesthetized using inhaled isoflurane and imaged with an IVIS Spectrum in vivo imaging system with a heated chamber containing inhaled isoflurane Nanoparticles containing dextran (10 kDa) conjugated with AlexaFluor680 were prepared and injected subcutaneously into the lateral flank of mice at a total nanoparticle dose of 8 mg/kg Images were acquired using filter sets of 640/760, medium binning, an F-stop of 1, and an exposure time of 1 s Living Image software was used to analyze the fluorescence efficiency and total flux of the images.

Histology. At 1, 7, and 28 days following administration, animals were euthanized, and skin sections surrounding the injection site were biopsied with a 5 mm biopsy punch The tissue was fixed in 10% formalin overnight at room temperature After fixation, the tissue was washed with 70% ethanol and processed for histological analysis and H&E staining A pathologist was consulted in analysis of the samples.

In vivo glycemic control studies. The safety and efficacy of Ac-dex nanoparticles were evaluated using healthy and diabetic C57BL/6 mice (Jackson Labs) To induce diabetes, adult male mice were injected with a single dose of 150 mg/kg streptozotocin Groups of at least 4 mice were fasted for 12 h and subcutaneously injected with nanoparticles, long-acting insulin, or naked insulin. Their blood glucose levels were monitored every 30 min following injection with Clarity BG1000 Blood Glucose Meters Glucose tolerance tests were performed by administering 1.5 – 3 g/kg glucose to the mice intraperitoneally To measure serum insulin concentration, blood was collected by terminal cardiac punctures into serum gel microtubes (BD SST™ Microtainer) After centrifugation (5 min, 7000 rcf), serum was collected and analyzed immediately using an insulin ELISA kit (ALPCO) according to the manufacturer's instructions

Statistical analysis Data are expressed as mean ± standard deviation, unless otherwise indicated, and N = 4 – 6 randomly assigned mice per time point and per group These sample sizes where chosen based on statistical power analysis and previous literature Data were analyzed for statistical significance by unpaired, two-tailed Student's t-tests.

2.9 Acknowledgements

This work was supported in part by project funding provided by Sanofi, the Helmsley Charitable Trust, and the Koch Institute Support (core) Grant P30-CA14051 from the National Cancer Institute L V was supported by a NSF Graduate Research Fellowship. We thank the Koch Institute Swanson Biotechnology Center for technical support, specifically the Animal Imaging & Preclinical Testing Core, the Histology Core, the High Throughput Screening Core, and the Nanotechnology Materials Core We thank Dong Soo Yun for assistance with cryo-TEM and Roderick Bronson for assistance with histological analysis The authors declare no competing financial interest

Chapter 3: Microgel-Encapsulated Nanoparticles for Glucose-Responsive Insulin Delivery

The work presented in this chapter is in preparation for publication

L R Volpatti, A L Facklam, A B Cortinas, M Hill, M A Matranga, R Langer, D G Anderson, Microgel encapsulated nanoparticles for glucose-responsive insulin delivery *In preparation*

3.1 Introduction

Microgels are a versatile class of biomaterials that have been used extensively in applications of drug delivery,[174] tissue engineering,[175-176] and cell therapy.[177] They have similar molecular properties as their bulk hydrogel counterparts in addition to being injectable and modular with decreased diffusion distances for drug release or nutrient exchange. Alginate is commonly used to form microgels for biomedical applications due to its inherent biocompatibility and natural availability. Furthermore, alginate readily forms porous hydrogels via crosslinking with divalent cations, including calcium and barium.[178]

To extend the functional lifetime of glucose-responsive insulin delivery systems, we can encapsulate nanoparticles into porous alginate microgels (Figure 3.1). The microgels allow for the preconcentration of the Ac-dex nanoparticles discussed in Chapter 2 and serve as a long-term subcutaneous depot of glucose-responsive insulin in vivo. By combining the large surface area of Ac-dex nanoparticles with the stable porous network of microgels, we create a fast responding system that achieves prolonged normoglycemia for over three weeks with two doses in diabetic mice. Additionally, these microgels further limit the hypoglycemic effect associated with large doses of insulin needed for long-term release.

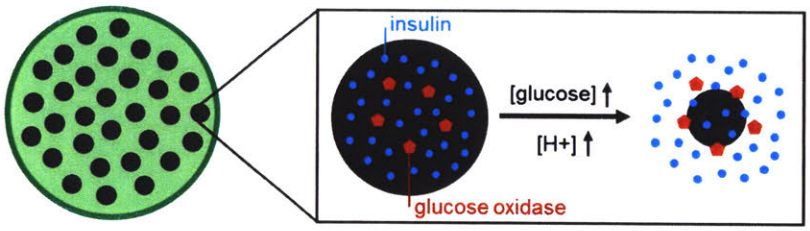

Figure 3.1. Schematic of microgel encapsulation and glucose-responsive insulin release from acid-degradable Ac-dex nanoparticles.

3.2 Encapsulation of NPs in Alginate Microgels

To encapsulate the NPs, we combine them with 1.4 wt% alginate in saline and use a custom-designed electro-spray system to form microdroplets (see methods), which are rapidly crosslinked in a divalent cation gelation bath. Due to the opacity of the NPs, the nanoparticle-encapsulated microgels ("microgels") do not allow light to pass through and appear dark in bright field microscopy images (Figure 3.2a). Upon the addition of glucose, the NPs are degraded, leaving the translucent alginate microgel shell (Figure 3.2b).

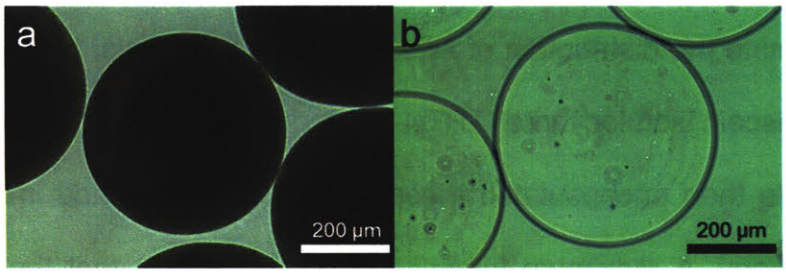

Figure 3.2. Ac-dextran nanoparticles can be encapsulated and degraded in alginate microgels. a) Bright field microscopy image of nanoparticle-encapsulated alginate microgels. b) Alginate microgels in (a) upon exposure to 400 mg/dL glucose for 24 h, showing the degradation of the nanoparticles.

Bright field images of a sample of > 2500 Ca^{2+}-crosslinked microgels formed from the electro-spray process were analyzed using ImageJ software (Figure 3.3a, A.3-1). Automatic thresholding was used to convert the bright field images into 8-bit binary images, and watershed was used to separate nearby microgels (Figure 3.3b, A.3-1). The diameter of the particles was then estimated by averaging the major and minor axes microgels with an approximate diameter under 200 or over 600 excluded due to errors in the watershed process. The measured microgel diameters approximate a Gaussian distribution with a mean of 415 µm and a standard deviation of 93 µm (Figure 3.3c).

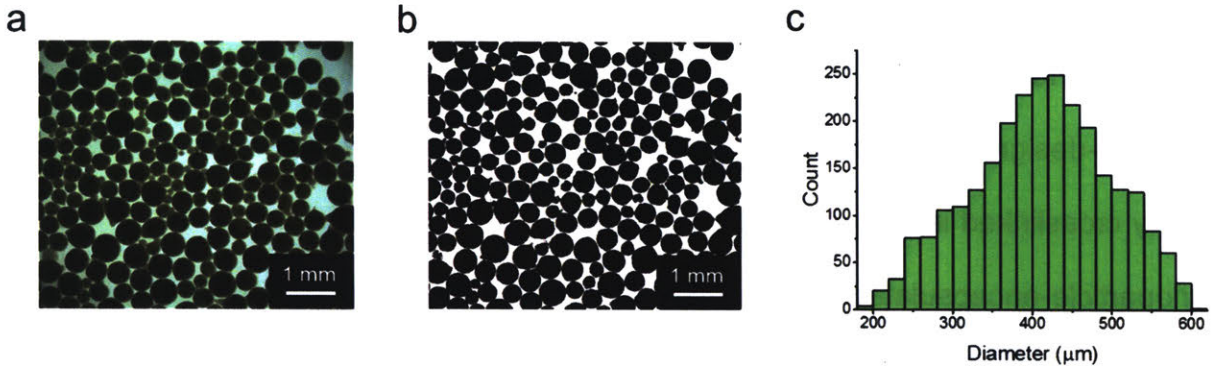

Figure 3.3. The average diameter of a sample of over 2500 microgels is 415 μm. a) Representative bright field image of microgels. b) 8-bit, processed image from (a). c) Histogram of microgel diameter, approximating a Gaussian distribution.

To determine the distribution of NPs within the microgels, NPs were synthesized containing fluorescein isothiocyante (FITC)-labeled insulin and Alexa Fluor 647 (AF647)-labeled GOx. We then encapsulated these NPs in microgels and imaged them using confocal microscopy. A maximum intensity projection shows that the proteins are co-localized and the NPs are evenly distributed throughout the microgels (Figure 3.4). Additional confocal images of a single z-plane of the microgels show a dark core due to the low transmittance of light through the densely packed nanoparticles (Figure A.3-2).

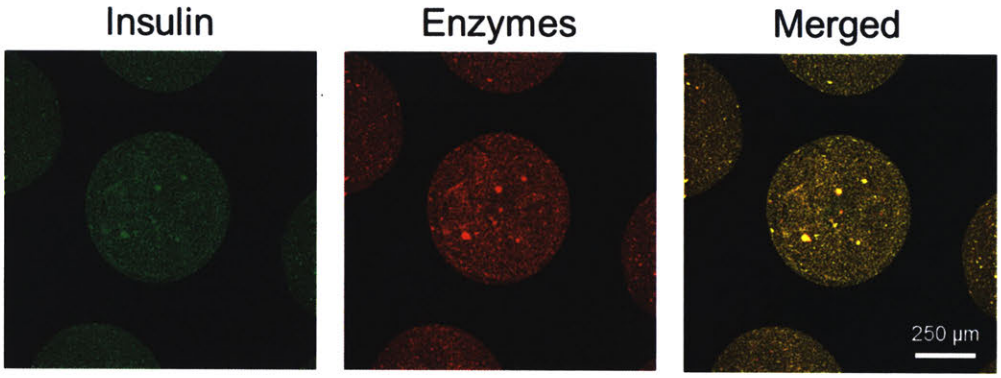

Figure 3.4. NPs are co-localized and evenly distributed throughout microgels. Maximum intensity projection of confocal microscopy images of microgels containing NPs encapsulated with FITC-insulin and AF647-GOx; left: 495 nm channel, center: 647 nm channel, right: overlay.

3.3 Insulin Release Kinetics from Microgels

Since Ba^{2+}-crosslinked alginate microgels and Ca^{2+}-crosslinked alginate microgels are known to have differing mechanical properties and porosity,[178] both cations were tested in this study to optimize microgel stability and insulin release kinetics. When Ba^{2+} is used as a crosslinker, there is an additional barrier to diffusion leading to a delay in acid-mediated insulin release in comparison to free NPs (Figure 3.5a). However, when the alginate is crosslinked with Ca^{2+}, the microgels exhibit insulin release kinetics similar to those of free NPs, with over 80% of insulin released in the first hour (Figure 3.5a). These results are consistent with previous studies which report a reduced permeability of Ba^{2+}-crosslinked microgels.[178-179] Both cations yield microgels that are stable under PBS at pH 7.4 with physiological concentrations of Ca^{2+} (2 mM), resulting in less than 10% of insulin being released over the first 11 h (Figure 3.5a).

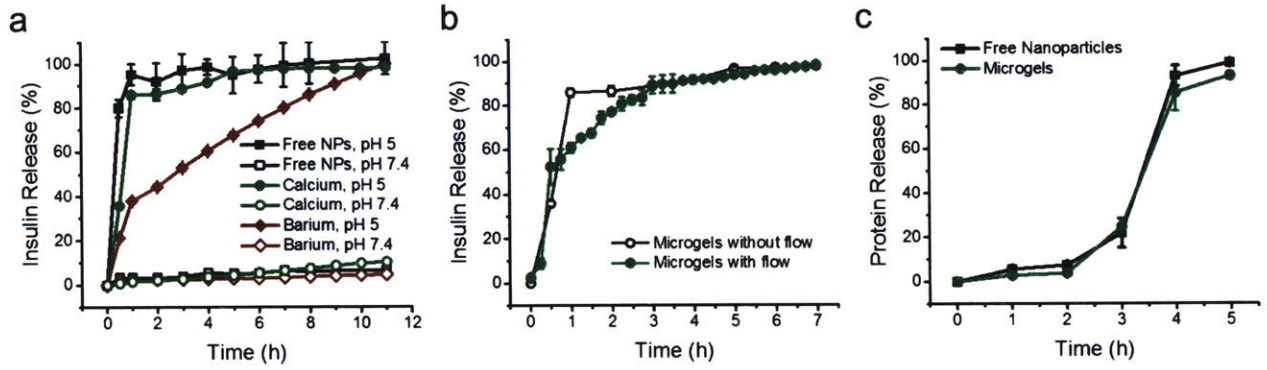

Figure 3.5. Insulin release from Ca^{2+}-crosslinked alginate microgels is similar to that from free NPs. a) Insulin release from free NPs, NPs encapsulated in Ca^{2+}-crosslinked microgels, or NPs encapsulated in Ba^{2+}-crosslinked microgels incubated in either acetate buffer (pH 5) or phosphate buffered saline (PBS, pH 7.4) at 37 °C with agitation. b) Acid-mediated insulin release from NP-encapsulated, Ca^{2+}-crosslinked microgels incubated in a centrifuge tube with acetate buffer at 37 °C with agitation (black open circles) compared to microgels in a perifusion system chamber at 37 °C subjected to a flow rate of 10 µL/min acetate buffer (green solid circles). c) Comparison of glucose-mediated insulin release from free NPs or NP-encapsulated microgels. NPs (2 mg) or microgels (100 µL) were incubated in a total of 200 µL PBS with 400 mg/dL glucose at 37 °C with agitation.

To further probe acid-mediated release kinetics from Ca^{2+}-crosslinked microgels, we analyzed the release profiles when microgels were subjected to fluid flow. When microgels are incubated in a perifusion chamber with a flow rate of 10 µL/min acetate buffer, they exhibit comparable insulin release kinetics as those without any fluid flow (Figure 3 5b) However, there is a slight delay in the onset of release, possibly due to the low flow rate and limited mixing occurring in the chamber Next, we used similar release conditions (10 mg/mL NPs, 50 µL buffer exchange every hour) to compare the glucose-mediated protein release kinetics from microgels and free NPs Under these conditions in response to 400 mg/dL glucose, the release profile from Ca^{2+}-crosslinked microgels shows excellent agreement to that from free NPs (Figure 3 5c).

Next, FITC-insulin NPs were loaded into microgels, and fluorescent images were taken at various time points following incubation in PBS with 400 mg/dL glucose to visualize glucose-mediated insulin release (Figure 3.6a) Fluorescent image quantification using ImageJ software shows that the fluorescence intensity decreases over time with the largest decrease occurring after 2 h of incubation (Figure 3 6b) After 3 h, the fluorescence remains approximately constant over the subsequent 2 h until the end of the study (Figure 3.6b). Microgels were then incubated in PBS alone, PBS containing 100 mg/dL glucose (normal glucose conditions), or PBS containing 400 mg/dL glucose (elevated glucose conditions) with complete buffer exchange every 2 h Under these conditions, the largest increase in protein release in the 400 mg/dL glucose solution occurs after 4 h of incubation (Figure 3 6c) Less than half of the total protein is released over a 10 h period under physiological concentrations of glucose, and minimal protein is released in PBS alone (Figure 3 6c)

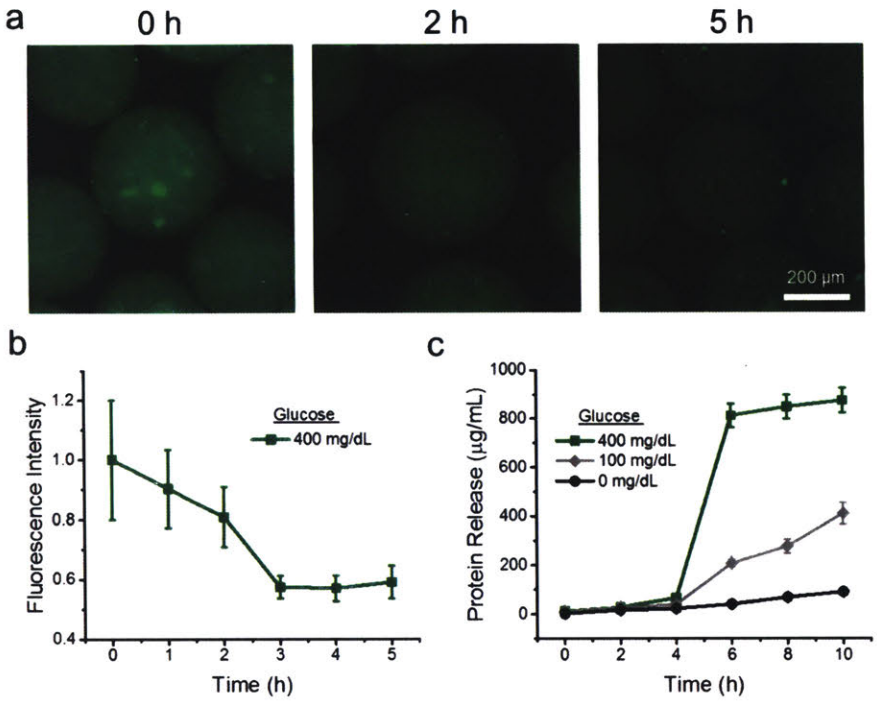

Figure 3.6. Insulin is released from NP-encapsulated microgels in response to elevated glucose concentrations. a) Fluorescence microscopy images of microgels loaded with FITC-insulin nanoparticles. At predetermined time points after incubation in PBS containing 400 mg/dL glucose, aliquots of microgels were rinsed with PBS and imaged. b) Quantification of fluorescence intensity of images from (a) over time. c) Total protein release from microgels incubated in PBS containing 400, 100, or 0 mg/dL glucose. Every 2 h, insulin content in the supernatant was analyzed and the buffer was replaced.

3.4 Insulin and NP Stability in Microgels

After probing insulin release kinetics, we analyzed the structure and activity of the released insulin in vitro. Naked insulin and microgels were incubated at 37 °C with agitation for 0, 3, or 9 days. At these time points, insulin was released from the microgels via acid-mediated Ac-dex degradation and analyzed in comparison to naked insulin. Circular dichroism (CD) was performed to characterize the secondary structure of insulin. As a protein high in α-helical content, insulin exhibits a CD spectrum with negative bands at 222 nm and 208 nm.[180-181] Prior to incubation, the spectra of both the naked insulin and the released insulin contain these characteristic bands. However, after 3 days of incubation, the spectrum of naked insulin begins to lose the band at 222 nm, and by Day 9 it is completely absent (Figure 3.7a). These results are consistent with previous reports of insulin aggregation or denaturation upon agitation at 37 °C in contact with hydrophobic surfaces.[182-183] The released insulin, on the other hand, retains both its characteristic bands and its α-helical structure throughout the duration of the experiment (Figure 3.7b).

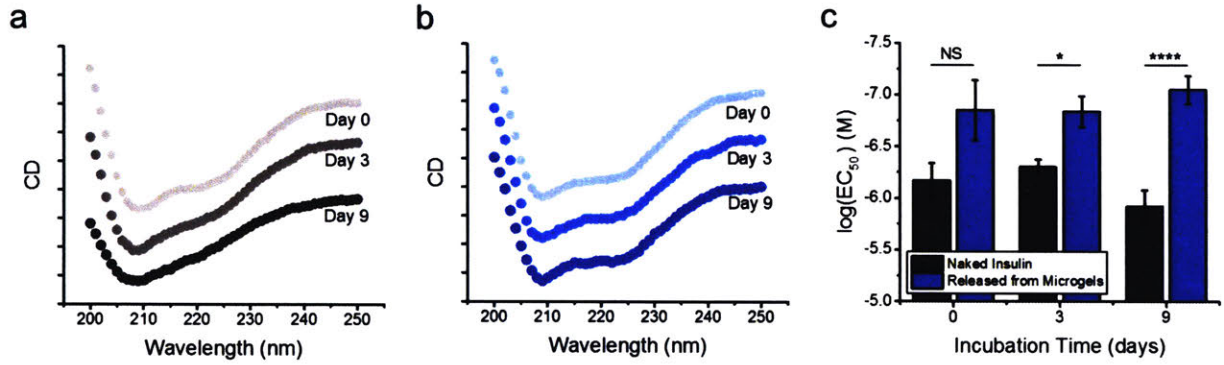

Figure 3.7. Insulin in microgels remains stable and active after 9 days of incubation. a) Circular dichroism spectra of insulin incubated in PBS at 37 °C with agitation for 0, 3, and 9 days, showing the loss of the negative band at 222 nm. b) Circular dichroism of insulin that has been released from microgels incubated in PBS at 37 °C with agitation for 0, 3, and 9 days, showing the retention of its secondary structure. c) EC_{50} determined by AKT phosphorylation of C2C12 cells exposed to naked insulin or insulin released from microgels after 0, 3, or 9 days of incubation. Statistical significance is indicated by *$p < 0.05$, ****$p < 0.0001$; NS: $p > 0.05$.

To determine if the retention of its secondary structure results in enhanced insulin activity, we performed a cell-based insulin receptor assay (see methods) By quantifying the extent of AKT phosphorylation resulting from the dose-dependent binding of insulin to its receptor, we can determine an EC_{50} of the protein After 3 and 9 days of incubation, the released insulin is significantly more potent than naked insulin due to the ability of the microgels to stabilize the protein and protect it from aggregation or denaturation (Figure 3 7c) These results also suggest that processing, encapsulating, and releasing insulin do not adversely affect its structure or activity Moreover, the nanoparticles and microgels stabilize the insulin for over a week in vitro, suggesting that they may have potential to act as long-term depots of insulin in vivo

We next tested the ability of the microgels to stabilize the NPs and enhance their retention at the site of injection for sustained release of insulin We encapsulated AF680-dextran into NPs, loaded them into microgels, and injected microgels or free NPs subcutaneously (s c) into immunocompetent, hairless, albino SKH1E mice (N = 4). The fifth mouse in each group received an injection of either empty microgels or empty NPs and was used to normalize the fluorescence values The mice were monitored over 4 weeks with an in vivo imaging system (IVIS) to track the fluorescence at the injection site (Figure 3 8, A 3-3) The initial fluorescence of the microgels is significantly lower than that of the free NPs, possibly due to the increased proximity of NPs and shielding of the fluorophore (Figure 3.8a) Both microgels and NPs exhibit peak fluorescence one week post-administration as the Ac-dex degrades and exposes the AF680-dextran (Figure 3 8b) Both groups subsequently experience a decrease in fluorescence when the AF680-dextran diffuses away or is cleared from the site of injection At Days 21 and 28, the

fluorescence of the NPs encapsulated in microgels is significantly higher than that of the free NPs.

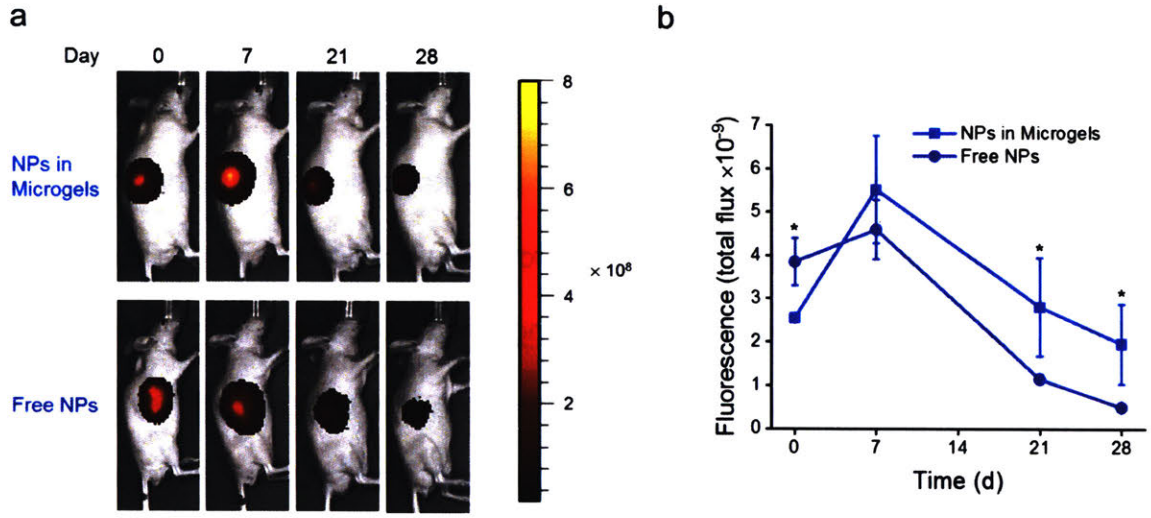

Figure 3.8. Microgels remain at the site of injection in healthy mice longer than free NPs. a) In vivo fluorescent images of NP-encapsulated microgels or free NPs containing AF680-dextran (10 kDa) subcutaneously injected in mice at a dose of 35 mg NP/kg. b) Quantification of total flux of fluorescence in (a). Data represent mean ± standard deviation, normalized to background fluorescence of a control mouse. Statistical significance is indicated by *$p < 0.05$.

3.5 In Vivo Glucose-Responsive Insulin Delivery

To determine whether the microgels offer enhanced protection from hypoglycemia in vivo, we monitored the blood glucose (BG) levels of fasted, healthy C57BL/6 mice following s.c. administration of microgels, free insulin, or an empty microgel control. Mice receiving microgels at an insulin dose of 60 IU/kg remained normoglycemic (70 mg/dL < BG < 200 mg/dL) for the 8.5 h period, suggesting there is minimal leakage of insulin at this dose under normal glucose conditions (Figure 3.9a). Conversely, the 3 IU/kg dose of free insulin causes the mice to experience hypoglycemia within the first hour with BG levels below 70 mg/dL (Figure 3.9a).

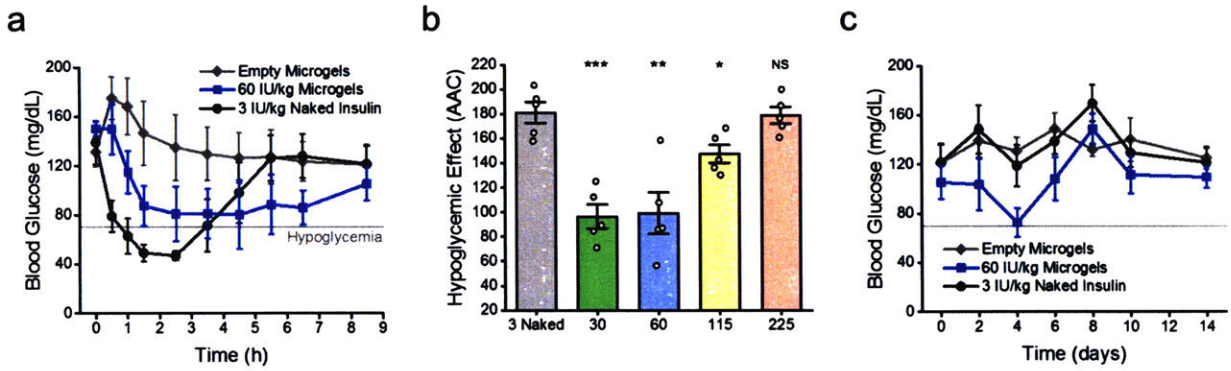

Figure 3.9. Microgels reduce the hypoglycemic effect of insulin in healthy mice. a) Blood glucose levels of healthy mice after administration of empty microgels, nanoparticle-encapsulated microgels at an insulin dose of 60 IU/kg, or naked insulin at a dose of 3 IU/kg. b) Quantification of treatments in (a) in addition to doses of 30, 115, and 225 IU/kg using the area above the curve (AAC) for the first 2.5 h to represent the hypoglycemic effect. c) Fasted blood glucose levels of mice in (a) over two weeks. Data represent mean ± standard deviation (a,c) or standard error of the mean (b). Statistical significance is indicated by *$p < 0.05$, **$p < 0.01$, *** $p < 0.001$ in comparison to naked insulin group; NS: $p > 0.05$.

This hypoglycemic effect is quantified by calculating the area above the curve (AAC) for the first 2.5 h, capturing the initial reduction in BG levels resulting from insulin administration. Using this metric, doses of 30, 60, and 115 IU/kg microgels show significantly lowered BG reduction in a dose escalation study compared to 3 IU/kg free insulin (Figure 3.9b, A.3-4). A dose of 25 IU/kg free NP was previously reported to have

a similar hypoglycemic effect to 3 IU/kg free insulin (Figure 2 15d), suggesting that the microgels protect the NPs from prematurely releasing insulin at high doses The mice were monitored over the following 2 weeks with average fasted BG levels remaining in the normoglycemic range (Figure 3 9c)

We next determined the efficacy of microgels in a streptozotocin-induced type 1 diabetic mouse model Fasted mice were subcutaneously injected with microgels, naked insulin, or an empty microgel control The microgels reduced BG levels at virtually the same rate as naked insulin over the first hour (Figure 3 10a), suggesting they can serve as a fast-acting system To test the ability of the microgels to combat an increase in blood sugar, mice were intraperitoneally administered glucose tolerance tests (GTTs 1 5 g/kg) every two hours after the first hour While the group receiving naked insulin reverted back to hyperglycemic after the first GTT, the group with microgels maintained tight glycemic control for the duration of the study following a total of 4 GTTs and 10 h (Figure 3.10a)

To provide more direct evidence of glucose-responsive insulin release in vivo, we performed pharmacokinetic (PK) studies by quantifying the amount of human insulin in diabetic mouse serum samples over time for mice receiving microgels with or without the glucose sensing enzyme The PK profile of the group receiving enzymes exhibits a peak in insulin release following administration with an additional spike directly after a GTT (3 g/kg, Figure 3.10b) The group without enzymes also shows a peak in insulin release after the first hour, indicative of nonspecific burst release, however, this peak is significantly reduced in comparison to the group receiving enzymes (Figure 3 10b) Furthermore, there is no increase in insulin release following the GTT, suggesting that enzymes are needed for glucose-responsiveness

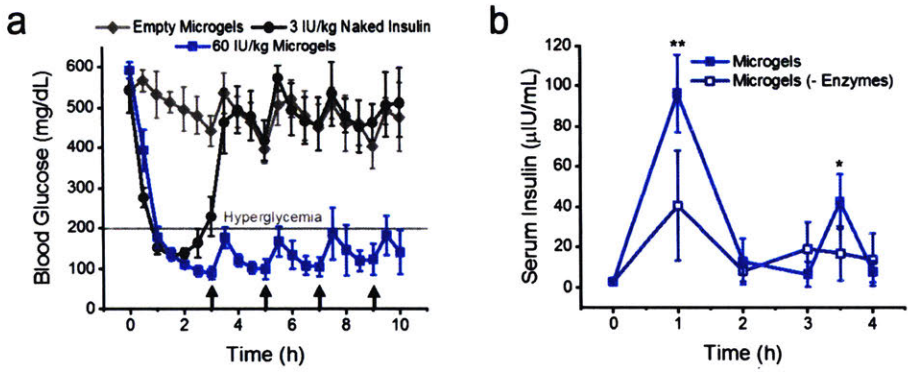

Figure 3.10. Microgels exhibit short-term glycemic control and glucose-responsive insulin release in diabetic mice. a) Blood glucose levels of streptozotocin-induced type 1 diabetic mice following subcutaneous administration of empty microgels, naked insulin, or NP-encapsulated microgels. Arrows represent intraperitoneal glucose tolerance tests (GTTs, 1.5 g/kg). b) Concentration of human insulin in diabetic mouse serum following the injection of microgels (with or without enzymes) with a GTT at 3 h (3 g/kg). Data represent mean ± standard deviation (N = 4+). Statistical significance is indicated by *$p < 0.05$, **$p < 0.01$.

3.6 Long-Term Glycemic Control in Diabetic Mice

To probe the efficacy of the microgels as a sustained insulin depot with prolonged glycemic control, we administered a GTT (3 g/kg) to fasted mice 5 days following microgel dosing. The BG response of the treated mice is consistent with that of healthy mice while mice receiving empty microgels remain diabetic and fail to achieve normoglycemia over the course of the study (Figure 3.11a). These results are quantified using the area under the curve (AUC), which shows that there is no significant difference between treated and healthy mice (Figure 3.11b). Both groups have significantly reduced AUCs compared to those from the empty microgel group (Figure 3.11b).

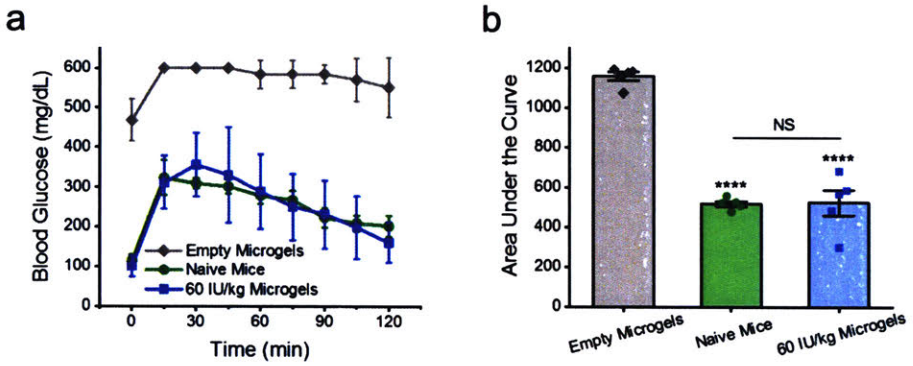

Figure 3.11. Mice receiving microgels respond to a glucose tolerance test similarly to healthy mice. a) Response of diabetic mice to a GTT (3 g/kg) 5 days following injection of empty or nanoparticle-encapsulated microgels compared to response of healthy mice. b) Area under the curve for (a). Data represent mean ± standard deviation (a) or standard error of the mean (b). Statistical significance is indicated by ****$p < 0.0001$, NS: $p > 0.05$.

Finally, we evaluated the long-term efficacy of the microgels by monitoring the BG levels of the mice for a total of 4 weeks. On Day 2 and 4 post-administration, the BGs of the microgel-treated group are in the normoglycemic range. On Day 6, the average BG levels of mice receiving microgels increased to over 300 mg/dL (Figure A.3-5a). The BGs of the mice receiving microgels without enzymes were significantly greater, with an average of greater than 450 mg/dL (Figure A.3-5a). At this point, both groups were given

a second dose of 60 IU/kg. The mice receiving microgels with enzymes remained cured, with average BGs between 70 and 200 for over two additional weeks, a total of 22 days with just 2 doses (Figure 3.12a). The group lacking enzymes experienced decreased glycemic control over the course of the study (Figure A.3-5b), as evidenced by the significantly elevated area under the BG curve for the first 20 days (Figure 3.12b). Therefore, the glucose-sensing enzyme provides both enhanced glucose-responsiveness (Figure 3.10b) and enhanced glycemic control (Figure 3.12b) in a diabetic mouse model.

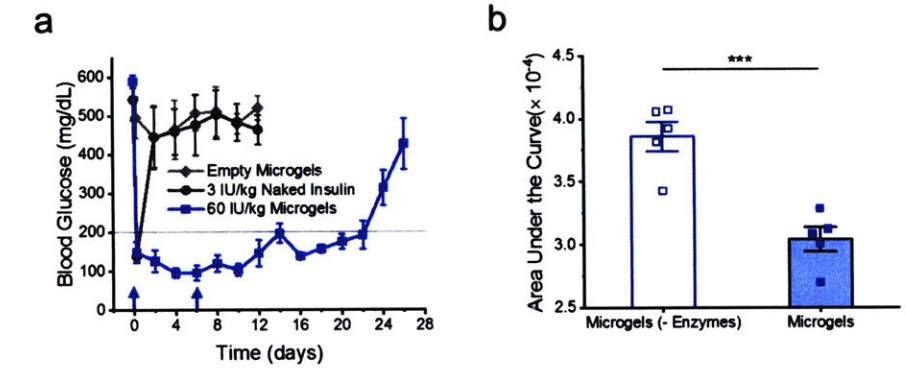

Figure 3.12. Microgels provide long-term glycemic control in diabetic mice. a) Blood glucose levels of diabetic mice following subcutaneous dosing of 60 IU/kg microgels at days 0 and 6 compared to a single dose of empty microgels or 3 IU/kg naked insulin. b) Area under the curve for the first 20 days of blood glucose levels comparing mice receiving two doses of microgels with or without enzymes. Data represent mean ± standard deviation (a) or standard error of the mean (b). Statistical significance is indicated by ***$p < 0.001$.

3.7 Discussion and Conclusions

In summary, by encapsulating glucose-responsive Ac-dex nanoparticles (~ 275 nm) into alginate microgels (~ 415 μm), we are able to control the kinetics of glucose-dependent insulin delivery. Nanoparticle release of insulin in response to enzyme-mediated acid generation was rapid, occurring on the order of minutes in response to elevated glucose levels The microgels provide protection and localization of the nanoparticles in the subcutaneous space, affording extended durations of glycemic control on the order of weeks

To further progress this approach, microgels may be fabricated from degradable biomaterials, for example from an oxidized derivative of alginate which hydrolytically degrades *in vivo* Furthermore, the exogenous enzymes glucose oxidase and catalase may be altered to prevent potential immunogenicity resulting from their repeated administration.

Using the model polysaccharide alginate and native enzymes, we show that this strategy may enhance the safety and efficacy of insulin administrations in healthy and diabetic mouse models The microgels limit the occurrence of hypoglycemia, retain the rapid glucose-responsiveness of the nanoparticles as shown by pharmacokinetic studies and glucose tolerance tests, and maintain glycemic control for over three weeks with two doses This generalizable strategy of encapsulating stimuli-responsive nanoparticles in porous microgels can be adapted for use in other systems to provide long-term, self-regulated drug delivery

3.8 Materials and Methods

Materials/reagents. All chemicals were obtained from Sigma-Aldrich (St Louis, MO) and cell culture reagents from Life Technologies (Carlsbad, CA) unless otherwise noted. Recombinant human insulin (Gibco™) was purchased from ThermoFisher Scientific (Waltham, MA) AlphaLISA SureFire ULTRA kits were purchased from Perkin-Elmer (Waltham, MA) to quantify AKT phosphorylation, and an insulin ELISA kit was purchased from ALPCO (Salem, NH) to measure serum insulin

Nanoparticle synthesis Ac-dextran nanoparticles were prepared with a double-emulsion, solvent evaporation technique Briefly, 50 mg insulin was dissolved in 0.5 mL carbonate buffer (pH 9 5) with or without 11 mg GOx (168 1 units/mg) and 1 5 mg catalase (≥20,000 units/mg) and added to 6 mL dichloromethane containing 240 mg Ac-Dex This two-phase mixture was sonicated for 90 s (Q-500, QSonica, 65% amplitude) with 1 s pulse and immediately added to 25 mL 3% poly(vinyl alcohol) (PVA) in PBS solution After a second round of sonication, the emulsion was added to 150 mL of a 0 3% PVA solution The mixture was stirred at room temperature for 2 h, centrifuged (15 min, 8000 rcf; Avanti JXN-26, Beckman Coulter) and washed twice with basic water (pH 8) The resultant nanoparticles were lyophilized and stored at -20 °C until use.

Microgel synthesis Alginate microgels were fabricated with a custom-designed, electro-spray system comprised of a vertically mounted syringe pump, a voltage generator, and a grounded metal collecting dish containing $CaCl_2$ (50 mM) or $BaCl_2$ (20 mM) gelling solution Microgels were formed from a 1.4% solution of PRONOVA SLG20 (NovaMatrix, Sandvika, Norway) dissolved in a 20 mg/mL suspension of nanoparticles in 0 9% saline A 25 G 1 5 in blunt needle with a voltage of 7.5 kV and a flow rate of 180

μL/min were used to generate microgels with an average diameter of 415 μm After crosslinking, the microgels were washed with saline with 2 mM $CaCl_2$ and stored at 4 °C until use

Bright field and fluorescence microscopy Microgels were imaged immediately prior to and following incubation (400 mg/dL glucose, 37 °C, 24 h) using an EVOS XI bright field microscope (Advanced Microscopy Group) ImageJ software was used to measure the diameter of > 2500 microgels from bright field images At predetermined time points after incubation in PBS containing 2 mM $CaCl_2$ and 400 mg/dL glucose, aliquots of microgels loaded with insulin conjugated with fluorescein isothiocyanate (FITC) were rinsed with PBS containing 2 mM $CaCl_2$ and imaged with an EVOS XI fluorescent microscope (Advanced Microscopy Group) ImageJ was used to quantify the decrease in fluorescence intensity.

Confocal microscopy Microgels were fabricated with nanoparticles containing FITC-insulin and glucose oxidase and catalase conjugated with Alexa Fluor 647. After washing the microgels with saline (+2 mM $CaCl_2$) several times, they were transferred to a black, glass bottom plate and imaged with a confocal microscope (Olympus FV1200) ImageJ was used to recolor the images and create a maximum intensity projection by stacking 45 images taken at ~ 10 μm increments

In vitro insulin release. Acid-mediated insulin release from free nanoparticles was determined by incubating 5 mg/mL nanoparticles without enzymes in PBS (pH 7 4) or acetate buffer (pH 5) at 37 °C with agitation At indicated time points, aliquots were withdrawn and centrifuged The supernatants were removed and insulin content was analyzed with a Coomassie Plus protein assay (Pierce) according to the manufacturer's

protocol To determine insulin release from microgels, 100 µL of microgels and 400 µL buffer (PBS or acetate) were incubated at 37 °C with agitation At indicated time points, 100 µL of buffer was exchanged and analyzed with a Coomassie Plus protein assay for total protein content For glucose-mediated release, 120 µL of suspended microgels with enzymes and 170 µL of buffer (PBS, 100 mg/dL glucose in PBS, or 400 mg/dL glucose in PBS) were added to 200 µL centrifuge tubes The tubes were incubated in a 37 °C shaker, and the buffer was completely exchanged every two hours. The total protein content of these samples was determined with a Coomassie Plus protein assay

Perifusion insulin release. To determine insulin release under flow conditions, microgels were inserted into a temperature-controlled (37 °C) perifusion system chamber (Biorep) Acetate buffer (+ 2 mM $CaCl_2$) was pumped through the chambers at a rate of 10 µL/min, collected into a 96-well plate every 15 min, and analyzed for protein content

Insulin structure Secondary structure motifs were elucidated using high-performance circular dichroism (CD). Naked recombinant human insulin and nanoparticle-encapsulated microgels were incubated in PBS at 37 °C over a period of 9 days At indicated time points, aliquots of naked insulin and microgels were withdrawn Insulin was released from the microgels following the addition of acid and both naked and released insulin (200 µg/mL) were analyzed with a high-performance CD spectrometer (J-1500, JASCO Inc) over a wavelength range of 200–250 nm using a 0 1 cm pathlength cell

In vitro activity. The in vitro activity of released insulin was determined with a cellular AKT assay To prepare for the AKT assay, C2C12 cells (American Type Culture Collection) were cultured in Dulbecco's modified Eagle medium (DMEM) containing L-

glutamine, 4.5 g/L D-glucose, and 110 mg/L sodium pyruvate supplemented with 10% fetal bovine serum and 1% penicillin–streptomycin. Cells were seeded and incubated in 96-well plates at a density of 5,000 cells per well. After 24 h, the cells were washed twice with serum-free DMEM and incubated for 4 h. The media was then removed, and the cells were stimulated with insulin samples or controls for 30 min. The cells were then washed twice with cold Tris-buffered saline and lysed with cold Lysis Buffer (Perkin-Elmer) for 10 min. Concentrations of pAKT 1/2/3 (Ser473) and total AKT 1 in the cell lysates were determined with AlphaLISA SureFire ULTRA kits (Perkin-Elmer) according to the manufacturer's instructions. Data were analyzed using GraphPad Prism 6.0 and fit to four parameter dose-response curves to determine the EC50 of each insulin sample.

In vivo imaging studies. All animal protocols were approved by the MIT Committee on Animal Care, and animals were cared for under supervision of MIT's Division of Comparative Medicine. For in vivo imaging, 8-week-old male SKH1E mice (hairless, immunocompetent) were fed an alfalfa-free diet (AIN-76A, Bio-Serv) for 1 week leading up to the study to limit background fluorescence. Mice were anesthetized using inhaled isoflurane and imaged with an IVIS Spectrum in vivo imaging system with a heated chamber containing inhaled isoflurane. Alginate microgels were prepared with nanoparticles containing dextran (10 kDa) conjugated with AlexaFluor 680. Mice were injected subcutaneously on the lateral flank with microgels or nanoparticles at a dose of 35 mg NP/kg and imaged at several time points using filter sets of 640/760, medium binning, an F-stop of 1, and an exposure time of 0.5 s. Living Image software was used to analyze the fluorescence efficiency and total flux of the images.

In vivo blood glucose studies. The safety and efficacy of nanoparticle-encapsulated microgels were evaluated using healthy and diabetic C57BL/6 mice (Jackson Labs) To induce diabetes, 8-week-old male mice were injected with a single dose of 150 mg/kg streptozotocin Blood glucose levels were monitored for the following week, and only mice with blood glucose levels consistently over 400 mg/dL were considered diabetic. Groups of 5 mice were fasted for 10 h and subcutaneously injected with microgels, nanoparticles, or naked insulin A ~ 5 μL drop of blood from the tail vain was used to monitor blood glucose levels every 30 min with Clarity BG1000 Blood Glucose Meters For long term studies, mice were fasted 10 h prior to measuring their blood glucose Glucose tolerance tests were performed by administering 1.5 – 3 g/kg glucose in saline solution to the mice intraperitoneally.

In vivo serum insulin studies To measure serum insulin concentration, blood was collected by terminal cardiac punctures into serum gel microtubes (BD SST™ Microtainer) After centrifugation (5 min, 7000 rcf), serum was collected and analyzed immediately using a human insulin enzyme-linked immunosorbent assay kit (ALPCO) according to the manufacturer's instructions

Statistical analysis Data are expressed as mean ± standard deviation, and N = 4 – 5 randomly assigned mice per time point and per group These sample sizes where chosen based on statistical power analysis and previous literature. Data were analyzed for statistical significance by unpaired, two-tailed Student's t-tests

3.9 Acknowledgments

This work was supported in part by project funding provided by Sanofi, the Helmsley Charitable Trust, and the Koch Institute Support (core) Grant P30-CA14051 from the National Cancer Institute. L V was supported by a NSF Graduate Research Fellowship We thank the Koch Institute Swanson Biotechnology Center for technical support, specifically the Animal Imaging & Preclinical Testing Core and the High Throughput Screening Core The authors declare no competing financial interest

Chapter 4: Electrostatic Complexation of Insulin and Polycations as a Glucose-Responsive Delivery System

The work presented in this chapter is in preparation for publication

L R Volpatti, D M Burns, A Basu, M Hill, M A Matranga, R Langer, D G Anderson, Electrostatic Complexation of Insulin and Polycations as a Glucose-Responsive Delivery System *In preparation*

4.1 Introduction

In addition to the physical encapsulation of drugs inside polymeric nanoparticles, the therapeutic agent can be covalently attached or electrostatically complexed to the delivery vehicle to enhance the loading capacity The insulin loading capacity of Ac-Dex NPs is ~ 5 – 8 wt%, and this percentage further decreases upon encapsulation in alginate microgels To increase the loading capacity of insulin and reduce the volume of material required for a single dose, we hypothesized that insulin could be electrostatically complexed to a polycation Insulin has a pKa around neutral pH it is slightly negatively charged at pH 7.4 and positively charged in acidic conditions Therefore, we hypothesized that electrostatic complexes (ECs) of insulin and a polycation would be stable under physiological pH When the pH of the microenvironment is reduced, for example through the enzymatic conversion of glucose to gluconic acid, the electrostatic interactions would be disrupted and insulin would become available to bind to the insulin receptor for blood sugar reduction (Figure 4 1) As a model polycation, we employ polyethylenimine (PEI) to determine the potential efficacy of insulin ECs.

An additional benefit of this delivery system is its enhanced stability in response to normoglycemic conditions due to the buffering capacity of the polycation In normal glucose concentrations, the polycation acts as a buffer and becomes more highly protonated to prevent drastic reductions in pH In elevated glucose concentrations, the generation of gluconic acid can overcome this buffering effect and reduce the pH of the surrounding environment. This enhanced stability also has the potential to extend the functional lifetime of the ECs compared to the Ac-Dex NPs.

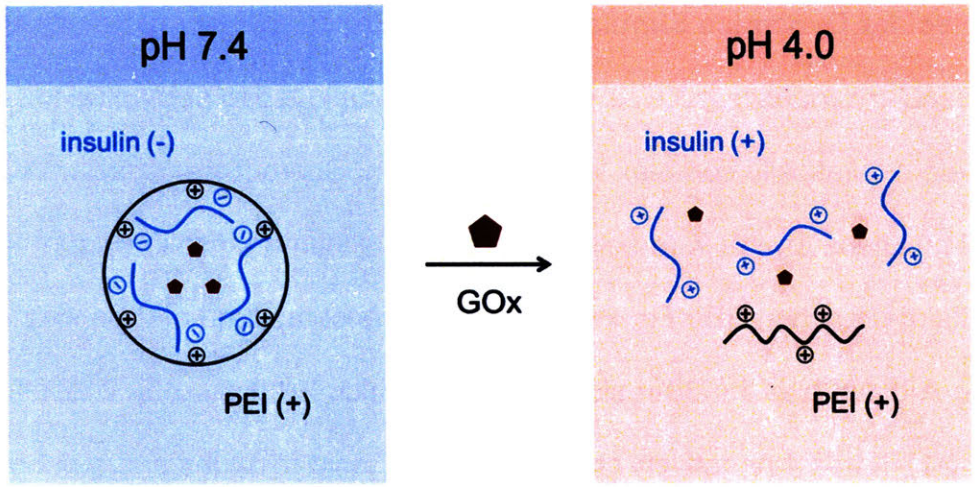

Figure 4.1. Schematic of insulin complexation with polyethyleneimine (PEI) and glucose-responsive release from the resulting electrostatic complex (EC).

4.2 Molecular Dynamics Simulations

Molecular dynamics (MD) simulations were employed to determine the potential of insulin to electrostatically complex with a polycation. Schrodinger software was used to perform simulations on the X-ray crystal structure of human insulin (Figure 4.2a) and 6 repeat units of branched PEI (Figure 4.2b). Insulin is comprised of 2 peptide chains, the 21-residue A chain and the 30-residue B chain, which are linked by 2 disulfide bridges (Figure A.4-1). It has 4 negatively charged glutamic acid residues and a net charge of -2 at physiological pH. Due to interactions with neighboring positively charged residues, 3 of the 4 glutamic acid residues are relatively inaccessible to complex with a polycation. The free glutamic acid is residue 21 on the B chain (B:GLU 21). Under physiological conditions, the PEI oligomer used in simulations has a net charge of +6.

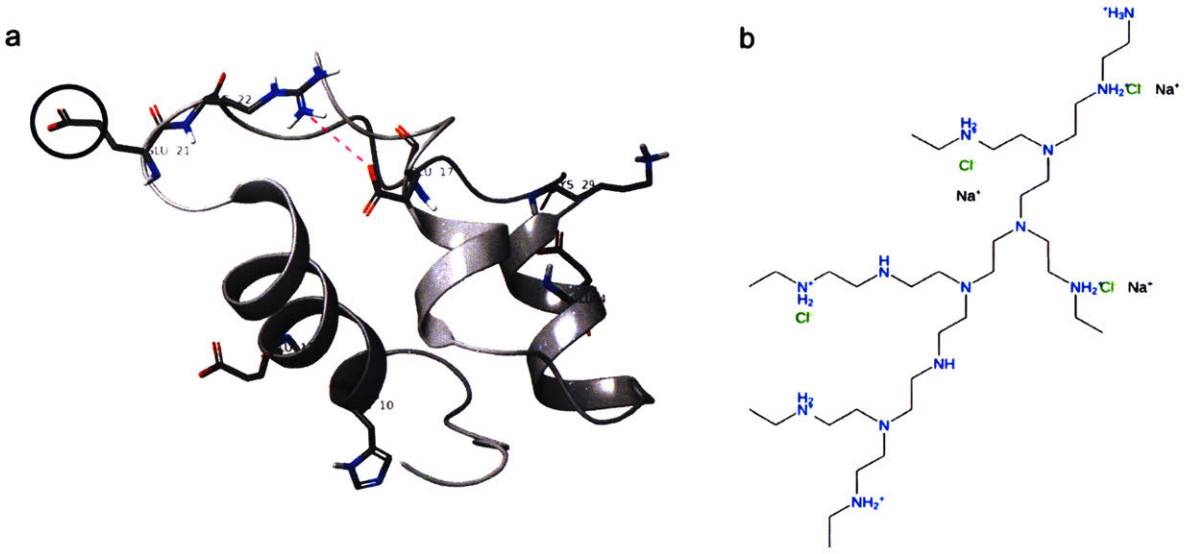

Figure 4.2. Depictions of insulin and polyethyleneimine oligomer. a) Ribbon diagram of insulin secondary structure. Glutamic acid residues are explicitly shown with neighboring positively charged residues. The single free glutamic acid (B:GLU 21) is circled. b) 6-mer of branched polyethyleneimine used for molecular dynamics simulations.

Within the first several ns of running the simulation, insulin and PEI begin interacting, and these interactions are maintained through the entire 500 ns simulation (Figure 4.3). Several of the amines on the PEI backbone interact with insulin for more than 30% of the simulation time (Figure A.4-2).

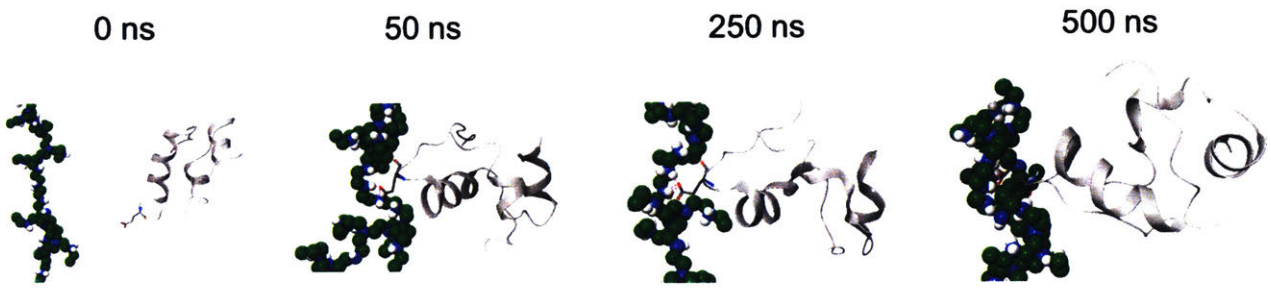

Figure 4.3. Visualization of insulin-PEI interactions over time.

The primary interactions that occur between the protein and polycation are hydrogen bonding and ionic, with hydrogen bonding accounting for the vast majority of interactions. Most interactions involve the free glutamic acid B:GLU 21 (Figure 4.4a). While other residues transiently interact with PEI, B:GLU 21 consistently experiences at least one contact with the polycation over the course of the simulation (Figure 4.4a). Additionally, a B chain tyrosine (B:TYR 16, Figure 4.4a) and an A chain glutamic acid (A:GLU 17, Figure 4.4b) participate in a small number of ionic interactions. The total number of contacts between insulin and PEI throughout the simulation is typically between 1 and 5 (Figure 4.4c). The root mean square deviation (RMSD), which measures conformational changes in the protein that occur over the course of the simulation, remains within a ~ 3 Å range throughout the simulation, indicative of small fluctuations around a thermal average structure and simulation convergence (Figure 4.4d). Taken together, these results suggest that the complexation of insulin with PEI is

thermodynamically favorable under physiological conditions and provides a theoretical basis for the formation of electrostatic complexes.

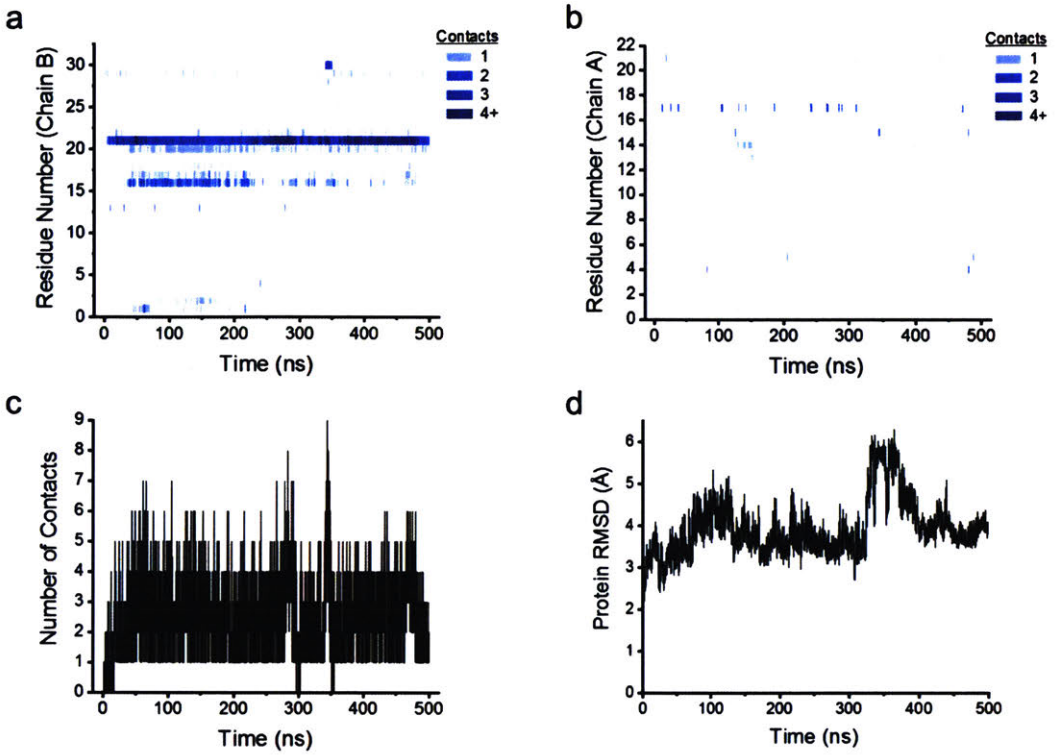

Figure 4.4. The free glutamic acid of insulin continuously interacts with PEI for the duration of the simulation. Number of interactions (contacts) between PEI and each residue of insulin in the a) B chain and the b) A chain over the course of the simulation. Residues with more than one contact are represented by a darker shade of blue, according to the scale at the right. c) Total number of contacts between PEI and insulin over the course of the simulation. d) Root mean square deviation (RMSD) measuring conformational changes in the protein over the course of the simulation.

4.3 Characterization of Electrostatic Complexes

After completing the MD simulations, we synthesized electrostatic complexes (ECs) through a double emulsion, solvent evaporation method. ECs were formulated with a 1:1 weight ratio of insulin to PEI and varying initial amounts of GOx (0.63:1, 0.31:1, or 0.16:1 mg GOx:mg PEI). The ECs were then characterized according to their composition, size, and charge. The concentration of GOx in the EC was measured according to an activity assay, which suggests that only a small fraction of the initial GOx is entrapped in the EC. The final amount of GOx correlates with the starting concentration with values ranging from ~ 0.2 to ~ 0.9 U/mg EC (Figure 4.5a). The concentration of insulin in the EC was then measured by high performance liquid chromatography (HPLC). For all formulations, the amount of insulin in the EC is similar and comprises over 50% of the mass of the complex (Figure 4.5a).

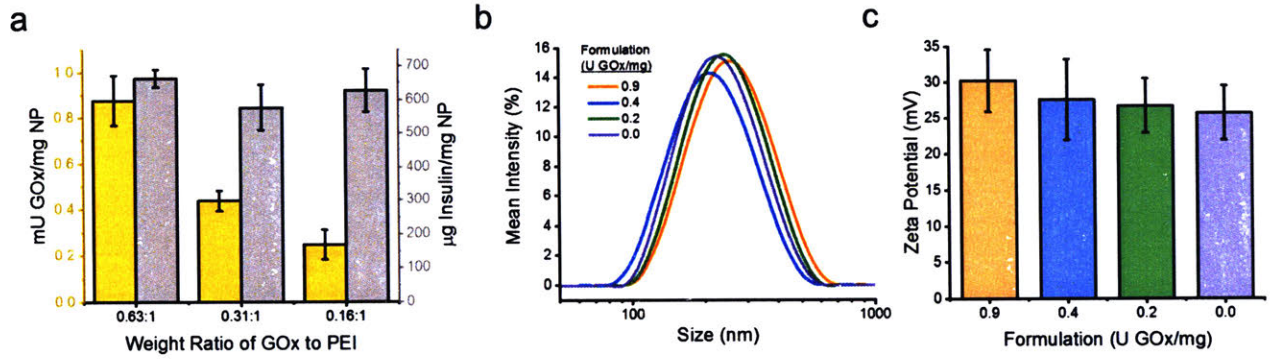

Figure 4.5. Varying the amount of glucose oxidase (GOx) in ECs does not significantly affect insulin loading, size, or surface charge. a) GOx and insulin content of different formulations of EC according to the initial GOx concentration. b) Dynamic light scattering of different formulations of EC according to the final GOx concentration. c) Zeta potential of different formulations of EC according to the final GOx concentration.

The size of the ECs was then determined by dynamic light scattering (DLS) intensity measurements. The mean diameters of formulations containing 0.9, 0.4, 0.2, and 0.0 U GOx/mg EC average to 248.5 nm ± 19.5 nm, and the average polydispersity

index is 0.26 (Figure 4.5b). Due to the high charge density of the PEI, the ECs have a corresponding highly positive surface charge. The average zeta potential of the different EC formulations ranges from +25 to +30 mV, with the lowest average charge corresponding to the formulation with no GOx (Figure 4.5c). Since the different formulations have similar insulin content, size, and surface charge, we can attribute differences in release kinetics to the amount of GOx present in the ECs.

4.4 Insulin Release Kinetics from Electrostatic Complexes

Next we studied the kinetics of insulin release in response to normal (100 mg/dL) and elevated (400 mg/dL) glucose concentrations. ECs were incubated in 37 °C with agitation, and the amount of insulin released at each time point was quantified by HPLC. After 2 h, there is significantly more insulin release in the high glucose conditions compared to the low glucose conditions for each of the formulations (Figure 4.6).

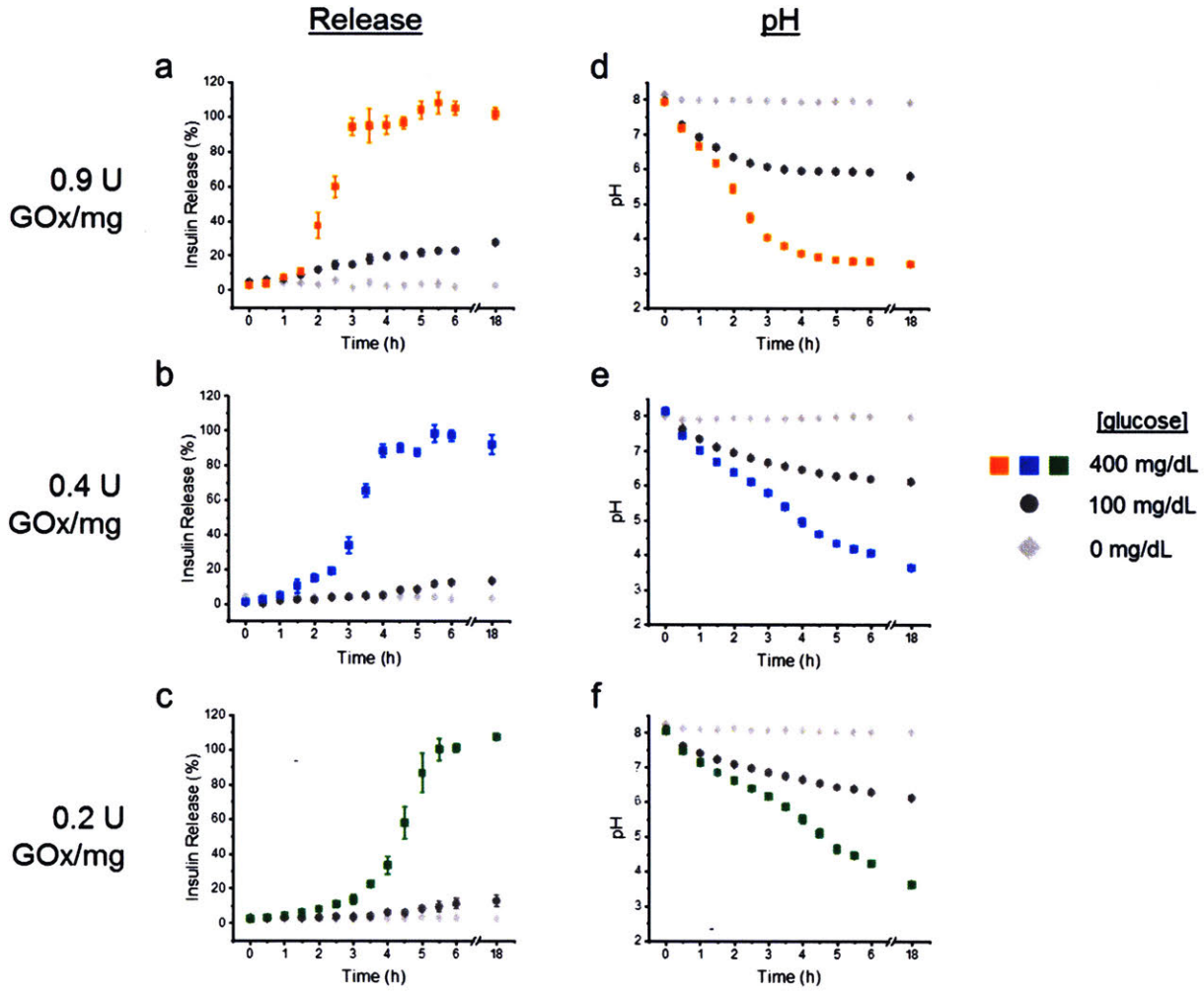

Figure 4.6. Increasing the amount of GOx in the EC results in faster insulin release and corresponding pH reduction. Insulin release kinetics (a-c) and pH curves (d-f) for EC formulations with varying amounts of GOx. ECs were incubated at 37 °C with agitation in PBS containing 0, 100, or 400 mg/dL glucose.

At this point, the formulation with 0.9 U GOx/mg EC has released over 2 and 4 times the amount of insulin as compared to the 0.4 U and 0.2 U formulations, respectively. The time it takes for 50% of insulin to be released from each formulation is then linearly interpolated from the plots as a single measure of release kinetics. The 0.9 U formulation releases 50% of insulin in ~ 2 h while the 0.4 U and 0.2 U release 50% of insulin in ~ 3 and ~ 4 h, respectively (Figure 4.7a).

To more directly evidence the effect of GOx concentration on insulin release, the pH of the solution was also measured at each time point. The pH curves support the insulin release kinetics, with a pH of around 5 resulting in enhanced insulin release (Figure 4.6). The area under the pH curve (AUC) was then calculated as a single measure of pH reduction. The AUC of the 0.9 U formulation is about 20% reduced compared to the 0.2 U formulation in 400 mg/dL glucose but is comparable for 100 and 0 mg/dL (Figure 4.7b). Therefore, the 0.9 U formulation allows for faster pH reduction at elevated glucose concentrations with pH values remaining above 5.5 throughout the study in response to normoglycemic conditions.

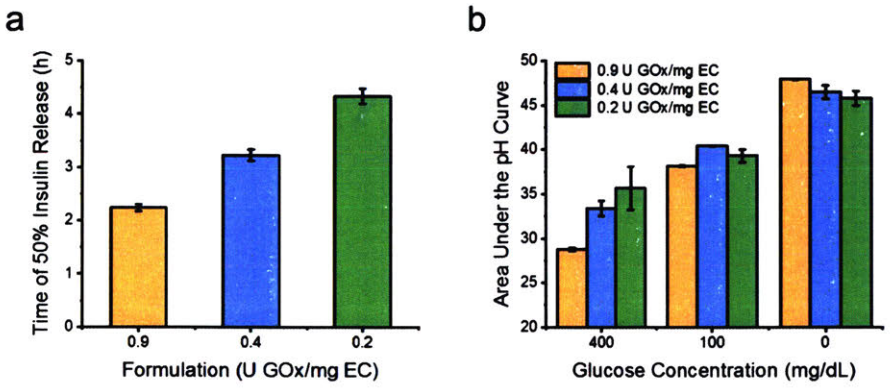

Figure 4.7. The time of 50% insulin release and area under the pH curve in elevated glucose conditions is significantly reduced with 0.9 U GOx/mg EC. a) The time of 50% insulin release in 400 mg/dL glucose for each formulation. Values are linearly interpolated from the data in Figure 4.6. b) Area under the pH curves in Figure 4.6 for each formulation and glucose concentration.

The 0.9 U GOx/mg formulation was then used to probe the potential for changes in release following changes in glucose concentration. First, we repeatedly alternated between hyperglycemic and normal glucose levels every hour for 4 cycles, beginning with an incubation in the high glucose condition (Figure 4.8a). The first two incubations in high glucose release approximately 3.5 times the amount of insulin that is released in response to the lower glucose condition. This pulsatile behavior continues, though is slightly diminished, over the course of the 8 h experiment.

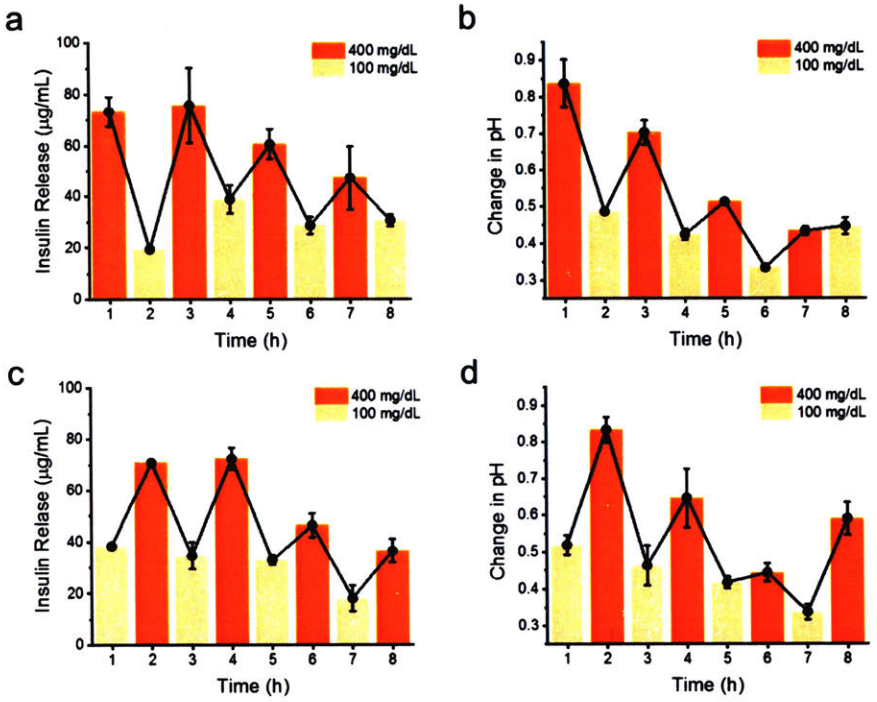

Figure 4.8. Insulin release rates and pH values repeatedly alternate between high and low according to glucose concentration. a) The amount of insulin released at each time point for alternating glucose concentrations starting with 400 mg/mL. b) The pH curves corresponding to (a). c) The amount of insulin released at each time point for alternating glucose concentrations starting with 100 mg/mL. d) The pH curves corresponding to (c).

The corresponding changes in pH similarly show a pulsatile pattern that trends downward over time (Figure 4.8b). The diminished responsiveness is likely caused by the dissociation of the EC and release of enzyme over time. Importantly, similar pulsatile

release patterns are also observed when the ECs are first incubated in low glucose conditions, suggesting that the release is glucose-mediated with limited non-specific burst release of insulin at early time points (Figure 4.8c,d).

Next, the rate of insulin release was assessed in response to increasing concentrations of glucose over time. The ECs were first incubated in PBS alone. After 2 hours, glucose was added to the solution at a concentration of 100 mg/dL. Every subsequent 2 h period, the glucose concentration was doubled. The resulting rates of insulin release correspondingly increased with increasing glucose concentration (Figure 4.9a). The rate of change in solution pH also increased over time with higher glucose concentrations (Figure 4.9b). Collectively, the in vitro experiments suggest that the pH change and subsequent insulin release from ECs is mediated by the concentration of glucose in the surrounding environment.

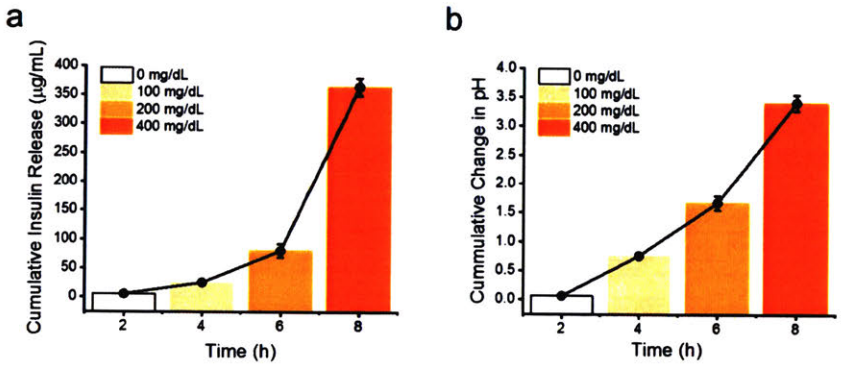

Figure 4.9. Increasing the concentration of glucose over time results in enhanced insulin release and changes in pH. a) Cumulative amount of insulin released over time for increasing glucose concentrations. b) Cumulative changes in pH corresponding to (a).

4.5 Insulin Stability and In Vivo Activity

Finally, we wanted to confirm that the released insulin retains its structure and function. To probe the secondary structural motifs, we used circular dichroism (CD). Insulin released from the ECs on Day 0 and Day 9 retains the negative bands at 208 nm and 222 nm characteristic of α-helical proteins (Figure 4.10a). These data suggest that the complexation and de-complexation of insulin do not alter its secondary structure, supporting the MD simulations. Furthermore, the ECs can stabilize the insulin and prevent aggregation or denaturation for up to 9 days in vitro, suggesting that they may extend the shelf-life of insulin.

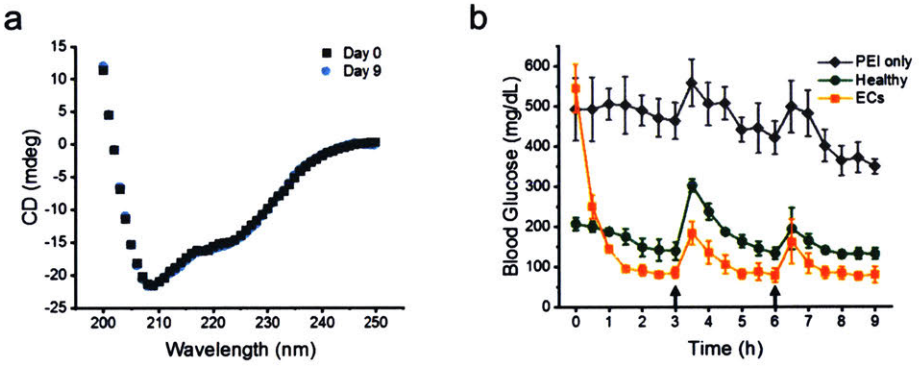

Figure 4.10. Insulin retains its structure and bioactivity after release from ECs. a) Circular dichroism of insulin upon formulation and after 9 days of incubation at 37 °C. b) Blood glucose correction of type 1 diabetic mice receiving a dose of 15 IU/kg insulin in ECs compared to PEI only and healthy mice. Arrows represent intraperitoneal glucose tolerance tests (1.5 g/kg). Data represent mean ± standard deviation, and N=5 mice for each group.

To assess the bioactivity of the released insulin, we performed an in vivo study using streptozotocin-induced Type 1 diabetic mice. After overnight fasting, we injected the mice subcutaneously with ECs at a dose of 15 IU/kg insulin or PEI alone. The ECs successfully reduced the blood glucose (BG) levels of the diabetic mice from hyperglycemic to normoglycemic regimes (Figure 4.10b). Intraperitoneal glucose tolerance tests (GTTs, 1.5 g/kg) were administered at the 3 and 6 h time points. The

response of the treated mice to the GTTs was comparable to that of healthy mice. After a modest rise in BG level, the mice treated with ECs were able to recover and remain in the normoglycemic range throughout the duration of the study.

4.6 Discussion and Conclusions

In summary, we have developed a novel, nanoscale electrostatic complex between insulin and a polycation that encapsulates GOx These complexes have a high loading efficiency and are comprised of over 50% insulin by weight, thus limiting the total amount of material injected in each dose In elevated glucose concentrations, approximately 50% of encapsulated insulin is released within the first 2 h In normoglycemic conditions, on the other hand, the polycation buffers the reduction of the environmental pH, allowing for enhanced stability with less than 30% of insulin released after 18 h of incubation. Furthermore, the complexation of insulin does not alter its secondary structure or activity and extends the therapeutic effect of insulin for at least 9 h with one dose

Since PEI and GOx have the potential for toxic side effects, alternate strategies should be pursued in the future to increase the biocompatibility of this approach For example, highly positively charged poly(β-amino esters) could be used as a more biocompatible and biodegradable alternative to PEI Additionally, the PEI-insulin ECs could be embedded in microneedles made out of a porous hydrogel Since the molecular weight of insulin is an order of magnitude smaller than either PEI or GOx, the insulin could diffuse out the matrix, with the polycation and enzymes remaining in the microneedle when it is removed from the skin Nevertheless, these initial studies demonstrate the potential for electrostatically-complexed insulin nanoparticles as promising candidates in glucose-responsive insulin delivery.

4.7 Materials and Methods

Materials/reagents. All chemicals were obtained from Sigma-Aldrich (St Louis, MO) and cell culture reagents from Life Technologies (Carlsbad, CA) unless otherwise noted. Recombinant human insulin (Gibco™) was purchased from ThermoFisher Scientific (Waltham, MA)

Molecular modeling. We have chosen 6 repeat units of the polyethyleneimine for representing the atomistic interactions mimicking the insulin and polymer interaction. All molecules were drawn, and their three dimensional structures were built using the Maestro Interface of Schrodinger Suite 2018-1 The constructed polymer was then subjected to ligprep to assign appropriate ionization states at pH 7.0 Thereafter, the initial geometries were relaxed by energy minimization of 50,000 steps of steepest descent at converging gradient of 0.01 kcal/mol, using OPLS2003e force field Simulations were performed on the X-ray crystal structure of human Insulin (PDB ID 4INS) All the water molecules in the crystal structure three-dimensional, bond orders were assigned, hydrogens were added, and insulin was then further subjected to restrained energy minimization with relatively higher convergence criteria of 0 30 Å using Schrodinger's Protein preparation wizard, using OPLS-2003e force field

Molecular dynamics studies. The optimized structures of Insulin and polymer were placed at a random position ~ 10 Å apart from each other. Each system was then subjected to molecular dynamics simulations as follows. MD simulations were carried out using the Desmond program, an explicit solvent MD package (version 3.1, Desmond Molecular Dynamics System, D E Shaw Research, New York, NY, USA and version 3 1, Maestro-Desmond Interoperability Tools, Schrodinger) with inbuilt optimized potentials

for liquid simulation (OPLS 2005) force field The system was set up for simulation using a predefined water model (simple point charge, SPC) as a solvent in a cubic box with periodic boundary conditions specifying the shape and size of the box as 10 Å × 10 Å × 10 Å distance The desirable electrically neutral system for simulation was built with 0.15 M NaCl (physiological concentration of monovalent ions) in 10 Å buffer using the system-built option. All the MD simulations were performed on a local EXXACT Corp workstation equipped with K40-NVIDIA GPU The system was allowed to minimize at 50,000 steps using steepest descent. This was followed by 100 ps of constant volume (NVT) simulation, and finally by two 12 ns followed by 24 ns of constant pressure (NPT) simulation Once the system was relaxed, a short 5 ns MD simulation (NPT) was performed, followed by a relatively long-range 500 ns NPT MD simulation. The data obtained were plotted as a function of a number of contacts (characterized by hydrogen bonding interactions and ionic salt bridge formation between insulin and the polymer) vs simulation time

Electrostatic complex synthesis. Electrostatic complexes were prepared using a double-emulsion, solvent evaporation technique. Briefly, insulin was dissolved in carbonate buffer (pH 9 5, 100 mg/mL) with or without GOx (168 1 units/mg) and added to PEI in dichloromethane (DCM, 100 mg/mL) prior to sonication for 90 s (Q-500, QSonica, 65% amplitude) with 1 s pulse This mixture was added to a 3% poly(vinyl alcohol) (PVA) in PBS solution and sonicated for a second time After stirring for 2 h, the resultant electrostatic complexes were centrifuged (15 min, 8000 rcf, Avanti JXN-26, Beckman Coulter) and washed once with basic water (pH 8) before lyophilization

Loading capacity The loading capacities of protein were determined by degrading a known mass of ECs in a solution of PBS + acetic acid (pH 2) and measuring protein content. Insulin was quantified by high performance liquid chromatography (HPLC, Agilent 1100 Series) with an Atlantis® T3 column (5 µm, Waters) The activity of GOx was measured using an Amplex® Red Glucose/Glucose Oxidase Assay Kit (Life Technologies)

Electrostatic complex characterization The size and surface charge of ECs were characterized by dynamic light scattering (DLS) and zeta potential (Zetasizer Nano ZS, Malvern Instruments), respectively Lyophilized ECs were suspended in ultrapure water and filtered through 0 8 µm membrane filters before analysis by DLS or zeta potential.

In vitro insulin release. ECs (2 mg/mL) were suspended in triplicate in PBS alone or with the addition of 100 mg/dL, 200 mg/dL or 400 mg/dL glucose and incubated at 37 °C with agitation At indicated time points, aliquots were withdrawn and centrifuged. The supernatants were removed, and protein content was analyzed by HPLC

Insulin structure Secondary structural motifs were elucidated using high-performance circular dichroism (CD). ECs (500 µg/mL) were incubated in a PBS at 37 °C with agitation for 0 or 9 days. At indicated time points, the ECs were washed once and degraded with HCl (pH 2) NaOH was used to return the pH to 7.4 before analysis with a high-performance CD spectrometer (J-1500, JASCO Inc.) using a 0.1 cm pathlength cell

In vivo glycemic control studies. The activity of ECs was evaluated using diabetic C57BL/6 mice (Jackson Labs). To induce diabetes, adult male mice were injected with a single dose of 150 mg/kg streptozotocin Groups of 5 mice were fasted for 12 h and

subcutaneously injected with ECs or PEI alone Their blood glucose levels were monitored every 30 min following injection with Clarity BG1000 Blood Glucose Meters Glucose tolerance tests were performed by administering 1 5 g/kg glucose to the mice intraperitoneally

Statistical analysis Data are expressed as mean ± standard deviation, unless otherwise indicated, and N = 5 randomly assigned mice per time point and per group These sample sizes where chosen based on statistical power analysis and previous literature Data were analyzed for statistical significance by unpaired, two-tailed Student's t-tests

4.8 Acknowledgments

This work was supported in part by project funding provided by Sanofi, the Helmsley Charitable Trust, and the Koch Institute Support (core) Grant P30-CA14051 from the National Cancer Institute. L V was supported by a NSF Graduate Research Fellowship We thank the Koch Institute Swanson Biotechnology Center for technical support, specifically the Animal Imaging & Preclinical Testing Core. The authors declare no competing financial interest.

Chapter 5: Conclusions

5.1 Thesis Summary

In summary, this Thesis described three projects that have made progress toward achieving the goal of glucose-responsive insulin delivery The first project focused on a nanoparticle-based insulin delivery system comprised of a pH-sensitive modified dextran, glucose oxidase, and catalase These nanoparticles afford rapid insulin release with up to 16 h of glycemic control in diabetic mice The second project detailed the potential of this nanoparticle system to be encapsulated in porous microgels to allow for extended glucose-responsive insulin delivery. This system is able to achieve over 3 weeks of glycemic control with just two doses Finally, the third project discussed an alternative method to achieve glucose-responsive insulin release based on the electrostatic complexation of insulin to polycations These nanoparticles demonstrated enhanced stability with less than 30% of insulin being released in vitro after 18 h of incubation in normoglycemic conditions

5.2 Future Perspectives

Further optimization of these systems may enhance their potential for translation into the clinic. For example, in the second project, the weekly injection of non-degradable polymers may cause unintended side effects and potential immunogenicity in patients The development of a degradable system, such as an oxidized form of alginate, would greatly enhance the potential for translation of this project. For the third project, polycations tend to be toxic in vivo Additionally, daily dosing of exogeneous enzymes could also pose a concern of immunogenicity Therefore, future work, such as developing a microneedle delivery system, may enhance the potential impact of this work

Another important feature of a translatable glucose-responsive insulin delivery system is the existence of a "shut-off" valve in the event of hypoglycemia. One way this could be achieved is through the addition of glucose-responsive glucagon delivery, which releases the counter-regulatory hormone when glucose levels are too low. Such a dual-hormonal system has already been commercialized in insulin pumps and may be an exciting new direction in the field of chemically glucose-responsive insulin delivery

Appendix A: Supplementary Figures

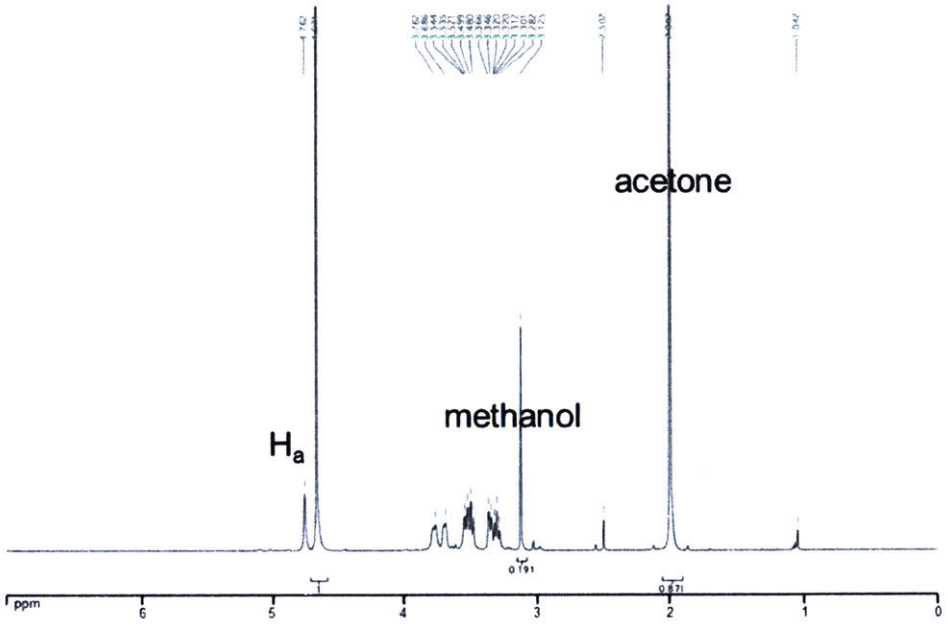

Figure A.2-1. ^{1}H NMR of Ac-dex degradation products. Example ^{1}H NMR spectrum upon incubation in deuterium chloride showing the methanol and acetone peaks used to determine percent cyclic and acyclic modifications.

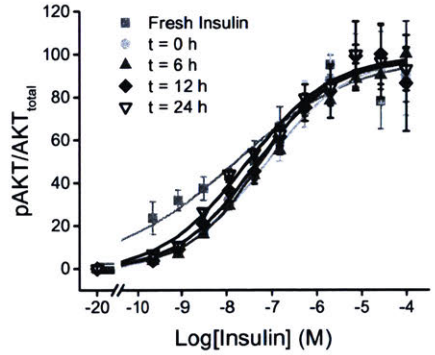

Figure A.2-2. Dose response curves of cellular receptor assay. The ratio of phosphorylated AKT to total AKT as a function of insulin concentration for naked insulin and encapsulated insulin released after various incubation times. Lines represent a four parameter fit using GraphPad Prism 6.0.

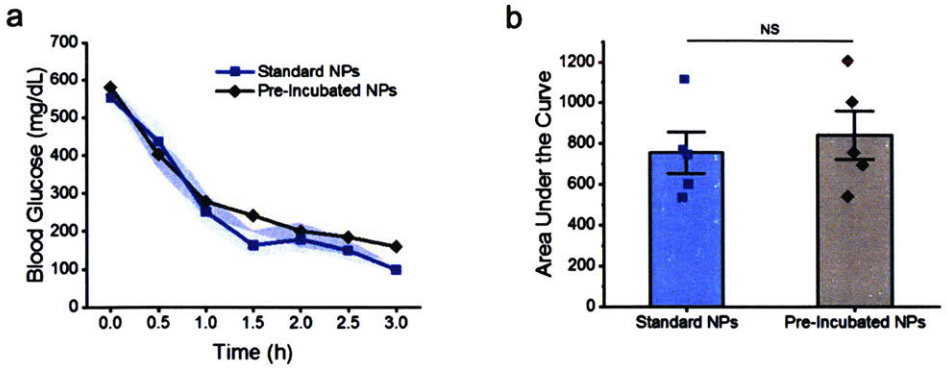

Figure A.2-3. Comparison of standard and pre-incubated NPs in reducing the blood glucose (BG) levels of diabetic mice. a) BG levels of nanoparticles or nanoparticles that were first incubated for 1 h in vitro and resuspended in fresh buffer prior to injection. b) Area under the curve for NPs in (a). Shaded regions and error bars represent standard error of the mean. Statistical significance is indicated by NS: $p > 0.05$.

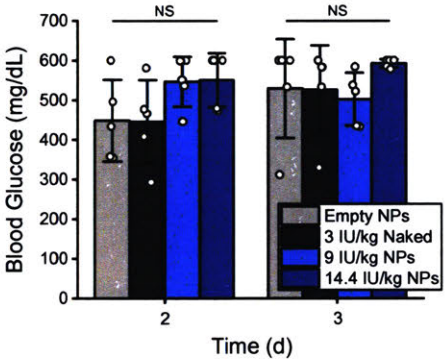

Figure A.2-4. BG levels of diabetic mice receiving empty NPs, 3 IU/kg naked insulin, or NPs at insulin doses of 9 and 14.4 IU/kg 2 and 3 days post injection. Statistical significance is indicated by NS: $p > 0.05$.

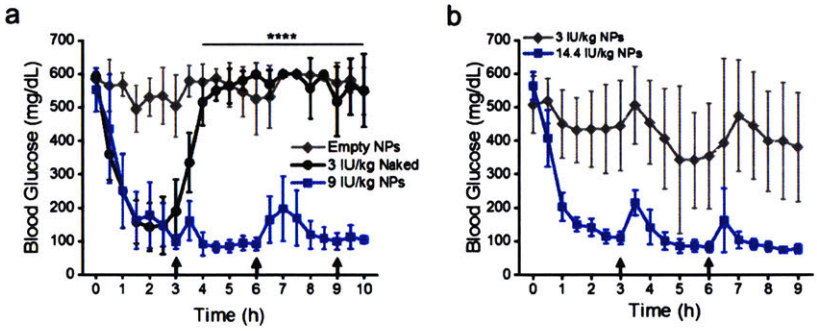

Figure A.2-5. BG levels of diabetic mice receiving NPs at insulin doses of 3, 9, and 14.4 IU/kg. a) BG levels of diabetic mice upon injection of empty NPs, 3 IU/kg naked insulin, or NPs containing 9 IU/kg insulin. Arrows represent intraperitoneal glucose tolerance tests (GTTs) at 3 h (1.5 g/kg), 6 h (2 g/kg), and 9 h (1.5 g/kg). b) BG levels of diabetic mice upon injection of 3 or 14 IU/kg NPs. Arrows represent 1.5 g/kg GTTs. Statistical significance is indicated by ****$p < 0.0001$.

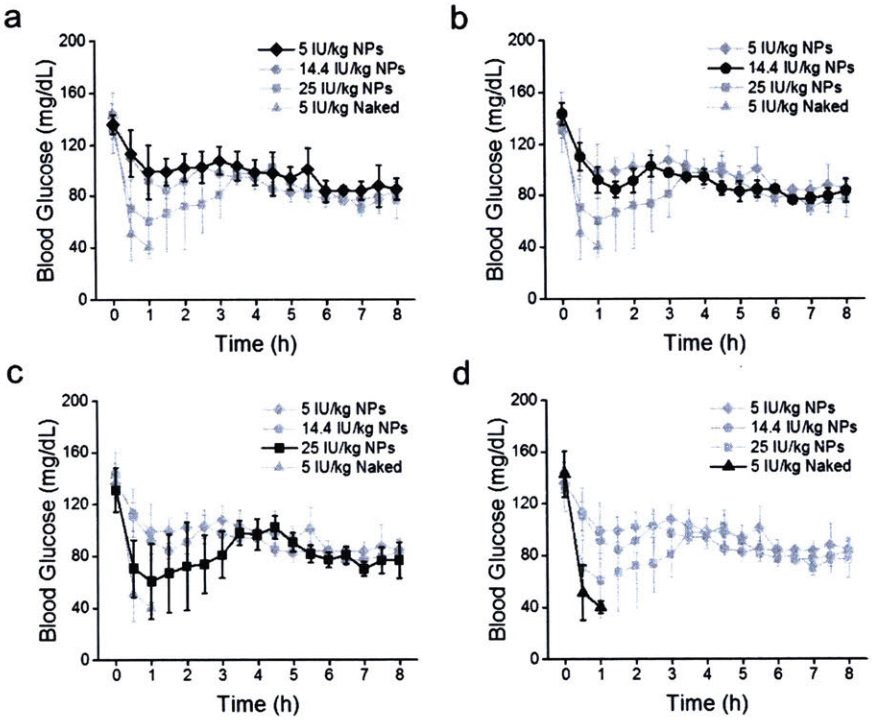

Figure A.2-6. BG levels of healthy mice receiving NPs at insulin doses of 5, 14.4, and 25 IU/kg. BG levels of healthy mice upon injection of a) NPs at an insulin dose of 5 IU/kg, b) NPs at an insulin dose of 14.4 IU/kg, c) NPs at an insulin dose of 25 IU/kg, and d) 5 IU/kg naked insulin. Severely hypoglycemic mice in (d) were administered glucose after 1 h.

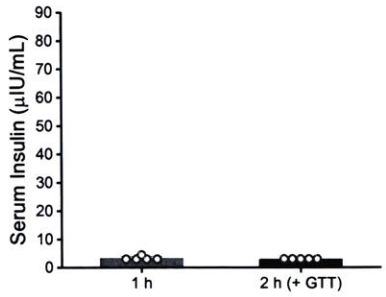

Figure A.2-7. Supplemental serum human insulin levels of healthy mice. Serum insulin levels of healthy mice 1 h after administration of NP(– Insulin) or 2 h after administration with a GTT at 1 h (3 g/kg). Values below the standard curve are reported as less than or equal to 3 μIU/mL, the limit of detection of the ELISA.

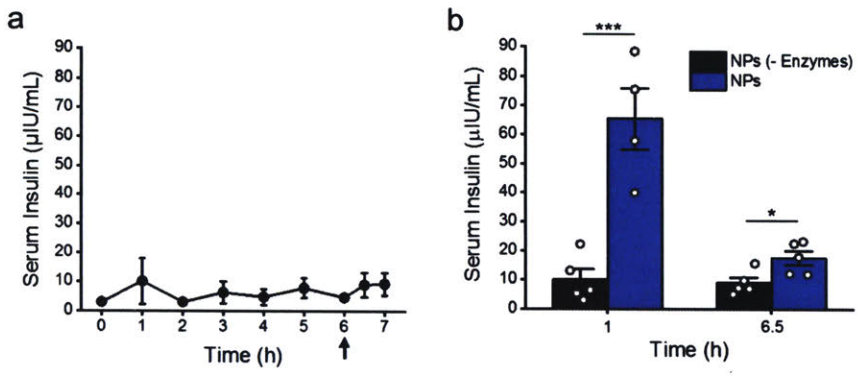

Figure A.2-8. Supplemental serum human insulin levels of diabetic mice. a) Serum insulin levels of diabetic mice upon injection of NP(– Enzymes) at an insulin dose of 9 IU/kg with a GTT at 6 hours (2 g/kg). b) Serum insulin levels of diabetic mice receiving NP(– Enzymes) or NPs at an insulin dose of 9 IU/kg 1 h and 6.5 h after administration. Data represent mean ± standard deviation (a) or standard error of the mean (b). Statistical significance is indicated by *$p < 0.05$, ***$p < 0.001$.

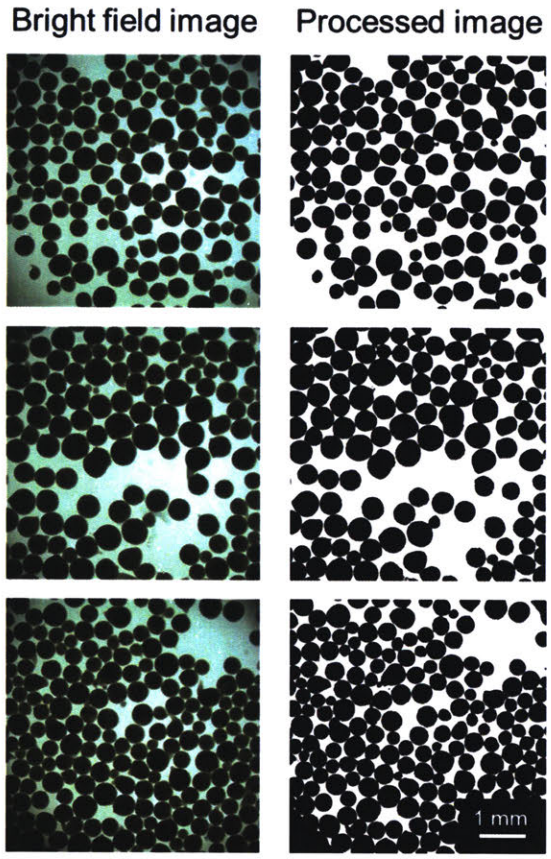

Figure A.3-1. Additional bright field and 8-bit images processed using ImageJ software.

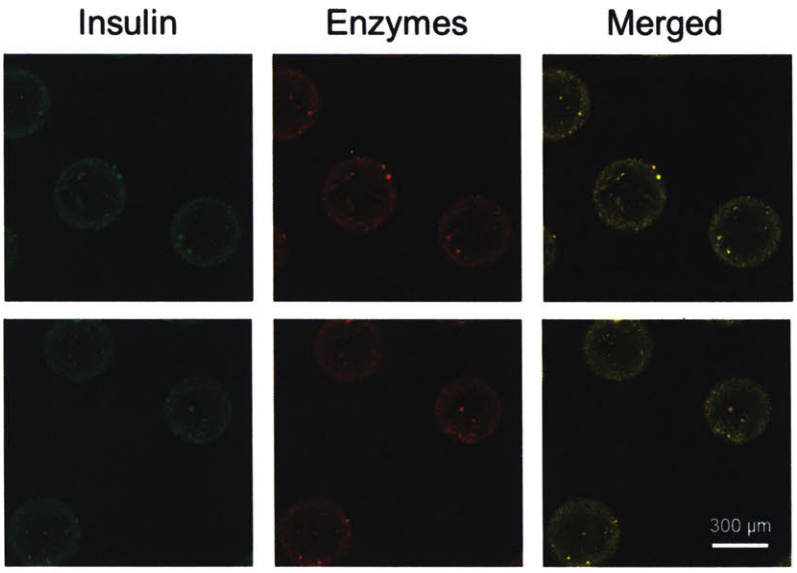

Figure A.3-2. Single z-plane confocal images. Microgels containing NPs encapsulated with FITC-insulin and AF647-GOx; left: 495 nm channel, center: 647 nm channel, right: overlay.

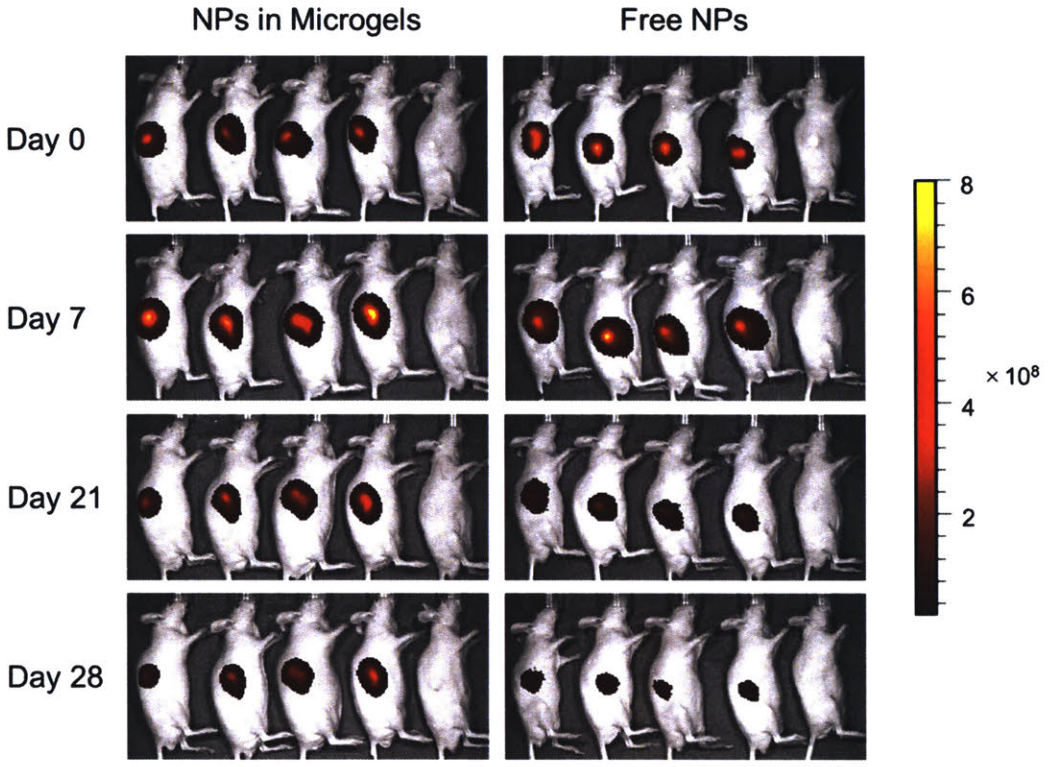

Figure A.3-3. Additional in vivo fluorescent images. NP-encapsulated microgels or free NPs containing AF680-dextran (10 kDa) subcutaneously injected in mice at a dose of 35 mg NP/kg.

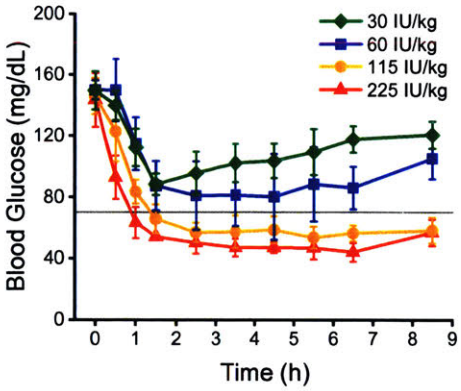

Figure A.3-4. BG levels of healthy mice receiving microgels at insulin doses of 30, 60, 115, and 225 IU/kg. Data represent mean ± standard deviation.

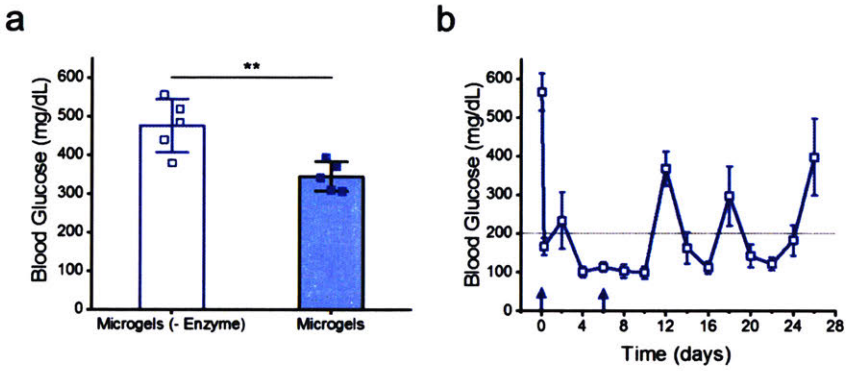

Figure A.3-5. Supplemental BG levels of diabetic mice. a) BG levels of diabetic mice 6 days after receiving a dose of 60 IU/kg microgels with or without enzymes, prior to administration of a second dose.b) BG levels of diabetic mice following subcutaneous dosing of 60 IU/kg microgels without enzymes at days 0 and 6. Data represent mean ± standard deviation. Statistical significance is indicated by **p < 0.01.

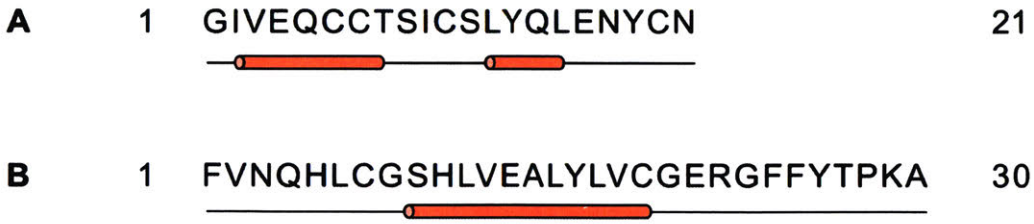

Figure A.4-1. Primary structure of insulin. Alpha helicies are represented beneath their contributing residues.

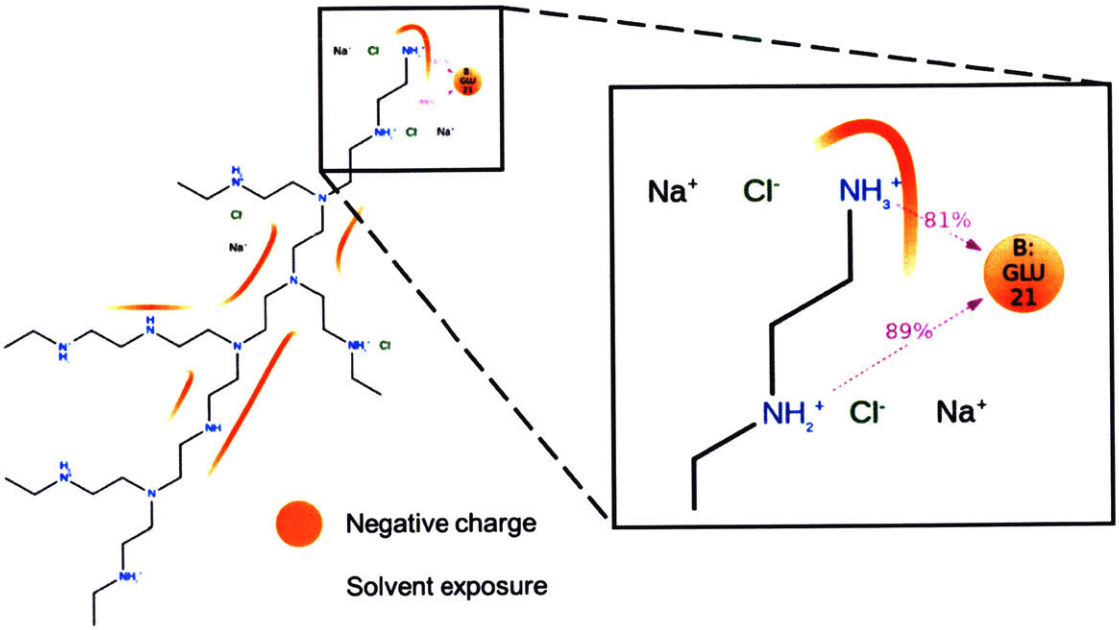

Figure A.4-2. PEI interactions in molecular dynamics simulations. Interactions that occur for more than 30% of the simulation time are shown in orange. The box depicts an example interaction between the positively charged amines of PEI and the free glutamic acid residue of insulin.

Appendix B: References

1 Cho, N , Shaw, J , Karuranga, S , Huang, Y , da Rocha Fernandes, J , Ohlrogge, A , Malanda, B , IDF Diabetes Atlas Global estimates of diabetes prevalence for 2017 and projections for 2045 *Diabetes Res Clin Pract* **2018,** *138*, 271-281
2 Association, A D , Economic costs of diabetes in the US in 2017 *Diabetes Care* **2018,** *41* (5), 917-928
3 Banting, F , Best, C H , Collip, J B , Campbell, W R , Fletcher, A A , Pancreatic extracts in the treatment of diabetes mellitus *Can. Med Assoc. J* **1922,** *12* (3), 141
4 Matthews, D , Hosker, J , Rudenski, A , Naylor, B , Treacher, D , Turner, R , Homeostasis model assessment insulin resistance and β-cell function from fasting plasma glucose and insulin concentrations in man *Diabetologia* **1985,** *28* (7), 412-419
5 Maechler, P , Wollheim, C B , Mitochondrial function in normal and diabetic β-cells *Nature* **2001,** *414* (6865), 807-812
6 Daneman, D , Type 1 diabetes *The Lancet* **2006,** *367* (9513), 847-858
7 Butler, A E , Janson, J , Bonner-Weir, S , Ritzel, R , Rizza, R A , Butler, P C , β-cell deficit and increased β-cell apoptosis in humans with type 2 diabetes *Diabetes* **2003,** *52* (1), 102-110
8 Group, D P P R , Reduction in the incidence of type 2 diabetes with lifestyle intervention or metformin *The New England journal of medicine* **2002,** *346* (6), 393
9 Nathan, D M , Long-term complications of diabetes mellitus *New Engl J Med* **1993,** *328* (23), 1676-1685
10 Giovannucci, E , Harlan, D M , Archer, M C , Bergenstal, R M , Gapstur, S M , Habel, L A , Pollak, M , Regensteiner, J G , Yee, D , Diabetes and cancer a consensus report *CA Cancer J. Clin* **2010,** *60* (4), 207-221
11 Control, D , Group, C T R , The effect of intensive treatment of diabetes on the development and progression of long-term complications in insulin-dependent diabetes mellitus *N. Engl J Med* **1993,** *1993* (329), 977-986
12 Ohkubo, Y , Kishikawa, H , Araki, E , Miyata, T , Isami, S , Motoyoshi, S , Kojima, Y , Furuyoshi, N , Shichiri, M , Intensive insulin therapy prevents the progression of diabetic microvascular complications in Japanese patients with non-insulin-dependent diabetes mellitus a randomized prospective 6-year study *Diabetes Res Clin Pract* **1995,** *28* (2), 103-117
13 Claxton, A J , Cramer, J , Pierce, C , A systematic review of the associations between dose regimens and medication compliance *Clin Ther* **2001,** *23* (8), 1296-1310
14 Peyrot, M , Barnett, A , Meneghini, L , Schumm-Draeger, P M , Insulin adherence behaviours and barriers in the multinational Global Attitudes of Patients and Physicians in Insulin Therapy study *Diabet Med* **2012,** *29* (5), 682-689
15 Seaquist, E R , Miller, M E , Bonds, D E , Feinglos, M , Goff, D C , Peterson, K , Senior, P , Investigators, A , The impact of frequent and unrecognized hypoglycemia on mortality in the ACCORD study *Diabetes Care* **2012,** *35* (2), 409-414
16 Cryer, P E , Hypoglycemia, functional brain failure, and brain death *J Clin Invest* **2007,** *117* (4), 868
17 McCoy, R G , Van Houten, H K , Ziegenfuss, J Y , Shah, N D , Wermers, R A , Smith, S A , Increased mortality of patients with diabetes reporting severe hypoglycemia *Diabetes Care* **2012,** *35* (9), 1897-1901
18 Siebenhofer, A A , Plank, J J , Berghold, A A , Narath, M M , Gfrerer, R R , Pieber, T R , Short acting insulin analogues versus regular human insulin in patients with diabetes mellitus *Cochrane Database of Systematic Reviews* **2004,** (4)
19 Peterson, G E , Intermediate and long-acting insulins a review of NPH insulin, insulin glargine and insulin detemir *Curr Med Res Opin* **2006,** *22* (12), 2613-2619
20 Horvath, K , Jeitler, K , Berghold, A , Ebrahim, S H , Gratzer, T W , Plank, J , Kaiser, T , Pieber, T R , Siebenhofer, A , Long-acting insulin analogues versus NPH insulin (human isophane insulin) for type 2 diabetes mellitus *Cochrane database of systematic reviews* **2007,** (2)
21 Pickup, J , Keen, H , Continuous subcutaneous insulin infusion at 25 years *Diabetes Care* **2002,** *25* (3), 593-598
22 Hovorka, R , Closed-loop insulin delivery from bench to clinical practice *Nature Reviews Endocrinology* **2011,** *7* (7), 385-395
23 Bequette, B W , Challenges and recent progress in the development of a closed-loop artificial pancreas *Annual reviews in control* **2012,** *36* (2), 255-266

24 DeSalvo, D , Buckingham, B , Continuous glucose monitoring current use and future directions *Curr Diab Rep* **2013,** *13* (5), 657-662
25 Klueh, U , Liu, Z , Feldman, B , Henning, T P , Cho, B , Ouyang, T , Kreutzer, D , Metabolic biofouling of glucose sensors in vivo role of tissue microhemorrhages SAGE Publications 2011
26 Rodbard, D , Continuous glucose monitoring: a review of successes, challenges, and opportunities *Diabetes Technol Ther* **2016,** *18* (S2), S2-3-S2-13
27 Cramer, J , Benedict, A , Muszbek, N , Keskinaslan, A , Khan, Z , The significance of compliance and persistence in the treatment of diabetes, hypertension and dyslipidaemia a review *Int J. Clin Pract* **2008,** *62* (1), 76-87
28 Rubin, R R , Adherence to pharmacologic therapy in patients with type 2 diabetes mellitus *The American journal of medicine* **2005,** *118* (5), 27-34
29 Richter, A , Anton, S E , Koch, P , Dennett, S L , The impact of reducing dose frequency on health outcomes *Clin Ther* **2003,** *25* (8), 2307-2335
30 Ravaine, V , Ancla, C , Catargi, B , Chemically controlled closed-loop insulin delivery *J Controlled Release* **2008,** *132* (1), 2-11
31 Yang, J , Cao, Z , Glucose-responsive insulin release Analysis of mechanisms, formulations, and evaluation criteria *J Controlled Release* **2017**
32 Oda, Y , Kasai, K -i , Ishii, S -i , Studies on the specific interaction of concanavalin A and saccharides by affinity chromatography Application of quantitative affinity chromatography to a multivalent system *The Journal of Biochemistry* **1981,** *89* (1), 285-296
33 Shimura, K , Kasai, K -i , Determination of the affinity constants of concanavalin A for monosaccharides by fluorescence affinity probe capillary electrophoresis *Anal Biochem* **1995,** *227* (1), 186-194
34 Brownlee, M , Cerami, A , A glucose-controlled insulin-delivery system semisynthetic insulin bound to lectin *Science* **1979,** *206* (4423), 1190-1191
35 Taylor, M J , Tanna, S , Sahota, T , In vivo study of a polymeric glucose-sensitive insulin delivery system using a rat model *J. Pharm Sci* **2010,** *99* (10), 4215-4227
36 Wu, S , Huang, X , Du, X , Glucose-and pH-responsive controlled release of cargo from protein-gated carbohydrate-functionalized mesoporous silica nanocontainers *Angew Chem Int Ed* **2013,** *52* (21), 5580-5584
37 Kaarsholm, N C , Lin, S , Yan, L , Kelly, T , van Heek, M , Mu, J , Wu, M , Dai, G , Cui, Y , Zhu, Y , Engineering glucose responsiveness into insulin *Diabetes* **2018,** *67* (2), 299-308
38 Zion, T C , Lancaster, T C , Conjugate based systems for controlled drug delivery Google Patents 2010
39 Krug, A W , Visser, S A , Tsai, K , Kandala, B , Fancourt, C , Thornton, B , Morrow, L , Kaarsholm, N C , Bernstein, H S , Stoch, S A , Clinical Evaluation of MK-2640 An Insulin Analog With Glucose-Responsive Properties *Clin Pharmacol Ther* **2019,** *105* (2), 417-425
40 Wang, C , Ye, Y , Sun, W , Yu, J , Wang, J , Lawrence, D S , Buse, J B , Gu, Z , Red blood cells for glucose-responsive insulin delivery *Adv Mater* **2017,** *29* (18), 1606617
41 Wang, J , Yu, J , Zhang, Y , Kahkoska, A R , Wang, Z , Fang, J , Whitelegge, J P , Li, S , Buse, J B , Gu, Z , Glucose transporter inhibitor-conjugated insulin mitigates hypoglycemia *Proceedings of the National Academy of Sciences* **2019,** *116* (22), 10744-10748
42 Yin, R , Wang, K , Han, J , Nie, J , Photo-crosslinked glucose-sensitive hydrogels based on methacrylate modified dextran–concanavalin A and PEG dimethacrylate *Carbohydr Polym* **2010,** *82* (2), 412-418
43 Yin, R , He, J , Bai, M , Huang, C , Wang, K , Zhang, H , Yang, S -M , Zhang, W , Engineering synthetic artificial pancreas using chitosan hydrogels integrated with glucose-responsive microspheres for insulin delivery *Materials Science and Engineering. C* **2019,** *96*, 374-382
44 Lin, K , Yi, J , Mao, X , Wu, H , Zhang, L -M , Yang, L , Glucose-sensitive hydrogels from covalently modified carboxylated pullulan and concanavalin A for smart controlled release of insulin *React Funct Polym* **2019,** *139*, 112-119
45 Yin, R , Wang, K , Du, S , Chen, L , Nie, J , Zhang, W , Design of genipin-crosslinked microgels from concanavalin A and glucosyloxyethyl acrylated chitosan for glucose-responsive insulin delivery *Carbohydr Polym* **2014,** *103*, 369-376
46 Yin, R , Tong, Z , Yang, D , Nie, J , Glucose-responsive microhydrogels based on methacrylate modified dextran/concanavalin A for insulin delivery *J Controlled Release* **2011,** *152*, e163-e165

47 Yin, R., Tong, Z., Yang, D., Nie, J., Glucose-responsive insulin delivery microhydrogels from methacrylated dextran/concanavalin A preparation and in vitro release study *Carbohydr Polym* **2012,** *89* (1), 117-123

48 Yin, R., Tong, Z., Yang, D., Nie, J., Glucose and pH dual-responsive concanavalin A based microhydrogels for insulin delivery *Int J Biol Macromol* **2011,** *49* (5), 1137-1142

49 Yin, R., Han, J., Zhang, J., Nie, J., Glucose-responsive composite microparticles based on chitosan, concanavalin A and dextran for insulin delivery *Colloids Surf B Biointerfaces* **2010,** *76* (2), 483-488

50 Ye, T., Yan, S., Hu, Y., Ding, L., Wu, W., Synthesis and volume phase transition of concanavalin A-based glucose-responsive nanogels *Polymer Chemistry* **2014,** *5* (1), 186-194

51 Yan, J., Springsteen, G., Deeter, S., Wang, B., The relationship among pKa, pH, and binding constants in the interactions between boronic acids and diols—it is not as simple as it appears *Tetrahedron* **2004,** *60* (49), 11205-11209

52 Zhdankin, V. V., Persichini III, P., Zhang, L., Fix, S., Kiprof, P., Synthesis and structure of benzoboroxoles novel organoboron heterocycles *Tetrahedron Lett* **1999,** *40* (37), 6705-6708

53 Wulff, G., Lauer, M., Bohnke, H., Rapid proton transfer as cause of an unusually large neighboring group effect *Angewandte Chemie International Edition in English* **1984,** *23* (9), 741-742

54 Kitano, S., Hisamitsu, I., Koyama, Y., Kataoka, K., Okano, T., Sakurai, Y., Effect of the incorporation of amino groups in a glucose-responsive polymer complex having phenylboronic acid moieties *Polym Adv Technol* **1991,** *2* (5), 261-264

55 Tomsho, J. W., Pal, A., Hall, D. G., Benkovic, S. J., Ring Structure and Aromatic Substituent Effects on the p K a of the Benzoxaborole Pharmacophore *ACS Med Chem Lett* **2011,** *3* (1), 48-52

56 Yesilyurt, V., Webber, M. J., Appel, E. A., Godwin, C., Langer, R., Anderson, D. G., Injectable Self-Healing Glucose-Responsive Hydrogels with pH-Regulated Mechanical Properties *Adv Mater* **2016,** *28* (1), 86-91

57 Dong, Y., Wang, W., Veiseh, O., Appel, E. A., Xue, K., Webber, M. J., Tang, B. C., Yang, X.-W., Weir, G. C., Langer, R., Injectable and glucose-responsive hydrogels based on boronic acid–glucose complexation *Langmuir* **2016,** *32* (34), 8743-8747

58 Kotsuchibashi, Y., Agustin, R. V. C., Lu, J.-Y., Hall, D. G., Narain, R., Temperature, pH, and glucose responsive gels via simple mixing of boroxole-and glyco-based polymers *ACS Macro Letters* **2013,** *2* (3), 260-264

59 Ma, R., Yang, H., Li, Z., Liu, G., Sun, X., Liu, X., An, Y., Shi, L., Phenylboronic acid-based complex micelles with enhanced glucose-responsiveness at physiological pH by complexation with glycopolymer *Biomacromolecules* **2012,** *13* (10), 3409-3417

60 Sinha, A., Chakraborty, A., Jana, N. R., Dextran-gated, multifunctional mesoporous nanoparticle for glucose-responsive and targeted drug delivery *ACS applied materials & interfaces* **2014,** *6* (24), 22183-22191

61 Yilmaz, M. D., Xue, M., Ambrogio, M. W., Buyukcakir, O., Wu, Y., Frasconi, M., Chen, X., Nassar, M. S., Stoddart, J. F., Zink, J. I., Sugar and pH dual-responsive mesoporous silica nanocontainers based on competitive binding mechanisms *Nanoscale* **2015,** *7* (3), 1067-1072

62 Chou, D. H.-C., Webber, M. J., Tang, B. C., Lin, A. B., Thapa, L. S., Deng, D., Truong, J. V., Cortinas, A. B., Langer, R., Anderson, D. G., Glucose-responsive insulin activity by covalent modification with aliphatic phenylboronic acid conjugates *Proceedings of the National Academy of Sciences* **2015,** *112* (8), 2401-2406

63 Tang, Z., Guan, Y., Zhang, Y., Contraction-type glucose-sensitive microgel functionalized with a 2-substituted phenylboronic acid ligand *Polymer Chemistry* **2014,** *5* (5), 1782-1790

64 Tang, Z., Guan, Y., Zhang, Y., The synthesis of a contraction-type glucose-sensitive microgel working at physiological temperature guided by a new glucose-sensing mechanism *Polymer Chemistry* **2018,** *9* (8), 1012-1021

65 Matsumoto, A., Ishii, T., Nishida, J., Matsumoto, H., Kataoka, K., Miyahara, Y., A synthetic approach toward a self-regulated insulin delivery system *Angew Chem Int Ed* **2012,** *51* (9), 2124-2128

66 Matsumoto, A., Tanaka, M., Matsumoto, H., Ochi, K., Moro-Oka, Y., Kuwata, H., Yamada, H., Shirakawa, I., Miyazawa, T., Ishii, H., Synthetic "smart gel" provides glucose-responsive insulin delivery in diabetic mice *Science advances* **2017,** *3* (11), eaaq0723

67 Chen, S , Matsumoto, H , Moro-oka, Y , Tanaka, M , Miyahara, Y , Suganami, T , Matsumoto, A , Microneedle-array patch fabricated with enzyme-free polymeric components capable of on-demand insulin delivery *Adv Funct Mater* **2019,** *29* (7), 1807369

68 Chen, S , Matsumoto, H , Moro-oka, Y , Tanaka, M , Miyahara, Y , Suganami, T , Matsumoto, A , Smart Microneedle Fabricated with Silk Fibroin Combined Semi-interpenetrating Network Hydrogel for Glucose-Responsive Insulin Delivery *ACS Biomaterials Science & Engineering* **2019**

69 Zhao, L , Ding, J , Xiao, C , He, P , Tang, Z , Pang, X , Zhuang, X , Chen, X , Glucose-sensitive polypeptide micelles for self-regulated insulin release at physiological pH *J Mater Chem* **2012,** *22* (24), 12319-12328

70 Yao, Y , Zhao, L , Yang, J , Yang, J , Glucose-responsive vehicles containing phenylborate ester for controlled insulin release at neutral pH *Biomacromolecules* **2012,** *13* (6), 1837-1844

71 Kim, H , Kang, Y J , Kang, S , Kim, K T , Monosaccharide-responsive release of insulin from polymersomes of polyboroxole block copolymers at neutral pH *J Am Chem Soc* **2012,** *134* (9), 4030-4033

72 Zhang, G , Zhang, X , Shen, H , Yang, J , Yang, J , Smarter glucose-sensitivity of polymeric micelles formed from phenylborate ester-co-pyrenylboronic ester for insulin delivery at physiological pH *RSC Advances* **2014,** *4* (91), 49964-49973

73 Jiang, G , Jiang, T , Chen, H , Li, L , Liu, Y , Zhou, H , Feng, Y , Zhou, J , Preparation of multi-responsive micelles for controlled release of insulin *Colloid Polym Sci* **2015,** *293* (1), 209-215

74 Wen, N , Gao, C , Lu, S , Xu, X , Bai, X , Wu, C , Ning, P , Zhang, S , Liu, M , Novel amphiphilic glucose-responsive modified starch micelles for insulin delivery *RSC Advances* **2017,** *7* (73), 45978-45986

75 Wang, J , Yu, J , Zhang, Y , Zhang, X , Kahkoska, A R , Chen, G , Wang, Z , Sun, W , Cai, L , Chen, Z , Charge-switchable polymeric complex for glucose-responsive insulin delivery in mice and pigs *Science advances* **2019,** *5* (7), eaaw4357

76 Liang, J , Ma, Y , Sims, S , Wu, L , A patterned porous polymer film for localized capture of insulin and glucose-responsive release *Journal of Materials Chemistry B* **2015,** *3* (7), 1281-1288

77 Shan, M , Gong, C , Li, B , Wu, G , A pH, glucose, and dopamine triple-responsive, self-healable adhesive hydrogel formed by phenylborate–catechol complexation *Polymer Chemistry* **2017,** *8* (19), 2997-3005

78 Lee, J , Ko, J H , Mansfield, K M , Nauka, P C , Bat, E , Maynard, H D , Glucose-Responsive Trehalose Hydrogel for Insulin Stabilization and Delivery *Macromol Biosci* **2018,** *18* (5), 1700372

79 Cai, B , Luo, Y , Guo, Q , Zhang, X , Wu, Z , A glucose-sensitive block glycopolymer hydrogel based on dynamic boronic ester bonds for insulin delivery *Carbohydr Res* **2017,** *445*, 32-39

80 Yang, T , Ji, R , Deng, X -X , Du, F -S , Li, Z -C , Glucose-responsive hydrogels based on dynamic covalent chemistry and inclusion complexation *Soft Matter* **2014,** *10* (15), 2671-2678

81 Xu, X , Shang, H , Zhang, T , Shu, P , Liu, Y , Xie, J , Zhang, D , Tan, H , Li, J , A stimuli-responsive insulin delivery system based on reversible phenylboronate modified cyclodextrin with glucose triggered host-guest interaction *Int J Pharm* **2018,** *548* (1), 649-658

82 Yang, H , Sun, X , Liu, G , Ma, R , Li, Z , An, Y , Shi, L , Glucose-responsive complex micelles for self-regulated release of insulin under physiological conditions *Soft Matter* **2013,** *9* (35), 8589-8599

83 Wu, G , Li, C , Liu, X , Lv, J , Ding, Y , Liu, Y , Liu, Y , Huang, F , Shi, L , An, Y , Glucose-responsive complex micelles for self-regulated delivery of insulin with effective protection of insulin and enhanced hypoglycemic activity in vivo *Colloids Surf B Biointerfaces* **2019,** *180*, 376-383

84 Gaballa, H , Theato, P , Glucose-Responsive Polymeric Micelles via Boronic Acid–Diol Complexation for Insulin Delivery at Neutral pH *Biomacromolecules* **2019,** *20* (2), 871-881

85 Zhao, L , Xiao, C , Ding, J , Zhuang, X , Gai, G , Wang, L , Chen, X , Competitive binding-accelerated insulin release from a polypeptide nanogel for potential therapy of diabetes *Polymer Chemistry* **2015,** *6* (20), 3807-3815

86 Si, X , Song, W , Yang, S , Ma, L , Yang, C , Tang, Z , Glucose and pH Dual-Responsive Nanogels for Efficient Protein Delivery *Macromol Biosci* **2019**, 1900148

87 Guo, Q , Wu, Z , Zhang, X , Sun, L , Li, C , Phenylboronate-diol crosslinked glycopolymeric nanocarriers for insulin delivery at physiological pH *Soft Matter* **2014,** *10* (6), 911-920

88 Chai, Z , Ma, L , Wang, Y , Ren, X , Phenylboronic acid as a glucose-responsive trigger to tune the insulin release of glycopolymer nanoparticles *J Biomater Sci Polym Ed* **2016,** *27* (7), 599-610

89 Guo, H , Li, H , Gao, J , Zhao, G , Ling, L , Wang, B , Guo, Q , Gu, Y , Li, C , Phenylboronic acid-based amphiphilic glycopolymeric nanocarriers for in vivo insulin delivery *Polymer Chemistry* **2016,** *7* (18), 3189-3199

90 Guo, H , Guo, Q , Chu, T , Zhang, X , Wu, Z , Yu, D , Glucose-sensitive polyelectrolyte nanocapsules based on layer-by-layer technique for protein drug delivery *J. Mater Sci Mater Med* **2014,** *25* (1), 121-129

91 Matuszewska, A , Uchman, M , Adamczyk-Woźniak, A , Sporzyński, A , Pispas, S , Kováčik, L , Štěpánek, M , Glucose-responsive hybrid nanoassemblies in aqueous solutions ordered phenylboronic acid within intermixed poly (4-hydroxystyrene)-block-poly (ethylene oxide) block copolymer *Biomacromolecules* **2015,** *16* (12), 3731-3739

92 Wang, Y , Huang, F , Sun, Y , Gao, M , Chai, Z , Development of shell cross-linked nanoparticles based on boronic acid-related reactions for self-regulated insulin delivery *J Biomater Sci Polym Ed* **2017,** *28* (1), 93-106

93 Wang, Y , Zhang, X , Han, Y , Cheng, C , Li, C , pH-and glucose-sensitive glycopolymer nanoparticles based on phenylboronic acid for triggered release of insulin *Carbohydr Polym* **2012,** *89* (1), 124-131

94 Shi, D , Ran, M , Zhang, L , Huang, H , Li, X , Chen, M , Akashi, M , Fabrication of biobased polyelectrolyte capsules and their application for glucose-triggered insulin delivery *ACS applied materials & interfaces* **2016,** *8* (22), 13688-13697

95 Yang, H , Zhang, C , Li, C , Liu, Y , An, Y , Ma, R , Shi, L , Glucose-responsive polymer vesicles templated by α-CD/PEG inclusion complex *Biomacromolecules* **2015,** *16* (4), 1372-1381

96 Wang, W , Liao, L , Zhang, X , Lei, F , Zhang, Y , Liu, G , Xie, W , An Intelligent Nanoscale Insulin Delivery System *Molecules* **2018,** *23* (11), 2945

97 Matsumoto, A , Yuasa, M , Matsumoto, H , Sanjo, M , Tabata, M , Goda, T , Hoshi, T , Aoyagi, T , Miyahara, Y , Boronate-functionalized Polymer Gel-based Insulin Delivery System with Improved Stability in Performance A Comparative Structure–Function Study *Chem Lett* **2016,** *45* (4), 460-462

98 Elshaarani, T , Yu, H , Wang, L , Ullah, R S , Fahad, S , Rahman, K U , Khan, A , Nazir, A , Usman, M , Khan, R U , Glucose-responsive nanostructured hydrogels with enhanced elastic and swelling properties *Journal of Materials Science* **2019,** *54* (13), 10009-10023

99 Shen, Y , Xu, Z , Li, L , Yuan, W , Luo, M , Xie, X , Fabrication of glucose-responsive and biodegradable copolymer membrane for controlled release of insulin at physiological pH *New J Chem* **2019,** *43* (20), 7822-7830

100 Liu, G , Ma, R , Ren, J , Li, Z , Zhang, H , Zhang, Z , An, Y , Shi, L , A glucose-responsive complex polymeric micelle enabling repeated on–off release and insulin protection *Soft Matter* **2013,** *9* (5), 1636-1644

101 Wen, N , Lu, S , Gao, C , Xu, X , Bai, X , Wu, C , Ning, P , Liu, M , Glucose-responsive zwitterionic dialdehyde starch-based micelles with potential anti-phagocytic behavior for insulin delivery *Chem Eng. J* **2018,** *335*, 52-62

102 Zhang, X , Lu, S , Gao, C , Chen, C , Zhang, X , Liu, M , Highly stable and degradable multifunctional microgel for self-regulated insulin delivery under physiological conditions *Nanoscale* **2013,** *5* (14), 6498-6506

103 Belbekhouche, S , Charaabi, S , Carbonnier, B , Glucose-sensitive capsules based on hydrogen-bonded (polyvinylpyrrolidone/phenylboronic–modified alginate) system *Colloids Surf B. Biointerfaces* **2019,** *177*, 416-424

104 Wu, J -Z , Williams, G R , Li, H -Y , Wang, D -X , Li, S -D , Zhu, L -M , Insulin-loaded PLGA microspheres for glucose-responsive release *Drug Deliv* **2017,** *24* (1), 1513-1525

105 Lee, D , Choe, K , Jeong, Y , Yoo, J , Lee, S M , Park, J -H , Kim, P , Kim, Y -C , Establishment of a controlled insulin delivery system using a glucose-responsive double-layered nanogel *RSC Advances* **2015,** *5* (19), 14482-14491

106 Wu, Z , Zhang, X , Guo, H , Li, C , Yu, D , An injectable and glucose-sensitive nanogel for controlled insulin release *J Mater Chem* **2012,** *22* (42), 22788-22796

107 Kim, H , Kang, Y J , Jeong, E S , Kang, S , Kim, K T , Glucose-responsive disassembly of polymersomes of sequence-specific boroxole-containing block copolymers under physiologically relevant conditions *Acs Macro Letters* **2012,** *1* (10), 1194-1198

108 Wilson, R , Turner, A , Glucose oxidase an ideal enzyme *Biosensors Bioelectron* **1992,** *7* (3), 165-185

109 Bankar, S B , Bule, M V , Singhal, R S , Ananthanarayan, L , Glucose oxidase—an overview *Biotechnol. Adv* **2009,** *27* (4), 489-501

110 Ishihara, K , Kobayashi, M , Ishimaru, N , Shinohara, I , Glucose induced permeation control of insulin through a complex membrane consisting of immobilized glucose oxidase and a poly (amine) *Polym J* **1984,** *16* (8), 625

111 Kost, J , Horbett, T A , Ratner, B D , Singh, M , Glucose-sensitive membranes containing glucose oxidase Activity, swelling, and permeability studies *Journal of Biomedical Materials Research Part A* **1985,** *19* (9), 1117-1133

112 Ito, Y , Casolaro, M , Kono, K , Imanishi, Y , An insulin-releasing system that is responsive to glucose *J Controlled Release* **1989,** *10* (2), 195-203

113 Brown, L R , Edelman, E R , Fischel-Ghodsian, F , Langer, R , Characterization of glucose-mediated insulin release from implantable polymers *J Pharm Sci* **1996,** *85* (12), 1341-1345

114 Podual, K , Doyle, F , Peppas, N , Preparation and dynamic response of cationic copolymer hydrogels containing glucose oxidase *Polymer* **2000,** *41* (11), 3975-3983

115 Podual, K , Doyle, F J , Peppas, N A , Glucose-sensitivity of glucose oxidase-containing cationic copolymer hydrogels having poly (ethylene glycol) grafts *J Controlled Release* **2000,** *67* (1), 9-17

116 Podual, K , Doyle Iii, F J , Peppas, N A , Dynamic behavior of glucose oxidase-containing microparticles of poly (ethylene glycol)-grafted cationic hydrogels in an environment of changing pH *Biomaterials* **2000,** *21* (14), 1439-1450

117 Gordijo, C R , Koulajian, K , Shuhendler, A J , Bonifacio, L D , Huang, H Y , Chiang, S , Ozin, G A , Giacca, A , Wu, X Y , Nanotechnology-enabled closed loop insulin delivery device In vitro and in vivo evaluation of glucose-regulated insulin release for diabetes control *Adv. Funct Mater* **2011,** *21* (1), 73-82

118 Gu, Z , Aimetti, A A , Wang, Q , Dang, T T , Zhang, Y , Veiseh, O , Cheng, H , Langer, R S , Anderson, D G , Injectable nano-network for glucose-mediated insulin delivery *ACS nano* **2013,** *7* (5), 4194-4201

119 Gu, Z , Dang, T T , Ma, M , Tang, B C , Cheng, H , Jiang, S , Dong, Y , Zhang, Y , Anderson, D G , Glucose-responsive microgels integrated with enzyme nanocapsules for closed-loop insulin delivery *ACS nano* **2013,** *7* (8), 6758-6766

120 Fu, M , Zhang, C , Dai, Y , Li, X , Pan, M , Huang, W , Qian, H , Ge, L , Injectable self-assembled peptide hydrogels for glucose-mediated insulin delivery *Biomaterials science* **2018,** *6* (6), 1480-1491

121 Fu, Y , Liu, W , Wang, L y , Zhu, B y , Qu, M k , Yang, L q , Sun, X , Gong, T , Zhang, Z r , Lin, Q , Erythrocyte-Membrane-Camouflaged Nanoplatform for Intravenous Glucose-Responsive Insulin Delivery *Adv Funct Mater.* **2018,** *28* (41), 1802250

122 Xu, B , Jiang, G , Yu, W , Liu, D , Zhang, Y , Zhou, J , Sun, S , Liu, Y , H 2 O 2-responsive mesoporous silica nanoparticles integrated with microneedle patches for the glucose-monitored transdermal delivery of insulin *Journal of Materials Chemistry B* **2017,** *5* (41), 8200-8208

123 Hu, X , Yu, J , Qian, C , Lu, Y , Kahkoska, A R , Xie, Z , Jing, X , Buse, J B , Gu, Z , H2O2-responsive vesicles integrated with transcutaneous patches for glucose-mediated insulin delivery *ACS nano* **2017,** *11* (1), 613-620

124 Wang, J , Ye, Y , Yu, J , Kahkoska, A R , Zhang, X , Wang, C , Sun, W , Corder, R D , Chen, Z , Khan, S A , Core–Shell Microneedle Gel for Self-Regulated Insulin Delivery *ACS nano* **2018,** *12* (3), 2466-2473

125 Xia, D , He, H , Wang, Y , Wang, K , Zuo, H , Gu, H , Xu, P , Hu, Y , Ultrafast glucose-responsive, high loading capacity erythrocyte to self-regulate the release of insulin *Acta Biomater* **2018,** *69*, 301-312

126 Yu, J , Zhang, Y , Ye, Y , DiSanto, R , Sun, W , Ranson, D , Ligler, F S , Buse, J B , Gu, Z , Microneedle-array patches loaded with hypoxia-sensitive vesicles provide fast glucose-responsive insulin delivery *Proceedings of the National Academy of Sciences* **2015,** *112* (27), 8260-8265

127 Yu, J , Qian, C , Zhang, Y , Cui, Z , Zhu, Y , Shen, Q , Ligler, F S , Buse, J B , Gu, Z , Hypoxia and H2O2 dual-sensitive vesicles for enhanced glucose-responsive insulin delivery *Nano Lett* **2017,** *17* (2), 733-739

128 Lim, Z W, Ping, Y, Miserez, A, Glucose-Responsive Peptide Coacervates with High Encapsulation Efficiency for Controlled Release of Insulin *Bioconj Chem* **2018,** *29* (7), 2176-2180
129 Chen, X, Wu, W, Guo, Z, Xin, J, Li, J, Controlled insulin release from glucose-sensitive self-assembled multilayer films based on 21-arm star polymer *Biomaterials* **2011,** *32* (6), 1759-1766
130 Luo, J, Cao, S, Chen, X, Liu, S, Tan, H, Wu, W, Li, J, Super long-term glycemic control in diabetic rats by glucose-sensitive LbL films constructed of supramolecular insulin assembly *Biomaterials* **2012,** *33* (33), 8733-8742
131 Farahani, B V, Ghasemzaheh, H, Afraz, S, Intelligent semi-IPN chitosan–PEG–PAAm hydrogel for closed-loop insulin delivery and kinetic modeling *RSC Advances* **2016,** *6* (32), 26590-26598
132 Yang, X, Kim, J-C, β-Cyclodextrin grafted polyethyleneimine hydrogel immobilizing hydrophobically modified glucose oxidase *Int J Biol Macromol* **2011,** *48* (4), 661-666
133 Li, X, Fu, M, Wu, J, Zhang, C, Deng, X, Dhinakar, A, Huang, W, Qian, H, Ge, L, pH-sensitive peptide hydrogel for glucose-responsive insulin delivery *Acta Biomater* **2017,** *51*, 294-303
134 Gordijo, C R, Shuhendler, A J, Wu, X Y, Glucose-responsive bioinorganic nanohybrid membrane for self-regulated insulin release *Adv Funct Mater* **2010,** *20* (9), 1404-1412
135 Chu, M K, Chen, J, Gordijo, C R, Chiang, S, Ivovic, A, Koulajian, K, Giacca, A, Wu, X Y, Sun, Y, In vitro and in vivo testing of glucose-responsive insulin-delivery microdevices in diabetic rats *Lab on a Chip* **2012,** *12* (14), 2533-2539
136 Chu, L-Y, Li, Y, Zhu, J-H, Wang, H-D, Liang, Y-J, Control of pore size and permeability of a glucose-responsive gating membrane for insulin delivery *J Controlled Release* **2004,** *97* (1), 43-53
137 Duan, Y, Ye, F, Huang, Y, Qin, Y, He, C, Zhao, S, One-pot synthesis of a metal–organic framework-based drug carrier for intelligent glucose-responsive insulin delivery *Chem Commun* **2018,** *54* (42), 5377-5380
138 Chen, W-H, Luo, G-F, Vázquez-González, M, Cazelles, R, Sohn, Y S, Nechushtai, R, Mandel, Y, Willner, I, Glucose-Responsive Metal–Organic-Framework Nanoparticles Act as "Smart" Sense-and-Treat Carriers *ACS nano* **2018,** *12* (8), 7538-7545
139 Li, X, Shang, H, Wu, W, Li, S, Lin, Z, Duan, J, Xu, L, Li, J, Glucose-responsive micelles for controlled insulin release based on transformation from amphiphilic to double hydrophilic *Journal of nanoscience and nanotechnology* **2016,** *16* (6), 5457-5463
140 Wu, Y, Hu, H, Hu, J, Liu, S, Glucose-Regulated Insulin Release from Acid-Disintegrable Microgels Covalently Immobilized with Glucose Oxidase and Catalase *Macromol Rapid Commun* **2012,** *33* (21), 1852-1860
141 Ye, T, Bai, X, Jiang, X, Wu, Q, Chen, S, Qu, A, Huang, J, Shen, J, Wu, W, Glucose-responsive microgels based on apo-enzyme recognition *Polymer Chemistry* **2016,** *7* (16), 2847-2857
142 Kim, M Y, Kim, J, Chitosan microgels embedded with catalase nanozyme-loaded mesocellular silica foam for glucose-responsive drug delivery *ACS Biomaterials Science & Engineering* **2017,** *3* (4), 572-578
143 Di, J, Yu, J, Ye, Y, Ranson, D, Jindal, A, Gu, Z, Engineering synthetic insulin-secreting cells using hyaluronic acid microgels integrated with glucose-responsive nanoparticles *Cell Mol Bioeng* **2015,** *8* (3), 445-454
144 Zhao, W, Zhang, H, He, Q, Li, Y, Gu, J, Li, L, Li, H, Shi, J, A glucose-responsive controlled release of insulin system based on enzyme multilayers-coated mesoporous silica particles *Chem Commun* **2011,** *47* (33), 9459-9461
145 Aznar, E, Villalonga, R, Giménez, C, Sancenón, F, Marcos, M D, Martínez-Máñez, R, Díez, P, Pingarrón, J M, Amorós, P, Glucose-triggered release using enzyme-gated mesoporous silica nanoparticles *Chem Commun* **2013,** *49* (57), 6391-6393
146 Oroval, M, Díez, P, Aznar, E, Coll, C, Marcos, M D, Sancenón, F, Villalonga, R, Martínez-Máñez, R, Self-Regulated Glucose-Sensitive Neoglycoenzyme-Capped Mesoporous Silica Nanoparticles for Insulin Delivery *Chemistry–A European Journal* **2017,** *23* (6), 1353-1360
147 Jamwal, S, Ram, B, Ranote, S, Dharela, R, Chauhan, G S, New glucose oxidase-immobilized stimuli-responsive dextran nanoparticles for insulin delivery *Int J Biol Macromol* **2019,** *123*, 968-978
148 Anirudhan, T, Nair, A S, Nair, S S, Enzyme coated beta-cyclodextrin for effective adsorption and glucose-responsive closed-loop insulin delivery *Int J Biol Macromol* **2016,** *91*, 818-827

149. Xu, C.; Lei, C.; Huang, L.; Zhang, J.; Zhang, H.; Song, H.; Yu, M.; Wu, Y.; Chen, C.; Yu, C., Glucose-responsive nanosystem mimicking the physiological insulin secretion via an enzyme–polymer layer-by-layer coating strategy. *Chem. Mater.* **2017,** *29* (18), 7725-7732.
150. Tai, W.; Mo, R.; Di, J.; Subramanian, V.; Gu, X.; Buse, J. B.; Gu, Z., Bio-inspired synthetic nanovesicles for glucose-responsive release of insulin. *Biomacromolecules* **2014,** *15* (10), 3495-3502.
151. Suwa, K.; Sato, K.; Anzai, J., Preparation of multilayer films consisting of glucose oxidase and poly (amidoamine) dendrimer and their stability. *Colloid. Polym. Sci.* **2015,** *293* (9), 2713-2718.
152. Zhang, M.; Song, C.-C.; Du, F.-S.; Li, Z.-C., Supersensitive oxidation-responsive biodegradable PEG hydrogels for glucose-triggered insulin delivery. *ACS applied materials & interfaces* **2017,** *9* (31), 25905-25914.
153. Uchiyama, T.; Kiritoshi, Y.; Watanabe, J.; Ishihara, K., Degradation of phospholipid polymer hydrogel by hydrogen peroxide aiming at insulin release device. *Biomaterials* **2003,** *24* (28), 5183-5190.
154. Zhang, Y.; Wang, J.; Yu, J.; Wen, D.; Kahkoska, A. R.; Lu, Y.; Zhang, X.; Buse, J. B.; Gu, Z., Bioresponsive Microneedles with a Sheath Structure for H2O2 and pH Cascade-Triggered Insulin Delivery. *Small* **2018,** *14* (14), 1704181.
155. Scheja, S.; Domanskyi, S.; Gamella, M.; Wormwood, K. L.; Darie, C. C.; Poghossian, A.; Schöning, M. J.; Melman, A.; Privman, V.; Katz, E., Glucose-Triggered Insulin Release from Fe3+-Cross-linked Alginate Hydrogel: Experimental Study and Theoretical Modeling. *Chemphyschem* **2017,** *18* (12), 1541-1551.
156. Tong, Z.; Zhou, J.; Zhong, J.; Tang, Q.; Lei, Z.; Luo, H.; Ma, P.; Liu, X., Glucose-and H2O2-responsive polymeric vesicles integrated with microneedle patches for glucose-sensitive transcutaneous delivery of insulin in diabetic rats. *ACS applied materials & interfaces* **2018,** *10* (23), 20014-20024.
157. Yoshida, K.; Awaji, K.; Shimizu, S.; Iwasaki, M.; Oide, Y.; Ito, M.; Dairaku, T.; Ono, T.; Kashiwagi, Y.; Sato, K., Preparation of microparticles capable of glucose-induced insulin release under physiological conditions. *Polymers* **2018,** *10* (10), 1164.
158. Li, C.; Liu, X.; Liu, Y.; Huang, F.; Wu, G.; Liu, Y.; Zhang, Z.; Ding, Y.; Lv, J.; Ma, R., Glucose and H 2 O 2 dual-sensitive nanogels for enhanced glucose-responsive insulin delivery. *Nanoscale* **2019,** *11* (18), 9163-9175.
159. Zuo, M.; Qian, W.; Xu, Z.; Shao, W.; Hu, X. Y.; Zhang, D.; Jiang, J.; Sun, X.; Wang, L., Multiresponsive Supramolecular Theranostic Nanoplatform Based on Pillar [5] arene and Diphenylboronic Acid Derivatives for Integrated Glucose Sensing and Insulin Delivery. *Small* **2018,** *14* (38), 1801942.
160. Bachelder, E. M.; Beaudette, T. T.; Broaders, K. E.; Dashe, J.; Fréchet, J. M., Acetal-derivatized dextran: an acid-responsive biodegradable material for therapeutic applications. *J. Am. Chem. Soc.* **2008,** *130* (32), 10494-10495.
161. Broaders, K. E.; Cohen, J. A.; Beaudette, T. T.; Bachelder, E. M.; Fréchet, J. M., Acetalated dextran is a chemically and biologically tunable material for particulate immunotherapy. *Proceedings of the National Academy of Sciences* **2009,** *106* (14), 5497-5502.
162. Suarez, S.; Grover, G. N.; Braden, R. L.; Christman, K. L.; Almutairi, A., Tunable protein release from acetalated dextran microparticles: a platform for delivery of protein therapeutics to the heart post-MI. *Biomacromolecules* **2013,** *14* (11), 3927-3935.
163. Kurtzhals, P.; Havelund, S.; Jonassen, I.; Kiehr, B.; Larsen, U.; Ribel, U.; Markussen, J., Albumin binding of insulins acylated with fatty acids: characterization of the ligand-protein interaction and correlation between binding affinity and timing of the insulin effect in vivo. *Biochem. J.* **1995,** *312* (3), 725-731.
164. Havelund, S.; Plum, A.; Ribel, U.; Jonassen, I.; Vølund, A.; Markussen, J.; Kurtzhals, P., The mechanism of protraction of insulin detemir, a long-acting, acylated analog of human insulin. *Pharm. Res.* **2004,** *21* (8), 1498-1504.
165. Cramer, J. A.; Pugh, M. J., The Influence of Insulin Use on Glycemic Control: How well do adults follow prescriptions for insulin? *Diabetes Care* **2005,** *28* (1), 78-83.
166. Donnelly, L. A.; Morris, A. D.; Evans, J.; collaboration, D. M., Adherence to insulin and its association with glycaemic control in patients with type 2 diabetes. *Journal of the Association of Physicians* **2007,** *100* (6), 345-350.

167 Brod, M , Rana, A , Barnett, A H , Adherence patterns in patients with type 2 diabetes on basal insulin analogues missed, mistimed and reduced doses *Curr Med Res Opin* **2012,** *28* (12), 1933-1946
168 Peyrot, M , Barnett, A , Meneghini, L , Schumm-Draeger, P M , Factors associated with injection omission/non-adherence in the Global Attitudes of Patients and Physicians in Insulin Therapy study *Diabetes, Obesity and Metabolism* **2012,** *14* (12), 1081-1087
169 Peyrot, M , Rubin, R R , Kruger, D F , Travis, L B , Correlates of insulin injection omission *Diabetes Care* **2010,** *33* (2), 240-245
170 Ross, S A , Tildesley, H D , Ashkenas, J , Barriers to effective insulin treatment the persistence of poor glycemic control in type 2 diabetes *Curr Med Res Opin* **2011,** *27* (sup3), 13-20
171 Geller, A I , Shehab, N , Lovegrove, M C , Kegler, S R , Weidenbach, K N , Ryan, G J , Budnitz, D S , National estimates of insulin-related hypoglycemia and errors leading to emergency department visits and hospitalizations *JAMA internal medicine* **2014,** *174* (5), 678-686
172 Wang, H -C , Lee, A -R , Recent developments in blood glucose sensors *J Food Drug Anal* **2015,** *23* (2), 191-200
173 Vashist, S K , Zheng, D , Al-Rubeaan, K , Luong, J H , Sheu, F -S , Technology behind commercial devices for blood glucose monitoring in diabetes management A review *Anal Chim Acta* **2011,** *703* (2), 124-136
174 Oh, J K , Drumright, R , Siegwart, D J , Matyjaszewski, K , The development of microgels/nanogels for drug delivery applications *Prog Polym Sci* **2008,** *33* (4), 448-477
175 Khademhosseini, A , Langer, R , Microengineered hydrogels for tissue engineering *Biomaterials* **2007,** *28* (34), 5087-5092
176 Newsom, J P , Payne, K A , Krebs, M D , Microgels modular, tunable constructs for tissue regeneration *Acta Biomater* **2019**
177 Farina, M , Alexander, J F , Thekkedath, U , Ferrari, M , Grattoni, A , Cell encapsulation Overcoming barriers in cell transplantation in diabetes and beyond *Adv Drug Del Rev* **2018**
178 Mørch, Ý A , Donati, I , Strand, B L , Effect of Ca2+, Ba2+, and Sr2+ on Alginate Microbeads *Biomacromolecules* **2006,** *7* (5), 1471-1480
179 Bochenek, M A , Veiseh, O , Vegas, A J , McGarrigle, J J , Qi, M , Marchese, E , Omami, M , Doloff, J C , Mendoza-Elias, J , Nourmohammadzadeh, M , Alginate encapsulation as long-term immune protection of allogeneic pancreatic islet cells transplanted into the omental bursa of macaques *Nature biomedical engineering* **2018,** *2* (11), 810
180 Johnson Jr, W C , Protein secondary structure and circular dichroism a practical guide *Proteins. Structure, Function, and Bioinformatics* **1990,** *7* (3), 205-214
181 Greenfield, N J , Using circular dichroism spectra to estimate protein secondary structure *Nat Protoc.* **2006,** *1* (6), 2876
182 Sluzky, V , Tamada, J A , Klibanov, A M , Langer, R , Kinetics of insulin aggregation in aqueous solutions upon agitation in the presence of hydrophobic surfaces *Proceedings of the National Academy of Sciences* **1991,** *88* (21), 9377-9381
183 Sluzky, V , Klibanov, A M , Langer, R , Mechanism of insulin aggregation and stabilization in agitated aqueous solutions *Biotechnol Bioeng* **1992,** *40* (8), 895-903